Kinetics of Complete Methane Oxidation on Palladium Model Catalysts

by

Guanghui Zhu

A Dissertation

Submitted to the Faculty

of the

WORCESTER POLYTECHNIC INSTITUTE

in partial fulfillment of the requirements for the

Degree of Doctor of Philosophy

in

Chemical Engineering

January 2004

Committee Members:

Prof. Fabio H. Ribeiro
Department of Chemical Engineering, WPI

Prof. William M. Clark
Department of Chemical Engineering, WPI

Prof. Richard D. Sisson
Department of Mechanical Engineering, WPI

CONTENT

I. Abstract

The catalytic combustion of methane in excess of O_2 over Pd catalysts was studied on model catalysts, including polycrystalline palladium foil and palladium single crystals. The kinetics of this reaction could be measured at conditions not accessible to supported catalysts and, thus, the issues of structure sensitivity, mechanism, hysteresis on oxidation, and deactivation could be studied in detail.

Methane oxidation on PdO was insensitive to the original metal surface structure which PdO grew from, with turnover rates in the range of 1.3-4.7 s^{-1} on (111), (100) and (110) single crystals at 160 Torr O_2, 16 Torr CH_4, 1 Torr H_2O and 598 K. Methane oxidation on Pd metal was also insensitive to the original surface structure, with the turnover rate in the range of 2.0-2.8 s^{-1} on the three single crystals at 2.3 Torr O_2, 0.46 Torr CH_4, 0.05 Torr H_2O and 973 K. Since there is no support effect and the surface purity could be certified, these turnover rates for this reaction can be used as a benchmark.

The turnover rate for methane oxidation was found to decrease 95% when PdO decomposed to Pd metal at 888 K, showing that PdO was more active than Pd metal for methane combustion at this temperature. Water inhibition to the reaction was not observed at a temperature above 813 K on both PdO and Pd metal, while it was observed at 598 K on PdO. The activation energy on PdO was 32 kJ mol^{-1} in the range of 783-873 K, while it was 125 kJ mol^{-1} in the range of 568-623 K. The activation energy on Pd metal was 125 kJ mol^{-1} in the range of 930-980 K. The change of reaction orders and activation energies suggests that the reaction mechanism is a function of temperature and palladium chemical states. We propose that adsorbed water, the most abundant surface intermediate at 598 K, was not present in significant quantities at temperatures above 783 K. This change in surface inhibition by water is the reason for lower activation energy at temperatures above 783 K.

Interaction between the catalyst and support, or presence of impurities, is one of the factors for catalyst deactivation. The interaction between oxidized silicon and palladium was investigated on a polycrystalline palladium foil and on supported Pd/SiO_2 catalysts. During methane oxidation, oxidized silicon covered the palladium oxide surface as observed by TEM on Pd/SiO_2 catalysts and by XPS on palladium foil. On Pd foil, the source of silica was a silicon impurity, common on bulk metal samples. The migration of oxidized silicon onto PdO deactivated the catalysts by blocking the active sites for methane oxidation. Silicon oxide overlayers were also observed covering the Pd surface after reduction of Pd/SiO_2 by H_2 at 923 K.

Keywords: methane oxidation on palladium, kinetics, model catalyst, deactivation, hysteresis, structure sensitivity

II. Extended Abstract

Natural gas-fueled gas turbines are a preferred technology for power generation. One reason is that many of the large reserves of natural gas, which is composed mainly of methane, have very small amounts of sulfur and nitrogen compounds; as a consequence, when the natural gas is burned, the emission gases will contain correspondingly a low concentration of SOx and NOx formed from S and N compounds. Another reason is that methane has the highest hydrogen-to-carbon ratio in all hydrocarbons and thus it can produce less carbon dioxide, a greenhouse gas, per unit of power produced. In the conventional gas turbine combustors, flame can be sustained only within fixed flammability limits corresponding to temperatures (1800^{o}C) where the reaction of nitrogen and oxygen occurs at appreciable rates to form NOx. Procedures to reduce NOx formation, such as reducing the flame temperature or the residence time, could lead to increased operating expenses, increased emissions of CO and unburned hydrocarbons (UHC) as well as to an unstable combustion regime; while selective catalytic reduction of NOx with ammonia, commonly used as post-combustion clean up, is an expensive technology and handling of ammonia also poses problems. By contrast, catalytic combustion has the potential to reduce NOx emission to ultra low levels (less than 1 ppm) at a much lower cost, while avoiding the problems of lean premix combustors.

The catalyst for catalytic methane oxidation should have high activity for it to ignite at temperatures close to the compressor outlet temperature. Supported palladium catalysts have been found to be the most promising catalysts for catalytic methane combustion because they have the highest activity toward methane oxidation. However, methane combustion on palladium presents some practical challenging issues that need to be resolved: What is the rate of reaction at particular conditions? Is the reaction sensitive to the palladium surface structure? What is the reaction mechanism?

The approach in this study was to use a model system to address the issues mentioned above. In the model system, catalysts were planar replicas of the supported catalysts, including polycrystalline palladium foil and palladium single crystals. Those catalysts had all their area exposed at the surface and, thus, all the catalyst area was accessible to the powerful surface science techniques. Another advantage is that those catalysts were non-porous and free of internal mass and heat transfer limitations, making the kinetic study easier than on supported catalysts. The system for model studies consisted of a high-pressure reactor and an ultrahigh vacuum (UHV) analyzing chamber. The catalysts can be prepared and characterized in UHV by surface sensitive techniques and can then be moved with a welded bellows transfer arm to the reaction chamber. The reaction conditions are the same ones used to measure rates on high surface area catalysts. The catalyst surface can be studied after reaction. The techniques available in the UHV chamber are low energy electron diffraction (LEED), Auger electron spectroscopy (AES), X-ray photoelectron spectroscopy (XPS), and temperature programmed desorption (TPD). The attached reactor can be used to run reactions up to 1.5 atm and also to expose the sample to higher pressures of gases than is feasible in the UHV chamber. With this apparatus we were able, for example, to determine the maximum possible rate and determine the structure sensitivity of the reaction.

The background activity from the reactor was tested and its contribution to the experimental results was found to be negligible. The experimental data were acquired at conditions where no external mass transfer limitation was involved.

The turnover rate is defined as the number of methane molecules reacted on one active site per unit of time. This rate provided the foundation for all studies. The active sites were either PdO or Pd, depending on the oxygen pressure in the gas phase and reaction temperature. The number of PdO sites was measured by $^{18}O_2$ exchange. In this method, $^{18}O_2$ from the gas phase exchanged with ^{16}O on the $Pd^{16}O$ surface. The designed exchange conditions guaranteed that the exchange only occurred between gas phase $^{18}O_2$ and O in the first layer of palladium oxide, without appreciable diffusion of ^{18}O into the bulk. After exchange, the ^{18}O on the surface was released to the gas phase during temperature-programmed desorption and the amount released recorded. The surface area was then calculated based on the amount of ^{18}O released. The number of Pd metal sites was assumed to be the same as the amount of Pd atoms on the clean model catalyst surface.

Catalytic rates per unit of active area provide the quantitative measure to allow for comparison of catalysts. One difficulty in this quantification is that the rates may be dependent not only on the surface area but also on the particular structure of the active site, which would then have to be defined for each sample. Thus, to specify the rate of reaction one needs to find if the reaction is sensitive to the structure of the catalyst. One way to investigate this sensitivity is by realizing that a practical industrial catalyst is composed of nanometer clusters and that they are formed of single crystals surfaces. Comparing the rates on a set of large single crystal surfaces which make up the clusters can identify if the rates depend on the structure of the surface. In this research, we studied methane oxidation on three single crystals, Pd(111), Pd(100) and Pd(110). The surface during methane oxidation could be PdO or Pd metal, depending on the oxygen pressure and the reaction temperature; therefore both phases were studied. The turnover rates, reaction orders and activation energies on metal phase were similar for three single crystals, suggesting that methane oxidation on Pd metal is not sensitive to the original metal surface structure. Single crystals of PdO with different orientations are not available. Considering PdO in real catalysts is created by oxidizing the Pd particles which are composed mainly by facets of (111), (100) and (110), the oxide in this study was obtained by oxidizing the surface of the three crystals which should give the same PdO surface structure as on the corresponding facet in real catalysts. The turnover rates, reaction orders and activation energies on PdO phase were similar for three single crystals, suggesting that methane oxidation on PdO is not sensitive to the original metal surface structure where PdO grew from.

We studied methane oxidation on both PdO and Pd metal using palladium foil at the temperature near PdO decomposition point. Water inhibition to methane oxidation, which was observed at 598 K on PdO, was not observed at temperature above 813 K on both PdO and Pd metal. Reaction order was 0.6-0.8 for CH_4 and about zero for O_2 at 598-973 K on both PdO and Pd metal. On PdO, activation energy was 32 kJ mol^{-1} at temperature between 783-873 K; lower than the 125 kJ mol^{-1} obtained at temperature

between 568-623 K. On Pd metal, activation energy was 125 kJ mol^{-1} at temperatures between 930-1003 K. The variation of reaction orders and activation energies indicate that the reaction mechanism is a function of temperature and palladium chemical states. A reaction mechanism was proposed to explain the kinetic data. At 598 K, the catalyst surface could be mostly covered by adsorbed water which was in equilibrium with water vapor, and the adsorbed water blocked the active sites for methane oxidation. As the temperature increased, the concentration of adsorbed water decreased. When the concentration of adsorbed water was negligible compared with concentration of available sites for methane oxidation (such as at 813 K), the water inhibition effect disappeared. The lower activation energy on PdO at 783-873 K was attributed to the loss of water inhibition effect. At 888 K with 0.76 Torr O_2 and 0.15 Torr CH_4, the turnover rate was found to decrease from 1.9 s^{-1} to 0.1 s^{-1} when PdO decomposed to Pd metal, showing that PdO was more active toward methane oxidation than Pd metal at this temperature. The kinetic results obtained at temperatures around PdO decomposition point, together with the kinetic results obtained at 598 K, could stand for the reaction kinetics for the palladium catalyst inside a catalytic combustor with temperature varying from the inlet temperature of 630 K to outlet temperature of 1300 K.

Palladium catalyst exhibited activity hysteresis for methane oxidation at the temperature between PdO decomposition and reformation. The hysteresis was studied using temperature-programmed methane oxidation with 0.76 Torr O_2 and 0.15 Torr CH_4, which included heating and cooling cycles. In the heating cycle, the methane conversion initially increased as expected up to 873 K when PdO started to decompose to Pd. The conversion decreased by 90% after PdO fully decomposed to Pd. Methane conversion started to increase again as the temperature increased after PdO had fully decomposed. When the temperature reached 1003 K, the process was reversed by decreasing the temperature to the initial point. The conversion decreased as expected but as the transition temperature was reached the conversion remained at a level more than 90% lower than in the heating cycle. As the temperature reached 828 K, methane conversion increased to the same level observed in the heating cycle. Thus, there was a 45 K difference in the Pd-PdO transition temperature. Additional experiments showed that in the hysteresis temperature range (828-873 K), palladium oxidation could occur only if PdO could be first formed in the catalyst. This observation indicates that the PdO reformation at lower temperatures was not limited by the rate of oxidation but, possibly, by the formation of nucleation sites.

Catalyst activation and deactivation are important issues for methane combustion on palladium catalysts. Interaction between the catalyst and impurities from either reactants or source of catalyst materials is one of the factors for catalyst deactivation. Since silica is one of the most common supports and silicon is one of the common impurities in catalyst materials, we studied the effect of silica/silicon on palladium catalysts reactivity. The interaction between silica and palladium following complete oxidation of methane or following reduction in H_2 was investigated on a polycrystalline palladium foil and on supported Pd/SiO_2 catalysts. During methane oxidation, oxidized silicon covered the palladium oxide surface as observed by TEM on Pd/SiO_2 catalysts and by XPS on palladium foil. On the Pd foil, the source of silica was a silicon impurity, common on

bulk metal samples. The spreading of silica was not observed when the Pd foil was treated by pure oxygen reaction temperature (598 K) or by vapor water treatment at room temperature, suggesting that temperature and water vapor are the two necessary factors to promote silica spreading. The migration of oxidized silicon onto PdO deactivated the catalysts by blocking the active sites for methane oxidation. Silicon oxide overlayers were also observed covering the Pd surface after reduction of Pd/SiO_2 by H_2 at 923 K.

Keywords: methane oxidation on palladium, kinetics, model catalyst, deactivation, hysteresis, structure sensitivity

1 Research Motivations and Objectives

1.1 Research Motivation

Many of the large reserves of natural gas, which is composed mainly of methane, have very small amounts of sulfur and nitrogen compounds. As a consequence, when the natural gas is burned, the emission gases will contain correspondingly lower concentrations of SOx and NOx formed from S and N compounds. Methane has the highest hydrogen-to-carbon ratio in all hydrocarbons, and thus can produce the highest amount of energy per CO_2 formed when it is burned. Since CO_2 is a green house gas and consequently strict regulations on CO_2 emissions into the atmosphere is expected in the near future, natural gas becomes even more attractive as a fuel for the purposes of energy production. Due to those advantages, natural gas-fueled gas turbines are expected to provide a significant portion of the growing world demand for electric power generation.

Figure 1-1 gives the schematic diagram of a traditional gas turbine system using natural gas as fuel. The compressed air and the fuel are mixed and then combusted in a flame. The hot gas generated by the flame combustion expands and drives the turbine. The hot gas has to be cooled by by-passed compressed air to 2300^{o}F before being delivered to the gas turbine. The homogeneous combustion can be sustained only within fixed flammability limits corresponding to temperatures (3000^{o}F) where rapid coupling of nitrogen and oxygen occurs to form NOx (Figure 1-2, [1]). Procedures to reduce NOx formation, such as reducing the flame temperature or the residence time, could lead to the increasing emissions of CO and unburned hydrocarbons (UHC) as well as to an unstable combustion regime; while selective catalytic reduction of NOx with ammonia, commonly

used as post-combustion clean up, is an expensive technology and the handling of ammonia also poses problems.

Catalytic methane combustion was proposed to solve these issues without sacrificing the system performance. Catalytic methane combustion is a process in which methane and oxygen react on the surface of a catalyst to achieve complete oxidation. This process takes place without a flame and can be operated at much lower temperature than the conventional combustion system. Due to the lower operating temperature, catalytic methane combustion generates a lower emission of nitrogen oxides (NOx) than a conventional combustion system. This advantage becomes more and more economically and environmentally valuable with the increasingly stringent regulation of the NO_x emission.

Figure 1-3 gives the schematic diagram of a catalytic combustion system developed by Catalytic Energy Systems. In the non-flame combustors, fuel and air are thoroughly mixed and delivered to the catalytic combustion region. In the catalytic combustion region, part of the lean fuel-air mixture was catalytically combusted to raise the temperature at the outlet to about 1800^oF so that the remaining fuel can achieve a homogeneous combustion. [2-4]. This catalytic combustion system for gas turbines, which achieves combustion at temperatures at about 2300^oF, can reduce NOx formation dramatically to below 2.5 ppm.

The catalyst for catalytic methane oxidation should have high activity in order to obtain ignition at temperatures close to the compressor outlet temperature. Supported palladium

catalysts have been found to be the most promising catalysts for catalytic methane combustion [5] and are being used on the commercial catalytic combustors [3, 6]. Despite of the successful applications, methane combustion on palladium catalysts, however, presents some challenging problems that should be resolved to allow for a better performance. Some of these issues are related to the interaction of PdO with the reactants, and PdO with the support. The issues to be discussed in this dissertation are as follows:

(1) What is the reaction mechanism? Does the reaction mechanism change with temperature?

(2) Which phase is more active for methane combustion, PdO or Pd metal?

(3) What is the cause for the deactivation of catalysts?

(4) What causes the catalyst to limit its temperature under reaction conditions to 1073 K at 1 atm in air? Is it related to the transition between PdO and Pd?

(5) Is the reaction structure sensitive?

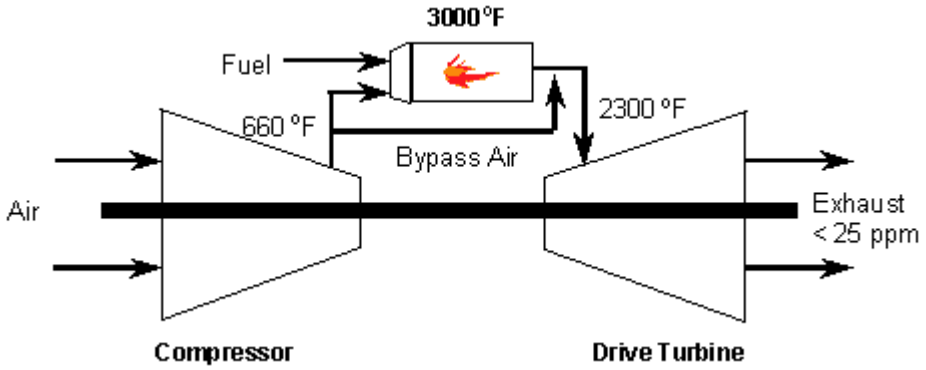

Figure 1-1 Schematic diagram of conventional flame combustion gas turbine system (Figure is cited from www.catalyticenergy.com)

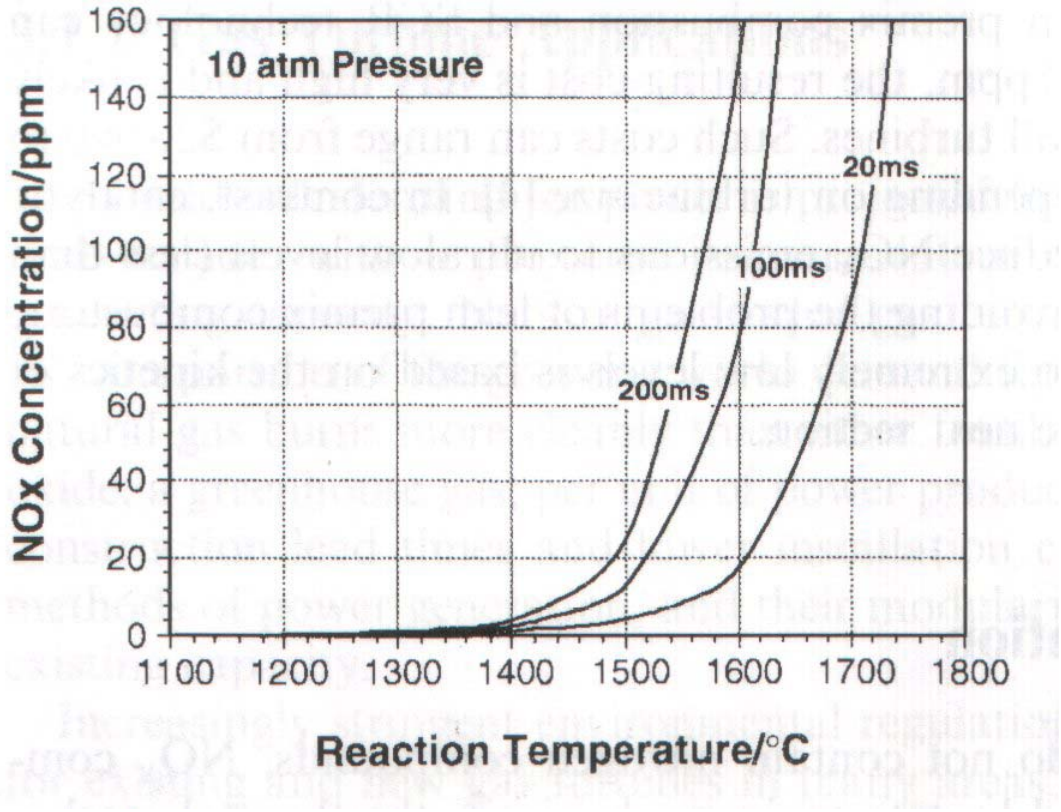

Figure 1-2 NOx formation as a function of temperature[1]

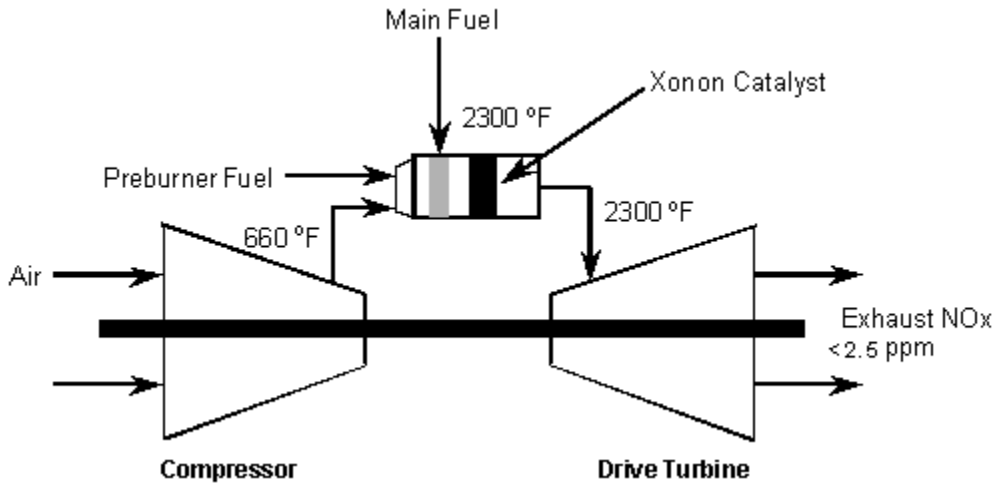

Figure 1-3 schematic diagram of catalytic combustion gas turbine system (Figure is cited from www.catalyticenergy.com)

1.2 Research Objectives

1.2.1 High Temperature Kinetics

Palladium catalysts for the oxidation of methane present an unusual situation in that the thermodynamically stable phase can be either Pd metal or PdO depending on the oxygen practical pressure and the temperature. In air, at atmospheric pressure, the stable phase is PdO at temperatures below 1073 K while is metallic Pd at temperature above 1073 K [7]. It is generally agreed that the reaction mechanism changes with reaction temperature and the thermodynamically stable phases [8-21], but quantitative studies of the reaction kinetics at temperatures around PdO decomposition point, including turnover rates, reaction orders and activation energies, were not available.

In this study, turnover rates, reaction orders and activation energies were obtained at various temperatures and palladium stable phases. These data set up benchmarks for any study of methane oxidation on palladium catalysts. The reaction mechanism was proposed to elucidate the kinetics results. By comparing the turnover rates on PdO and Pd metal under the same conditions at PdO decomposition temperature, we could tell which phase is more active for methane oxidation.

1.2.2 Catalyst Activation and Deactivation

Catalyst activation and deactivation have to be understood and controlled to allow a stable operation of the catalytic combustion system. The activation mostly occurred at the beginning of the reaction [8] and the activation period ranged from minutes to days [8, 14, 22-24]. Some catalysts started to deactivate as soon as the reaction started, some started to deactivate after an activation period, while some were rather stable [25-30]. There are no general agreements with reasons for these activations and deactivations.

Interactions between catalysts and impurities from either reactants or source of catalyst materials, were some of the factors for catalyst deactivation [27, 31-34]. Since silica is one of the most common supports and silicon is one of the most common impurities in catalyst materials, this study was to analyze the effect of silica/silicon on palladium catalysts reactivity. The catalysts studied include palladium foil with oxidized silicon impurities and palladium supported on silica.

1.2.3 Catalyst Activity Hysteresis during Palladium Phase Transition

Palladium catalyst exhibited hysteresis in the reaction rate for methane oxidation during PdO decomposition and reformation [17, 35-38]. In temperature-programmed methane oxidation, including heating and cooling cycles, the methane conversion initially increased as expected up to the temperature for PdO decomposition (Td). The methane conversion usually decreased along with the PdO decomposition. Methane conversion started to increase again as the temperature increased after PdO had fully decomposed.

The cooling cycle started from a temperature where PdO had fully decomposed to Pd metal. During cooling, the methane conversion decreased as expected but it could only return to the level observed during heating cycle at temperature lower than the PdO decomposition temperature. The temperature for PdO reformation (Tr) was found lower than the temperature for PdO decomposition (Td). At the temperature window between Tr~Td, the methane conversion in cooling cycle was generally lower than the methane conversion in heating cycle

The overall rate of catalytic methane combustion was the multiple of two factors: turnover rate and surface area. To understand quantitatively why the methane conversion dropped when palladium oxide decomposed to palladium metal, the turnover rates based on both PdO and Pd were obtained in this study at temperatures around PdO decomposition point.

For adiabatic catalytic reactor, reactivity hysteresis could cause the oscillation of reaction temperature and methane conversion [28, 39, 40], which would affect the performance of the catalytic combustion system. Understanding the mechanism for hysteresis would be helpful to solve the problem. In this study, a mechanism was proposed based on the experiment results, and methods with the potential to eliminate hysteresis were put forward.

1.2.4 Reaction Sensitivity to Surface Structure

One of the questions regarding methane combustion on palladium catalyst is structure sensitivity. For real catalyst, when metal particles are in the critical size of nanometer diameter, the relative concentrations of surface sites with given coordination neighbors changes rapidly when the particle size changes. This means the catalyst surface structure changes. If the turnover rates changes as the catalyst surface structure changes, then the reaction is structure sensitive. Turnover rate is commonly used as the quantitative measure for comparison of catalyst performance. Thus, it is necessary to specify whether the reaction is structure sensitive before comparing the turnover rate. The question of structure sensitivity on methane combustion has no unanimous answer so far [8, 15, 20, 21, 24, 41-45].

Most experiment results to address this issue were obtained on supported catalysts. The interaction between supports and catalyst varies depending on the support type, catalyst preparation method and catalyst treatment history. Those unpredictable interactions make the experimental results hard to interpret. One straightforward way to know whether a reaction is structure sensitive is to run the reaction on single crystal catalysts with different surface atom orientations and then to compare the turnover rates. In this study, the kinetics data were obtained on three palladium single crystals with the simplest orientations, Pd(111), Pd(110) and Pd(100). The surface during methane oxidation could be PdO or Pd metal, depending on the oxygen pressure and the reaction temperature; therefore both phases were studied. By comparing the kinetic results, the final conclusion was reached on whether methane oxidation is structure sensitive reaction.

2 Research System Setup

Model catalysts employed in this research were polycrystalline palladium foils and palladium single crystals. The palladium foils were 0.125 mm thickness (Goodfellow Cambridge Limited, 99.99+%) with geometric surface area between 0.5-1 cm^2. The single crystals, including Pd(111) (Princeton Scientific Co.), Pd(110) (Princeton Scientific Co.) and Pd(100) (Accumet Materials Co.), were about 1 mm thickness and 8.5 mm diameter. All single crystals were one side polished with orientation accuracy $\pm 0.5^o$.

The research system consisted of a high-pressure reactor cell attached to an ultra-high vacuum (UHV) analyzing chamber (Figure 2-1). The UHV chamber was isolated from the reaction cell by a gate valve. When gate valve was open, catalyst samples could be transferred between the high-pressure reactor and UHV analyzing chamber using a transfer arm without exposing the air, therefore the sample purity could be controlled and detailed surface analysis was feasible. The reactor (Figure 2-2) could be operated in two modes: batch reactor mode and continuous-stirred stank reactor (CSTR) mode. The batch mode was available by opening valve V4, and closing valve V1, V2, V3 and V5. The CSTR mode was available by opening valve V1, V2 and V3, and closing valve V4 and V5 (Figure 2-2). The gas phase concentration was monitored by an Agilent 6890 Series gas chromatograph (GC) equipped with a 15-ft Carboxen 1000, 60/80 mesh column and a thermal conductivity detector (TCD). The main components of the UHV analyzing chamber include a double-pass cylindrical mirror analyzer (PHI Model 15-255G) used for Auger electron spectroscopy (AES) and X-ray photoelectron spectroscopy (XPS), a 15 kV double-anode X-ray gun (PHI 4-548), a UTI-100C quadrupole mass spectrometer,

a sputtering gun (PHI model 04-164), an OCI low energy electron diffraction (LEED). The advantage of this approach is that one can apply surface science techniques and yet carry out reactions under the conditions described in the literature for supported catalysts.

Samples inside the reactor were mounted by spot-welding (Figure 2-3). For palladium foil, chromel-alumel thermocouples were spot-welded on the back of the foil for temperature measurement; stainless steel pins were spot-welded on the back of the foil to supply current for resistive heating. For single crystals, both the thermocouples and stainless steel pins were spot-welded on the edge of the crystals. An infrared lamp was mounted outside the reactor facing the viewport on the reactor. The infrared light generated by the lamp could go through the viewport and be focused on the sample. The sample was heated by both methods at the same time in the experiment (Figure 2-4). The sample temperature was controlled by using a temperature controller (Euortherm Model 2408) interfaced TCR power supply (Electronic Measurements Inc).

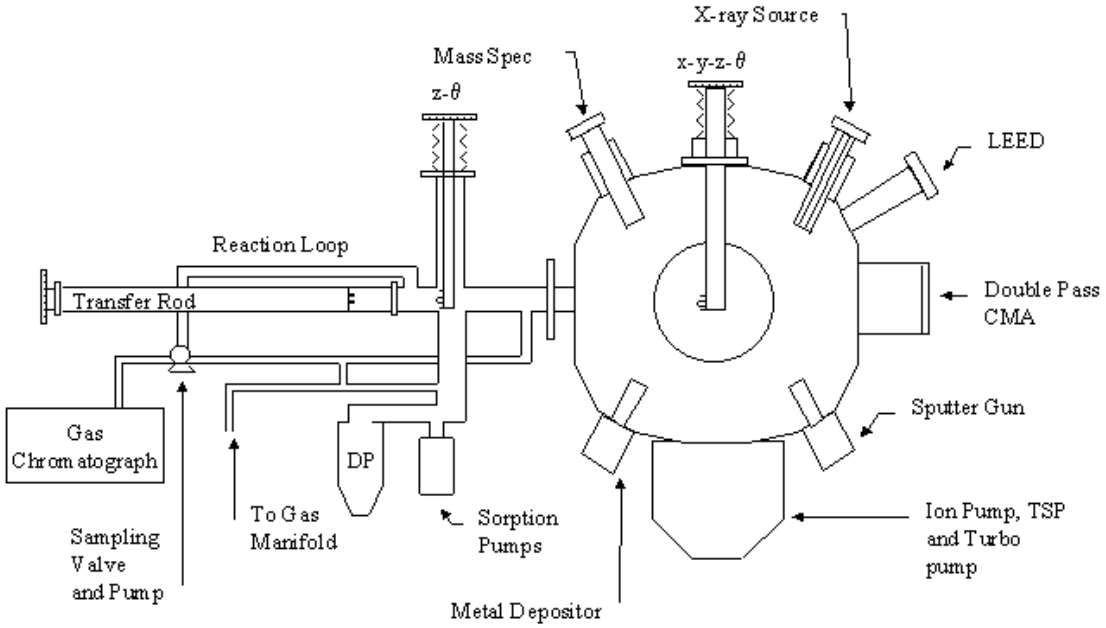

Figure 2-1 Schematic diagram of high pressure reactor/UHV chamber system

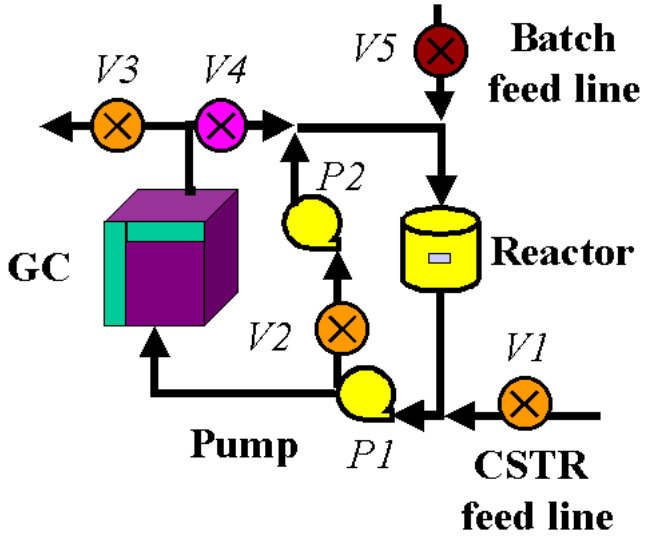

Figure 2-2 Schematic diagram of reaction and data collection system

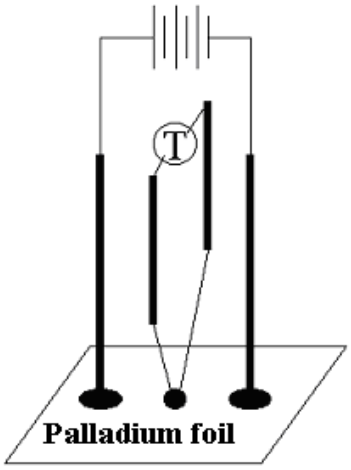

(a)

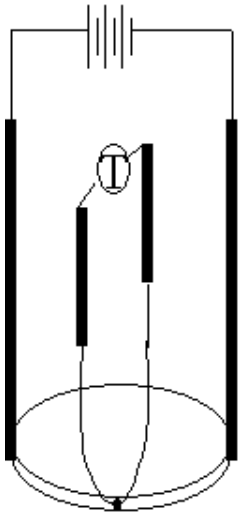

(b)

Figure 2-3 The construction of model catalysts (a) polycrystalline palladium foil (b) palladium single crystals

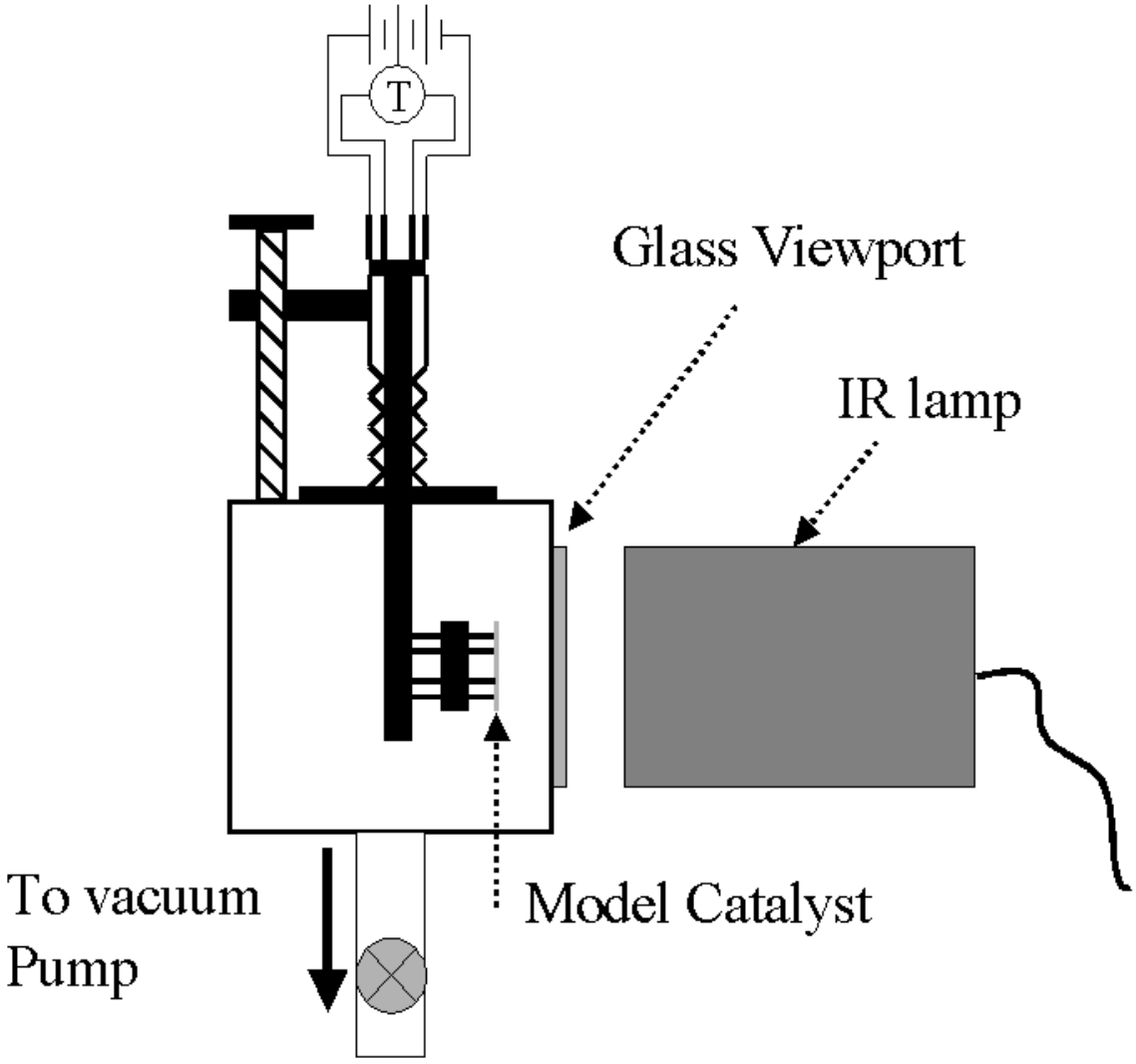

Figure 2-4 Schematic Diagram of High Pressure Reactor Cell

3 Temperature Dependence of Reaction Kinetics for Complete Oxidation of Methane on Palladium Foil

Abstract:

Kinetic data, including turnover rates, reaction orders and activation energies were obtained at temperatures between 813-1003 K on both PdO and Pd phases. At 888 K with 0.76 Torr O_2 and 0.15 Torr CH_4, the turnover rate decreased from 1.9 s^{-1} to 0.1 s^{-1} when PdO decomposed to Pd metal, suggesting that PdO is more active than Pd metal for methane oxidation at this temperature. Water inhibition to the reaction was not observed at temperature above 813 K on both PdO and Pd metal, while it was observed at 598 K on PdO in previous work. The reaction order was 0.6-0.8 for CH_4 and about zero for O_2, which was measured in the range of 598-973 K on both PdO and Pd metal. The activation energy was 32 kJ mol^{-1} at 783-873 K on PdO, while it was 125 kJ mol^{-1} at 933-1003 K on Pd metal. The variation of reaction orders and activation energies indicate that the reaction mechanism for methane oxidation on palladium catalyst is a function of temperature and palladium chemical states.

Keywords: methane oxidation on palladium; model catalyst; kinetics.

3.1 Introduction

There are large reserves of natural gas in the world which were mainly composed of methane with very low level of sulfur- and nitrogen- containing impurities. Methane has the highest C-H ratio among all the hydrocarbons; thus, combustion of methane produces the highest energy per unit of CO_2 (greenhouse gas) formed. Because of those advantages, natural gas-fueled gas turbines are expected to provide a significant portion of the growing world demand for electric power generation. Compared with the traditional flame combustion for the gas turbine, catalytic methane combustion is more attractive as it can be operated at a much lower temperature to reduce NOx formation. Palladium catalysts are the most active catalysts for catalytic methane combustion [5] and are currently being used on commercial catalytic combustors for gas turbine[3, 6].

In the practical operation, palladium catalysts for methane combustion present an unusual situation in that the thermodynamically stable phase can be either Pd metal or PdO depending on the oxygen practical pressure and the temperature. Kinetic data, such as turnover rates, reaction orders and activation energies, are necessary to understand the reaction mechanism on different catalyst phases. It is generally agreed that the reaction mechanism changes with reaction temperature and with the surface chemical states [8-21]. At temperatures below 600 K under normal working (dry feed) or excess water conditions, reaction order was reported 0.6-1 for methane, zero for oxygen, negative for water and zero for CO_2 [8, 10]. The magnitude of water inhibition on methane oxidation was smaller at higher temperatures. At 553 K, the reaction order of water was about -1[8]; when the temperature was above 723 K, water inhibition to the reaction was almost

invisible [9]. Inhibition to the reaction by CO_2 was observed only when excess CO_2 was added in the gas mixture [8, 9]; however, when both water and CO_2 were in the stream, the CO_2 effect was negligible, and the total decrease of activity was equal to the decrease of activity caused by water alone [9].

The activation energy was reported changing dramatically with reaction temperature and the chemical state of palladium catalyst. At low temperatures and PdO being thermodynamically stable phase, the activation energy was reported 125-184 kJ mol^{-1} by considering the water inhibition effect [8, 10, 43]. Numbers between 80-126 kJ mol^{-1} were obtained without considering the water inhibition effect [18-20] although these are not activation energies as the rate constants are effectively a function of water concentration. (k/[H2O]). Lower activation energy, with value about 24-45 kJ mol^{-1}, was reported at higher temperatures with PdO still being the thermodynamically stable phase [21]. The temperatures, where the lower activation energy were observed, started from between 654-820 K depending on the type of support and catalyst loading [11, 21]. The activation energy was about 157-200 kJ mol^{-1} [18, 19] when Pd metal was thermodynamically stable phase. The decomposition temperature of PdO varies with the oxygen pressure and the catalyst supports.

Until now, there is no general agreement on which state of palladium is more active for methane oxidation at high temperature conditions. Lyubovsky *et al.* [19] observed that Pd/α-Al_2O_3 after hydrogen reduction was more active than oxidized Pd/α-Al_2O_3 for methane oxidation. They also observed that the catalyst under stoichiometric mixture or fuel rich mixture was more active than the catalyst under fuel lean mixture, and they

attributed the higher activity to the metallic Pd which existed under stoichiometic or fuel rich mixture. On the contrary, Burch *et al.* [46] and Farrauto *et al.* [36, 47] claimed that the metal phase was inactive for methane oxidation.

In summary, the kinetic data at temperatures around PdO decomposition point are very crucial for people to understand the unusual behaviors of the catalyst occurred at this temperature range [17, 35, 36] due to PdO decomposition and reformation, but no systemic study was available. This study was to obtain the kinetic results in wide temperature range and two different phases, and then compare the catalytic activity of PdO and Pd metal. A model system was employed in this research to obtain the kinetic data. The advantages of this system are that catalyst can be easily examined by surface analytical techniques and yet reactions can be carried out at the conditions described in the literature for supported catalysts. The catalysts used in this study were non-porous solid palladium foil, which are free of internal mass and heat transfer limitation. The results obtained on the foil catalysts agree well with the kinetic results reported in the literature.

3.2 Experimental methods

The experiment system includes a high-pressure reactor cell and ultrahigh vacuum (UHV) surface analysis chamber. The reactor cell can be operated as continuous-stirred tank reactor (CSTR) and batch reactor. At temperature above 700 K, experiments were performed in CSTR mode to avoid total conversion of methane because of the high reaction rate; at temperature below 700 K, experiments were performed in batch mode so that CO_2 could accumulate inside the reactor to the level which the GC detector could

precisely monitor. Gas circulation pumps (Metal Bellows, MB-21) were employed to speed up reactants flow rate to avoid mass transfer limitation. The maximum flow rate was 4600 cc min^{-1}. The ultrahigh vacuum chamber was equipped with AES, XPS, mass spectrometer and sputtering gun for surface analysis and cleaning. Catalyst could be transferred between the reactor cell and the UHV chamber without exposing to air. Details about this system were described in previous paper[10].

The palladium catalysts were 0.1 mm thickness polycrystalline foil with surface area about 0.5 cm^2 (Alfa Aesar, 99.9%). It was spot-welded on the power pins so that electric current can go through to achieve resistive heating. Thermocouple wires were spot-welded on the back of the foil for temperature reading. Sample temperature was automatically controlled by interfacing a temperature controller (Euortherm Model 2408) with a TCR power supply (Electronic Measurements Inc). An infrared lamp was mounted outside the reactor facing the viewport on the reactor. Infrared light generated by the lamp could go through the viewport and be focused on the palladium foil. The sample was heated by both methods at the same time during the experiment. The clean procedures include running methane oxidation at 773 K and 873 K for 100 minutes respectively with reactants mixture of 4.5 Torr CH_4, 18 Torr O_2 and inert gases (He and N_2) balanced to atmospheric pressure, annealing at 873 K for 1 minute in vacuum, and sputtering with 2.0 keV Ar^+. Surface was regarded clean when no sulfur-, phosphorus- and silicon- species were detected by XPS. Before each independent experiment, the sample was sputtered by 2.0 keV Ar^+ and then annealed at 873 K for 1 minute.

The reaction temperature must be raised above PdO decomposition temperature to study the reaction mechanism of methane oxidation on palladium metal. The oxygen pressure reported in most publications was higher than 30 Torr (4% if the total pressure is 1 atm), which corresponds to PdO decomposition temperature higher than 1007 K [7]. Such kind of high temperature put a lot of stress on the equipment, especially when oxygen existed. In this study, the oxygen pressure was lowered to less than 3 Torr so that the metal phase could be obtained at a temperature lower than 930 K.

Except notation, turnover rate was calculated using the geometric Pd metal surface area assuming an average Pd surface atom density for a polycrystalline foil of $1.27*10^{15}$ atoms cm^{-2}[48]. The surface should not change or change slightly with the variation of temperature for activation energy measurement or with the variation of reactant concentration for reaction order measurement. Thus, using the geometric Pd metal surface area was feasible to measure the reaction orders and activation energies.

The real PdO surface area was measured by a surface exchange experiment with labeled oxygen (^{18}O isotope), which was done by exposing the oxidized foil to 5 Torr $^{18}O_2$ at 598 K for 12 seconds. These conditions were designed based on the results from Au-Yeung *et al.* [49] and ensured the exchange between ^{16}O in PdO and $^{18}O_2$ isotope mostly occur at the surface, without appreciable diffusion into the bulk. The reference point for oxygen coverage was made by assuming that a foil exposed to O_2 at room temperature will form an oxygen layer with 0.25 ML coverage at saturation. Since this coverage was well established for a Pd(111) single crystal [50, 51] and a foil is composed of mostly (111) planes, the reference point is reasonable. The exchange was proved to be an effective

method to measure PdO surface area [10, 52]. The surface area of the metal phase under reaction conditions was assumed to be the same as the surface area for clean Pd foil.

3.3 Results

3.3.1 System Test

A stainless steel foil with same size as palladium foil was used to test background activity of the catalytic reactor. The turnover rate was less than 0.15 s^{-1} on the stainless steel under conditions of 6 Torr O_2, 1.5 Torr CH_4, and at 1023 K, compared with the turnover rate of 9.3 s^{-1} on Pd foil. Therefore, the contribution from background activity of the catalytic reactor was less than 2%.

To obtain kinetic data, the experiment must be free of mass and heat transfer limitations. The palladium foil was non-porous solid metal, so there was no internal mass and heating transfer limitations. The temperature of the foil was automatically controlled by a temperature controller, which enabled the reaction free of external heat transfer limitation inherently. Thus, the only concern was external mass transfer limitation. Figure 3-1 shows the methane conversion as a function of gas circulation rate. Under the test conditions, methane conversion did not increase any more when circulation rate was raised to above 3800 cc min^{-1}. Therefore, when circulation rate was higher than 3800 cc min^{-1}, the reaction was free of external mass transfer limitation. The circulation rate was higher than 3800 cc min^{-1} during experiment, so no mass transfer limitation was involved in the experiment results.

3.3.2 Reaction Orders and Activation Energy

Table 3-1 summarizes the reaction orders and the activation energies obtained in this study under different conditions. The reaction order for CO_2, which is -2 when the concentration of CO_2 is higher than the concentration of H_2O [8], was not measured since the conditions of this work were outside the range where CO_2 could inhibit reaction. Reaction orders for CH_4, O_2, and H_2O were measured at 863 K and 973 K in fuel lean conditions (Figure 3-2 & Figure 3-3). To measure the reaction order for CH_4, for example, excess O_2 and H_2O were added into the gas mixture so that the change of reaction rate solely reflects the change of CH_4 concentration. Note that the thermodynamically stable phase was PdO at 863 K and Pd metal at 973 K. The reaction order for water was also measured at 813 K, and was 0.0 (Figure 3-4). Activation energy was 32 kJ mol^{-1} on PdO at 783-873 K and 125 kJ mol^{-1} on Pd metal at 933 K-1003 K (Figure 3-5).

3.3.3 Characterization

The chemical state of the foil surface was examined before and after reaction by X-ray photoelectron spectroscopy (XPS). The metallic Pd was characterized by the Pd $3d_{5/2}$ peak at 335.0 eV (Figure 3-5), which is in good agreement with the one in the literature [53]. Palladium oxide was observed on the foil surface after measuring the reaction orders at 863 K and activation energy at temperatures between 783-873 K. An example of XPS Pd_{3d} core level was shown in Figure 3-6 after reaction at 863 K with 0.76 Torr O_2, 0.15 Torr CH_4 and inert gases balanced to atmospheric pressure, and the binding

energy of Pd $3d_{5/2}$ was 336.85 eV, characteristic of PdO [53]. The Pd $3d_{5/2}$ peak obtained after methane oxidation did not show broadening comparing with the Pd $3d_{5/2}$ peak obtained on clean metal foil, indicating the major compound on the foil surface was PdO. If Pd metal were also present, metal Pd $3d_{5/2}$ peak at lower binding energy (335.0 eV) would have overlapped with the oxide Pd $3d_{5/2}$ peak and made it broader. When studying the reaction orders at 973 K and the activation energy at temperature between 933-1003 K, only metallic palladium was observed on the foil surface. An example of XPS Pd_{3d} core level was shown in Figure 3-6 after reaction at 903 K with 0.76 Torr O_2, 0.15 Torr CH_4 and inert gases balanced to atmospheric pressure, and the binding energy of $Pd3d_{5/2}$ was 335.0 eV.

The equilibrium oxygen pressure with temperature for PdO decomposition is [7]:

$$\log P = 31.905 - 6.29 \log T - \frac{14{,}510}{T} \pm 0.006$$

Where

P: O_2 pressure (atm)

T: temperature (K)

Calculations based on the above equation confirmed the XPS results.

3.3.4 Active Phase

In this study, the kinetic data including turnover rates, reaction orders and activation energies were obtained both on palladium oxide and palladium metal at temperatures around the PdO decomposition temperature. The turnover rate at PdO decomposition temperature (T_d) under certain O_2 pressure (P_d) could be calculated from the kinetic data (activation energy and turnover rate) on PdO or Pd metal as following:

$$TOR_{T_d} = TOR_T e^{-\frac{E_a}{R}(\frac{1}{T_d}-\frac{1}{T})}$$

Where T_d is the decomposition temperature (K)

T is the temperature to collect turnover rate (K)

Ea is the activation energy at temperature T (J mol^{-1})

R is universal gas constant (J mol^{-1} K^{-1})

Figure 3-7 shows the turnover rates on both palladium oxide and palladium metal at temperatures around the PdO decomposition temperature (888 K). The turnover rates on PdO were measured with 1.5 Torr O_2 and 0.30 Torr CH_4, while the turnover rates on Pd metal were measured with 2.3 Torr O_2 and 0.46 Torr CH_4. The methane oxidation rate was lower on Pd metal than on the oxide, thus higher methane pressure was used for experiment on metal phase to get reasonable concentration of CO_2 which GC can quantify. The O_2 pressure was also raised to keep the ratio of O_2 to CH_4 the same as on the oxide phase. Finally, all the turnover rates were corrected to 0.76 Torr O_2 and 0.15 Torr CH_4 using reaction order of 1 for CH_4, 0 for O_2 and H_2O. The surface area of PdO

corresponding to the reaction conditions of 1.5 Torr O_2, 0.3 Torr CH_4 at 843 K was 8.3 cm^2, based on 1 cm^2 geometric area of clean foil. With 0.76 Torr O_2, PdO decomposes to Pd metal at 888 K [7]. By extrapolating the data in Figure 3-7 to 888 K, turnover rates were found to be 1.9 s^{-1} on PdO and 0.10 s^{-1} on Pd metal at 888 K. The decrease of turnover rate from 1.9 s^{-1} to 0.10 s^{-1} when PdO decomposes to Pd shows that PdO is more active for methane oxidation than Pd metal at 888 K.

3.4 Discussion

The experiments in batch mode were carried out at 598 K with 160 torr O_2, 16 Torr CH_4 and N_2 balanced to 800 Torr. The turnover rate was 3.8 s^{-1} calculated at 598K, 160 Torr O_2, 16 Torr CH_4, 1 Torr H_2O. Comparison of turnover rates with literature reports was summarized in Table 3-2. The turnover rate in this study is close to the turnover rate obtained in our laboratory in former report [10], and is among the highest for all the palladium catalysts reported.

Monteiro *et al.* [10] observed that the surface area was two times the geometric area of palladium metal foil after reaction at 598 K with 160 Torr O_2, 16 Torr CH_4 and N_2 balanced to 800 Torr. In this study, the surface area was 8.3 times the geometric area of palladium metal foil after reaction at 843 K with 1.5 Torr O_2, 0.3 Torr CH_4 and inert gases balanced to atmospheric pressure. The surface area after treatment at 843 K was larger than the surface area after treatment at 598 K even though the O_2 pressure was much lower during treatment at 843 K, which indicates that high temperature was one of the driven forces for the surface area increase.

Table 3-1 summarizes the reaction orders at different temperatures. The reaction order was 0.6-0.7 for methane and around zero for oxygen at 598-973 K. Water inhibition effect was weaker at higher temperatures.

$CH_4 + * \leftrightarrows CH_4*$ (1)

$CH_4* + O \rightarrow \ldots.$ (rds) (2)

$H_2O + * \leftrightarrows H_2O*$ (3)

A reaction mechanism was proposed to explain the kinetic results. In this mechanism, methane is proposed to interact with lattice oxygen to break the initial C-H bond (step 2), which is regarded as the rate-determining step. Combustion of CH_4 and CD_4 gave a normal isotope effect ($k_H/k_D>1$, k is the reaction rate constant), suggesting that the rate-determining steps in the catalytic sequence involve H-atoms [54]. The rate of H-D exchange for the gas mixture of $CH_4/CD_4/O_2$ was found only 1/10 of the combustion rate at 573 K [54], indicating that the C-H bond activation could be treated as irreversible step. Isotopic studies showed that during methane oxidation, part of the O in products came from original O stored in PdO bulk [54-56]. While the other part of O came from gas phase O_2, it is not known whether gas phase O_2 transformed to lattice O before it was consumed by methane combustion. Therefore, at least part of the O (if not all) in the products came from lattice O. Oxygen scrambling was observed when $^{16}O_2/^{18}O_2$ mixture contacted with $Pd^{16}O/ZrO_2$ catalyst at 575 K without methane oxidation, but was not observed when methane oxidation was running at the same time [54]. This difference indicates that either the reaction consumed most of the adsorbed oxygen or the oxide

surface was blocked by other species during the reaction. Ciuparu *et al.* [57] observed water inhibition of the oxygen exchange between gas phase and PdO surface at 700 K, indicating that the slower exchange could be attributed to water blocking exchange sites (step 3). The most abundant surface intermediate (MASI) in the mechanism is assigned to H_2O* by considering its inhibition to the reaction. The positive reaction order of CH_4 and zero reaction order of CO_2 indicate that neither CH_4* nor CO_2* could be the MASI.

A pseudo-steady state treatment of the reaction mechanism proposed above gives rate expressed as:

$$r = k_2 K_1 \frac{[CH_4]L}{K_3[H_2O]+1}[O] \quad \text{(I)}$$

Where L is the concentration of active sites, $[H_2O^*]+[*]=L$

The concentration of O can be treated as constant (C) considering the lattice oxygen could be filled quickly. Step 4 should be exothermic reaction from left to right as it is water chemisorption; therefore, the equilibrium constant K_3 was greater at lower temperatures. At 598 K when water has inhibition effect on the reaction, the rate expression could be simplified to the following expression, which shows a reaction order of 1 for CH_4 and –1 reaction order for H_2O.

$$r = \frac{k_2 K_1}{K_3} CL \frac{[CH_4]}{[H_2O]} \quad \text{(II)}$$

As the temperature increases, K_3 became smaller and the expression (I) could be simplified to:

$$r = k_2 K_1 CL[CH_4] \qquad \text{(III)}$$

An abrupt decrease of activation energy on PdO was observed from 75-95 kJ mol^{-1} to 24-45 kJ mol^{-1} as the temperature increased, and the transition temperatures were in the range of 650-720 K [11, 21]. Those reports agree with the value of 32 kJ mol^{-1} obtained at temperatures between 783-873 K in this study. The apparent activation energy for equation (II) is $\Delta H_1+Ea_2-\Delta H_3$, while the apparent activation energy for equation (III) is ΔH_1+Ea_2. As ΔH_3 is negative, the activation energy should be higher at low temperature when water has inhibition effect.

As Pd metal became the thermodynamic stable phase, the surface species should be different from the surface species on PdO. Since most information on palladium for gas-surface interactions were reported on single crystals, here we will discuss the cases on Pd single crystals and then make comparable judgment on Pd foil. For heat of O_2 adsorption on Pd(110), Ertl *et al.* [58] reported 80 kcal mol^{-1} when the coverage reached some point where LEED image gave (1x3) pattern; 77 kcal mol^{-1} for (1x2) pattern; 62 kcal mol^{-1} for c(2x4) pattern and 48 kcal mol^{-1} for c(2x6) pattern. The heat of adsorption was obtained using Clausius-Clapeyron equation assuming a LEED pattern corresponds to same saturated oxygen coverage at different temperatures. Saturated coverage of 0.23 ML was reported for the (1x3) LEED pattern [59] and 0.48-0.5 ML was reported for c(2x4) LEED pattern [59, 60]. Jo *et al.* [61] believed that the (1x3) and (1x2) LEED patterns observed

by Ertl *et al.* [58] correspond to the streaky pattern they observed. Tanaka *et al.* [62] obtained a coverage of 0.2 ML for the (2x3)-1D pattern and a coverage of 0.3 ML for the streaky pattern. For Ni(110), which has the same crystal structure and the same surface atom orientation as Pd(110), coverage of 0.33-0.35 ML was reported for the (2x1) LEED pattern [63, 64]. Considering the same LEED pattern corresponds to same saturated overage of oxygen as long as the single crystals are in the structure and have same surface orientation, we think that the streaky LEED pattern reported on Pd(110) might be the (1x2) pattern Ertl *et al.* [58] observed. Thus, the coverage of 0.3 ML could be used for (1x2) LEED pattern. The c(2x6) LEED pattern was observed in our lab with the coverage in the range of 0.6-0.7 ML. On Rh(110), the oxygen coverage for the structure of c(2x2n) (n=3, 4 and 5) was proposed to be (n-1)/n [65], which agrees well with experimental results. Considering Rh(110) and Pd(110) have same crystal structure and surface orientation, the c(2x6) on Pd(110) should correspond to an oxygen coverage of 0.67 ML. In summary, the heat of adsorption at corresponding coverage is 80 kcal mol^{-1} at 0.23 ML, 77 kcal mol^{-1} at 0.30 ML, 62 kcal mol^{-1} at 0.50 ML and 48 kcal mol^{-1} at 0.67 ML. With the heat of adsorption, the equilibrium pressures at our experiment temperature (973 K) with oxygen coverage of 0.23 ML, 0.30 ML, 0.50 ML and 0.67 ML could be obtained using Clausius-Clapeyron equation. Then, the equilibrium oxygen pressure for 1 ML coverage at 973 K was found to be 0.8 Torr by empirical equation of Freundlich. Thus, from thermodynamic point of view, the surface of Pd(110) should be mostly covered by adsorbed oxygen at 973 K when exposing to 2.3 Torr O_2.

One concern is whether the oxygen adsorption rate could surpass methane adsorption rate under reaction conditions so that thermodynamically favored situation mentioned above could be reached. At temperatures between 273 K and 673 K, the sticking probability of oxygen on Pd(110) was about 1 at zero coverage of oxygen, and decreased to 0.1 at coverage about 0.5 ML [66]. The sticking probability of oxygen at 973 K with coverage less than 0.5 ML was found greater than 0.1 by extrapolating the sticking probability at lower temperatures. The initial sticking probability of methane on Pd(110) was found to increase exponentially with the average translational energy of methane which was calculated as:

$$E = \frac{m_h}{\overline{M}} \overline{C}_p T_g$$

Where m_h is the molecular mass of heavy species, $\overline{C}_p$ is the average heat capacity of the gas mixture, and $\overline{M}$ is the average molecular mass of the gas mixture[67, 68]. Meanwhile, The initial sticking probability was also found to increase strongly with methane molecule vibrational energy, but increase weakly with solid phase temperature [67-69]. When the turnover rate was measured in this study at 973 K, gas phase temperature could not be precisely determined but was estimated in the range between 600 K and 973 K. The average translational energy was then between 22 kJ mol^{-1} and 31 kJ mol^{-1} based on the fact that N_2 was the majority composition of gas mixture (>90 vol%) and also the heavy species. The sticking probability of methane on Pd(110) with zero coverage of oxygen was, therefore, in the range of $3*10^{-4}$ to $3*10^{-3}$ assuming it did not change with solid phase temperature. The sticking probability of methane on Pd(110) decreased linearly with oxygen coverage [68]:

$$S_{tot}(\theta_0) = S_{0,tot}(1 - \alpha\theta_0)$$

Where α has value about 2.3

S_{tot} is the sticking probability of methane at oxygen coverage of θ_0

$S_{0,tot}$ is the sticking probability of methane at oxygen coverage of 0

Based on these facts, the sticking probability of oxygen should be at least two orders of magnitude higher than the sticking probability of methane even with 0.5 ML oxygen coverage. Though the sticking probability of oxygen continuously decreases as the coverage increases, the large difference between the sticking probability of oxygen and methane indicate that oxygen adsorption rate should still surpass methane adsorption rate at higher oxygen coverage. Thus, the Pd(110) surface should be mostly covered by adsorbed oxygen under reaction conditions, from both thermodynamic and kinetic point of view.

The turnover rates on Pd(110) and Pd foil are very close at 973 K with 2.3 Torr O_2 and 0.46 Torr CH_4 [70], indicating that the surface of Pd foil under reaction conditions should be similar as the surface of Pd(110) which was mostly covered by oxygen. This conclusion is also reasonable considering the zero reaction order for oxygen on the Pd foil. If surface was mostly covered by other species, the reaction order for oxygen should be positive.

Experimental data in this study show that under steady operation the active phase should be temperature specific. At 888 K, turnover rate dropped from 1.9 s^{-1} to 0.1 s^{-1} under

0.76 Torr O_2 and 0.15 Torr CH_4 when PdO decomposed to Pd metal, indicating that PdO was more active than Pd metal for methane oxidation at this temperature. The two lines in Figure 3-7 intercept at 1160 K, suggesting that the turnover rate on PdO is the same as on Pd metal at 1160 K. At temperature below 1160 K, PdO is more active than Pd metal for methane oxidation; but at temperature above 1160 K, Pd metal is more active than PdO. McCarty [35] studied methane combustion on Pd/γ-Al_2O_3 with same methane pressure but different oxygen pressures and found that methane conversion dropped 60% when PdO decompose to Pd at 930 K, while no conversion drop when decomposition occurred at temperature above 1100 K, indicating the turnover rate on Pd metal surpassed PdO at temperature above 1100 K. This result is very close to our projection.

Lyubovsky *et al.* [19] observed a methane conversion increase when the oxygen pressure in the reaction mixture was reduced below the equilibrium and PdO decomposed. In their experiment when PdO decomposed to Pd, the oxygen pressure was reduced to the level that the ratio of O_2 to CH_4 was close to stoichiometric ratio or even under fuel rich conditions. The catalyst was reported to have a much higher activity in fuel rich conditions even when PdO was still in the stable phase [52], thus the activity improvement reported could be the result of changing O_2 to CH_4 ratio instead of PdO decomposition.

3.5 Conclusion

The reaction mechanism changed with temperature and palladium chemical states. The reaction orders for CH_4, O_2 and H_2O were 0.7, 0.2, 0.0 at 598 K, 0.6, 0.0, -0.0 at 863 K, and 0.7, -0.1, -0.1 at 973 K. The surface compound was PdO at 598 K [10] and 863 K,

and Pd metal at 973 K. The activation energy was 125 kJ mol^{-1} in the temperature range 568-628 K [10], 32 kJ mol^{-1} in 783-873 K and 125 kJ mol^{-1} in 933-1003 K. Note that the thermodynamically stable phase was PdO for the first two temperature regions and Pd for the last temperature region. A reaction mechanism was proposed to explain the kinetic data. In this mechanism, dissociative methane adsorption occurs on PdOx sites; the initial C-H bond breaking is achieved by methane interacting with lattice oxygen, which is the rate-determining step; water adsorbs on the active sites to block methane adsorption. The change of activation energy was caused possibly by the diminishing of water inhibition effect and the change of chemical properties of active sites. Surface area of PdO was measured by $^{18}O_2$ exchange, and the surface area of Pd metal was calculated based on atom density on the Pd foil of 1.27×10^{19} m^{-2}.

The active phase, PdO or Pd metal, is temperature dependent. At 888 K with 0.76 Torr O_2 and 0.15 Torr CH_4, the turnover rate decreased from 1.9 s^{-1} to 0.1 s^{-1} when PdO decomposed to Pd metal, suggesting that the active phase was PdO at 888 K.

Table 3-1: Comparison of reaction orders and activation energy at different temperatures and chemical states of the catalysts

Temperature	Reaction order			Activation Energy	Oxidation	Reference
K	CH_4	H_2O	O_2	(kJ mol^{-1})	state of foil	
598	0.7	-0.9	0.2	125	PdO	[10]
863	0.6	0	0	32	PdO	This work
973	0.7	-0.1	-0.1	125	Pd	This work

Table 3-2: Comparison of Turnover Rates on Palladium Catalysts

Catalyst	Activation Energy[a]		TOR[b] (s^{-1})	Reference
	Value ($kJ\ mol^{-1}$)	Measure Range (K)		
Pd foil	-	-	3.8	This work
Pd foil	125	570-630	5.3	[10]
Pd/Si-Al_2O_3	170-184	500-640	0.1[e]	[8]
Pd/Al_2O_3	150	500-640	0.07-0.16[e]	[8]
Pd/ZrO_2	170	500-640	0.1-0.7[e]	[8]
Pd/ZrO_2	185	-	0.5-3.0[e]	[43]
Pd/ZrO2	N/A	-	0.3[e]	[45, 71]

[a] Assuming reaction order for water is –1, the activation energy was corrected for the water inhibition effect.

[b]TOR calculated at 598 K, 16 Torr CH_4, 1 Torr H_2O, and N_2 balanced to 800 Torr. Reaction orders were assumed to be 1 for CH_4, 0 for O_2 and –1 for H_2O

[c]Surface area measured from $^{18}O_2$ exchange

[d]Number of sites measured from BET surface area (47 m^2g^{-1})

[e] For plug flow reactor, partial pressures for reactants and products are the average of values of inlet and exit concentration

Figure Captions:

Figure 3-1 Methane conversion as a function of reactants circulation rate at 863 K with 1.5 Torr O2, 0.38 Torr CH4 and inert gases balanced to atmospheric pressure

Figure 3-2 Reaction order dependence for Pd foil at 863 K on CH_4 (0.15-0.27 Torr CH_4, 0.76 Torr O_2, N_2 and He balanced to atmospheric pressure), O_2 (0.76-1.54 Torr O_2, 0.15 Torr CH_4, N_2 and He balanced to atmospheric pressure), and H_2O (0-1.5 Torr H_2O, 0.15 Torr CH_4, 0.76 Torr O_2, N_2 and He balanced to atmospheric pressure)

Figure 3-3 Reaction order dependence for Pd foil at 973 K on CH_4 (0.30-0.93 Torr CH_4, 2.28 Torr O_2, N_2 and He balanced to atmospheric pressure), O_2 (2.28-4.56 Torr O_2, 0.44 Torr CH_4, N_2 and He balanced to atmospheric pressure), and H_2O (0-0.7 Torr H_2O, 0.44 Torr CH_4, 2.28 Torr O_2, N_2 and He balanced to atmospheric pressure)

Figure 3-4 Reaction order dependence for Pd foil at 813 K on H_2O (0-1 Torr H_2O, 0.30 Torr CH_4, 1.52 Torr O_2, N_2 and He balanced to atmospheric pressure).

Figure 3-5 Arrhenius plot for the combustion of methane over Pd foil (solid circle: 1.5 Torr O_2, 0.3 Torr CH_4 and inert gases (N_2, He) balanced to atmospheric pressure; open circle: 2.3 Torr O_2, 0.46 Torr CH_4, 0.66 Torr H_2O and inert gases (N_2, He) balanced to atmospheric pressure).

Figure 3-6 Comparison of XPS Pd3d core level scan of clean metal foil, foil after lean reaction at 903 K and 863 K with 0.76 Torr O_2, 0.15 Torr CH_4 and inert gases (N2 and He) balanced to atmospheric pressure.

Figure 3-7 Prediction of Turnover Rates on Palladium Oxide and Palladium Metal with 0.76 Torr O_2 and 0.15 Torr CH_4

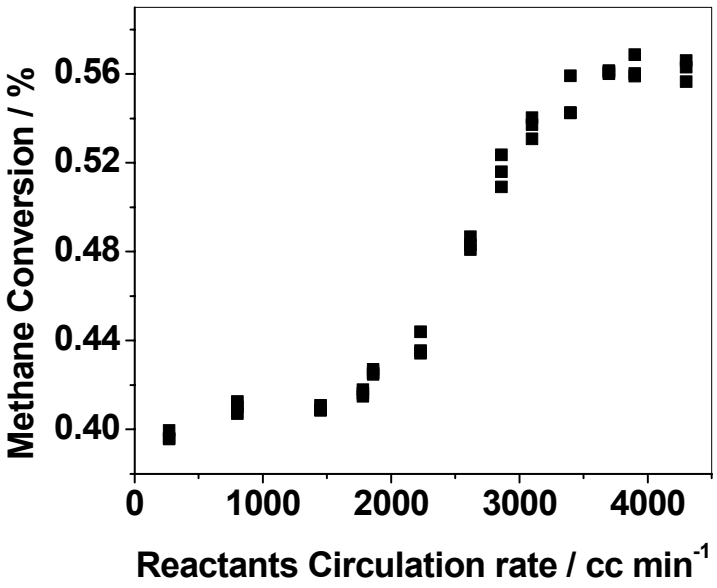

Figure 3-1 Methane conversion as a function of reactants circulation rate at 863 K with 1.5 Torr O_2, 0.38 Torr CH_4 and inert gases balanced to atmospheric pressure

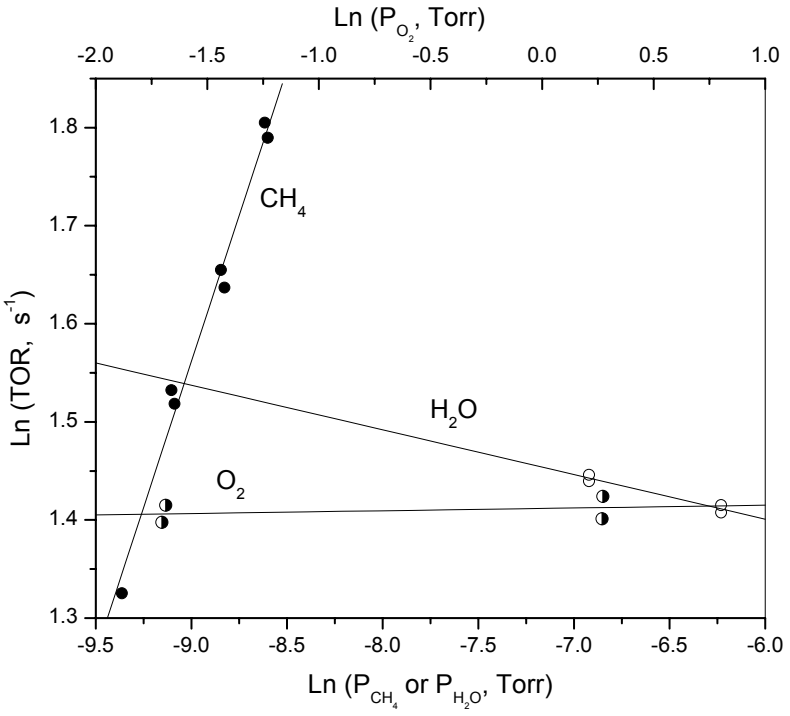

Figure 3-2 Reaction order dependence for Pd foil at 863 K on CH_4 (0.15-0.27 Torr CH_4, 0.76 Torr O_2, N_2 and He balanced to atmospheric pressure), O_2 (0.76-1.54 Torr O_2, 0.15 Torr CH_4, N_2 and He balanced to atmospheric pressure), and H_2O (0-1.5 Torr H_2O, 0.15 Torr CH_4, 0.76 Torr O_2, N_2 and He balanced to atmospheric pressure)

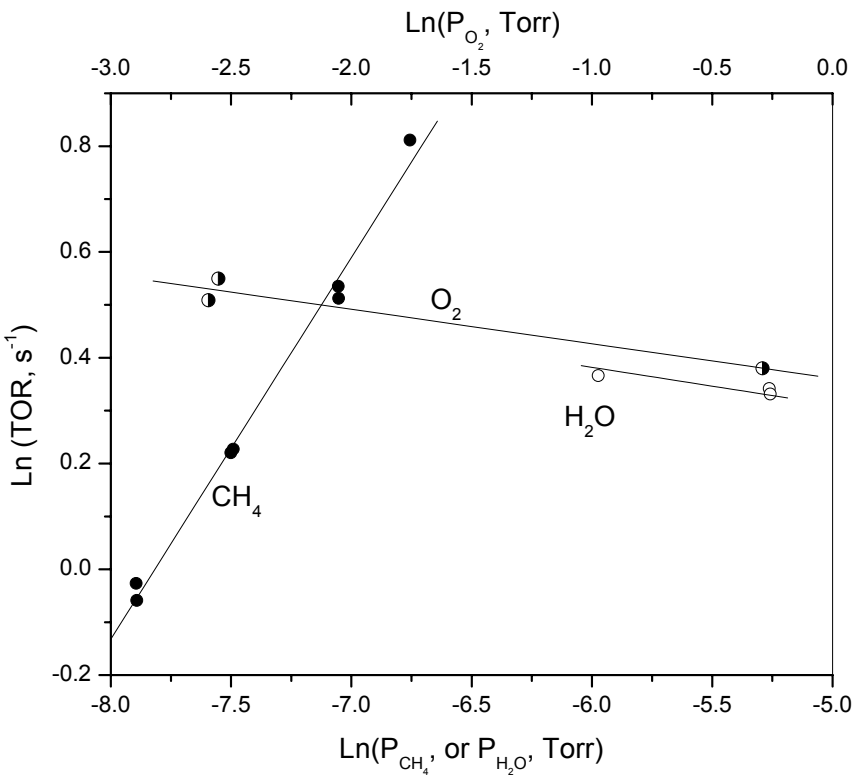

Figure 3-3 Reaction order dependence for Pd foil at 973 K on CH_4 (0.30-0.93 Torr CH_4, 2.28 Torr O_2, N_2 and He balanced to atmospheric pressure), O_2 (2.28-4.56 Torr O_2, 0.44 Torr CH_4, N_2 and He balanced to atmospheric pressure), and H_2O (0-0.7 Torr H_2O, 0.44 Torr CH_4, 2.28 Torr O_2, N_2 and He balanced to atmospheric pressure)

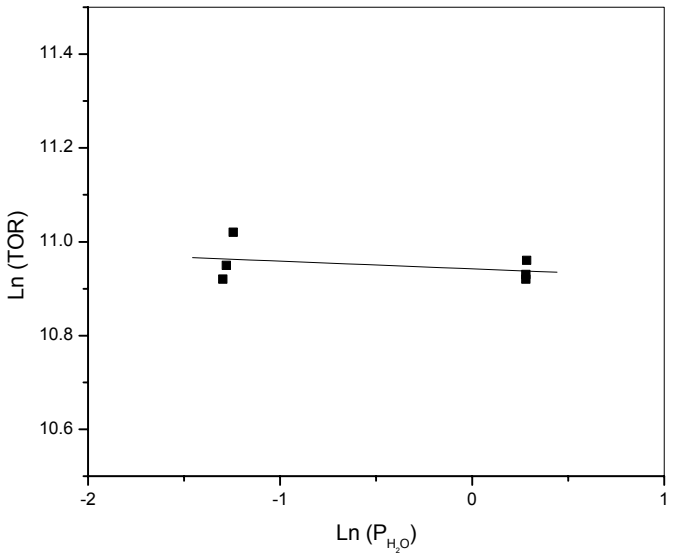

Figure 3-4 Reaction order dependence for Pd foil at 813 K on H_2O (0-1 Torr H_2O, 0.30 Torr CH_4, 1.52 Torr O_2, N_2 and He balanced to atmospheric pressure).

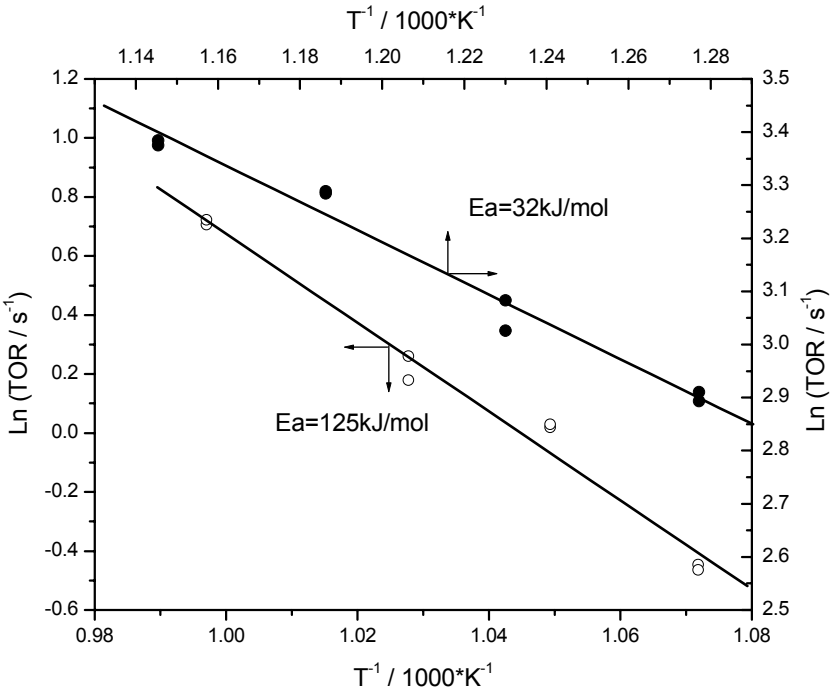

Figure 3-5 Arrhenius plot for the combustion of methane over Pd foil (solid circle: 1.5 Torr O_2, 0.3 Torr CH_4 and inert gases (N_2, He) balanced to atmospheric pressure; open circle: 2.3 Torr O_2, 0.46 Torr CH_4, 0.66 Torr H_2O and inert gases (N_2, He) balanced to atmospheric pressure).

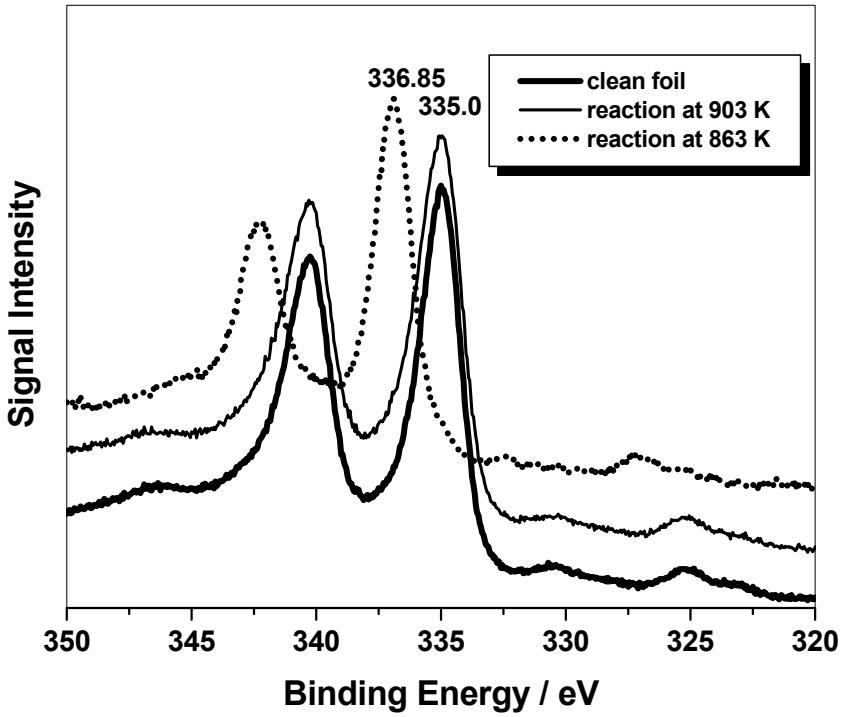

Figure 3-6 Comparison of XPS Pd3d core level scan of clean metal foil, foil after lean reaction at 903 K and 863 K with 0.76 Torr O_2, 0.15 Torr CH_4 and inert gases (N2 and He) balanced to atmospheric pressure.

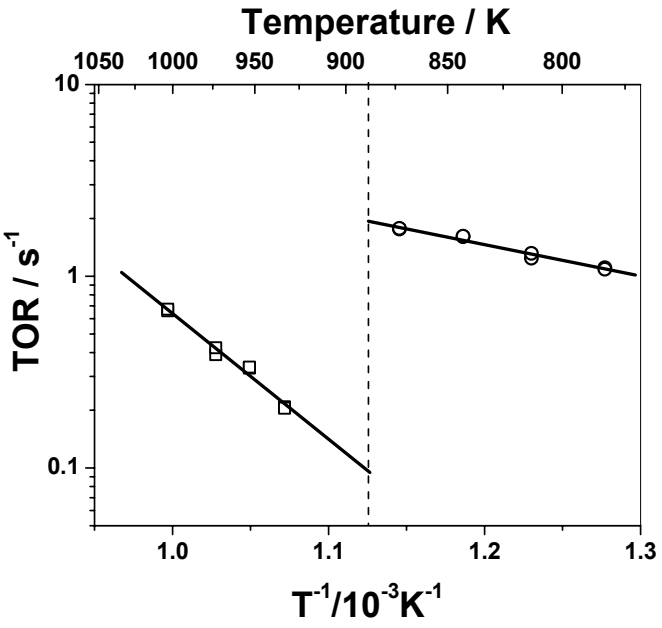

Figure 3-7 Prediction of Turnover Rates on Palladium Oxide and Palladium Metal with 0.76 Torr O_2 and 0.15 Torr CH_4

4 Coverage of Palladium Catalysts by Oxidized Silicon During Complete Oxidation of Methane*

*Contribution from Ken-ichiro Fujimoto (Nippon Steel Corp.) and Abhaya K. Datye (University of New Mexico) are acknowledged

Abstract

The interaction between silica and palladium following complete oxidation of methane or following reduction in H_2 was investigated on a polycrystalline palladium foil and on supported Pd/SiO_2 catalysts. During methane oxidation, oxidized silicon covered the palladium oxide surface as observed by TEM on Pd/SiO_2 catalysts and by XPS on palladium foil. On the Pd foil, the source of silica was a silicon impurity, common on bulk metal samples. The migration of oxidized silicon onto PdO deactivated the catalysts by blocking the active sites for methane oxidation. Silicon oxide overlayers were also observed covering the Pd surface after reduction of Pd/SiO_2 by H_2 at 923 K.

Key words: Complete methane oxidation on palladium; deactivation of Pd by silica; model catalysts

4.1 INTRODUCTION

Catalytic methane combustion is an environmentally benign process for power generation because of its potential to generate NOx emissions below 1 ppm; it can also be utilized to remove residual methane in the emission gases in vehicles powered by natural gas. The catalyst in methane combustion must be resistant to deactivation caused, for example, by interaction with the support and substrate materials and contaminants by air-borne dust [72]. Since palladium-based catalysts are the most effective catalysts for methane oxidation and silica (SiO_2) is a major component of air dust and a common contaminant in catalyst supports, it is of practical importance to understand the interaction between palladium and silica during catalytic methane oxidation. In addition, since silicon is a common impurity in Pd and it is difficult to analyze without surface science techniques, the results in the literature that use Pd as a foil or wire must be interpreted carefully.

The interactions between silica and the metal or metal oxide catalyst supported on silica and its effect on catalytic behavior have been reported before[25, 26, 73-81]. Reduction of Pd/SiO_2 in H_2 at a temperature above 723 K could form palladium silicides, such as Pd_2Si [73], Pd_3Si [74, 75], Pd_4Si[75], and the type of silicide formed is a function of reduction conditions. The interaction between Pd and silicide was responsible for the selectivity enhancement on the isomerization of neopentane[74]. Another example is the low temperature reduction of Pd/SiO_2 at 573 K by H_2, which created amorphous silica overlayers on the surface of palladium particles, presumably by silica migration[76]. Not only can H_2 facilitate the interaction between silica and metal or metal oxide, but also water. Silica migration was observed on iron oxide/silica model catalyst at 670 K upon

treatment in H_2O/CO or H_2O/H_2 gas mixture, but was not observed upon treatment in CO_2/CO or O_2[77]. After treating a silica-supported magnetite catalyst in a water-containing environment at 650 K and at near atmospheric pressure, the apparent turnover rate for water-gas shift was reduced by approximately one order of magnitude, although the capacity to chemisorb NO did not diminish significantly[78, 79]. Muto *et al*. [25, 26] tested Pd/SiO_2, Pd/Al_2O_3 and Pd/SiO_2-Al_2O_3 catalysts for methane oxidation. Their results showed that when the amount of silica on the surface of the support was enough to cover the entire surface of the catalyst, only deactivation was observed during reaction; otherwise, activation followed by deactivation was observed. Deactivation of silica supported cobalt catalyst was observed during Fischer-Tropsch synthesis. It was caused by a loss of active sites and BET surface area [80]. The deactivation increased with partial pressure of water. Cobalt-silicate formation and support breakdown, caused by the water produced during reaction, were proposed as the reasons for deactivation.

The objective of this contribution was to investigate the effect of silica on palladium catalysts during complete oxidation of methane and reduction in H_2. The investigations were carried out on model catalysts consisting of polycrystalline palladium foil and palladium supported on non-porous supports. The advantages of these catalysts are that they can be easily examined by surface sensitive techniques and by TEM [82], respectively. We conclude that silica poisons the catalyst by spreading and covering the surface of PdO in the presence of water at reaction temperature or H_2 reduction.

4.2 EXPERIMENTAL METHODS

4.2.1 Supported Model Catalysts

Two supported model catalysts, palladium supported on zirconia (Pd/ZrO_2) and palladium supported on silica (Pd/SiO_2), were studied for methane combustion. The silica support was prepared using the technique developed by Stoeber *et al.* [83]. By varying the reactant concentrations, monodisperse silica spheres were produced with average diameters between 100 and 500 nm. The material was non-porous and had a simple spherical geometry. The palladium was supported on the silica spheres by non-aqueous impregnations from Pd acetylacetonate (Aldrich) precursor followed by drying in air at room temperature. Palladium supported on zirconia was prepared by incipient wetness impregnation of zirconia (RC-100P, Daiichi Kigenso Kagaku Co., 16.5 m^2g^{-1}, air treatment at 1123 K, 10 hours) with $Pd(NH_3)_2(NO_2)_2/HNO_3$ solutions (Tanaka Kikinzoku Kogyo Co.) and then dried in air at 373 K for 24 hours.

The number of exposed Pd atoms was measured using H_2-O_2 titration after samples were reduced in H_2 (2-4 cm^3 H_2 $g^{-1}s^{-1}$) at 373 K for 1 h and evacuated at 373 K for 1 h to remove chemisorbed hydrogen. The uptake of O_2 during O_2 chemisorption and of H_2 during titration of chemisorbed oxygen by H_2 were measured at 373 K and 2.7-11 kPa H_2 or O_2. Monolayer values were obtained by extrapolating isotherms to zero pressure. The number of exposed Pd metal atoms was calculated using reported stoichiometries [84]:

$$Pd + \frac{1}{2}O_2 \rightarrow PdO \qquad (O_2 \text{ chemisorption})$$

$$PdO + \frac{3}{2}H_2 \rightarrow PdH + H_2O \qquad (\text{titration of adsorbed oxygen by } H_2)$$

Crystallite sizes were estimated from these dispersions by assuming hemispherical crystallites and a Pd surface density of 1.27×10^{19} m^{-2} [48].

The surface morphology of the supported model catalysts was examined by a Jeol 2000-FX transmission electron microscope. The reaction rate was measured in a tubular reactor with a thin layer of catalyst held above acid-washed quartz wool. This design achieved low methane conversion in a single pass, which made it possible to calculate the turnover rate by assuming a differential reactor behavior. The reaction was carried out at 553 K and at atmospheric pressure with reactants composition of 2% CH_4, 20% O_2 and 78% He.

4.2.2 Foil Catalyst

The palladium foil catalyst was a 0.125 mm thick polycrystalline foil (Goodfellow, 99.99+%) with a geometric area of ~1.0 cm^2. Methods to mount the catalyst were described previously [10].

Methane oxidation on palladium foil was performed in a batch reactor, which was attached to an ultrahigh vacuum (UHV) chamber equipped with surface analysis tools. Without exposure to the atmosphere, the foil could be transferred between the reactor and the UHV chamber by a welded bellows transfer arm. The batch reactor had a volume of

about 0.84 liters. Reactants were introduced into the reactor individually and were mixed by a pump (Metal Bellows model MB-21) at a nominal rate of 5000 cm^3 min^{-1} for 25 minutes before the reaction was started. The gas phase concentration was monitored by an Agilent 6890 Series gas chromatograph equipped with a 15-ft Carboxen 1000, 60/80 mesh column and a thermal conductivity detector (TCD). X-Ray Photoelectron Spectroscopy (XPS) and Temperature Programmed Desorption (TPD) were employed to characterize the foil surface. In the water treatment experiment, water was added by evaporation from the degassed liquid. Blank experiments on a stainless steel foil revealed that the turnover rate was negligible compared to the turnover rate on the palladium foil [10].

XPS spectra were collected using Al $K\alpha$ (1486.6 eV) radiation at 300W. The atomic sensitivity factor (ASF), used for surface composition calculation from XPS spectra, were 0.27 for Si 2s, 0.66 for O 1s and 4.6 for Pd 3d [85]. The relative atomic concentration for silicon was calculated by:

$$\text{Nominal atomic concentration of Si} = \frac{\frac{I_{Si2s}}{ASF_{Si2s}}}{\frac{I_{Si2s}}{ASF_{Si2s}} + \frac{I_{Pd3d}}{ASF_{Pd3d}} + \frac{I_{O1s}}{ASF_{O1s}}} \times 100\% \qquad (1)$$

where for example I_{Pd3d} is the signal intensity of Pd 3d.

The foil cleaning procedure consisted of sputtering with a 2 keV Ar ion beam, followed by annealing at 873 K for 1 minute under UHV conditions. For the clean foil, only metal palladium features were observed by XPS. Depth profiling of the deactivated foil consisted of cycles of sputtering with 500 eV Ar ions and XPS analysis.

Temperature-programmed-desorption was carried out in the UHV chamber by heating the foil from room temperature to 873 K at 3 K s^{-1}. Species desorbed from the surface were examined by an UTI-100C quadrupole mass spectrometer.

4.3 RESULTS

4.3.1 Surface Characterization Before Reaction

Supported Model Catalysts

Before reaction, each supported model catalyst was either reduced in H_2 at 923 K for 2 hours or oxidized in O_2 at 923 K for 2 hours. The specific surface area of treated catalysts is listed in Table 4-1. Oxidized Pd/ZrO_2 has 1.5 times the specific Pd surface area of the reduced Pd/ZrO_2; oxidized Pd/SiO_2 has 3 times the specific surface area of the reduced Pd/SiO_2. The turnover rate and the rate of reaction per gram of Pd after 24 h on stream are also shown in Table 4-1. The turnover rate for the sample supported on zirconia after reduction and oxidation is about the same, whereas the Pd catalyst supported on silica after reduction is less active in a factor of 15 than the sample after oxidation. This result shows a significant difference in rate between the samples supported on silica and zirconia, and for this reason, they were further investigated by TEM. Comparisons with rates from the literature are also presented in Table 4-1 [8, 10, 43].

The Pd samples supported on zirconia show the expected particle size and features after reduction (Figure 4-1) and oxidation (Figure 4-2). The same observation is true for the oxidized Pd/SiO_2 (Figure 4-3). However, on reduced Pd/SiO_2 sample amorphous overlayers covering the palladium particles were observed by TEM (Figure 4-4). The surface overlayers look amorphous, which is consistent with the migration of silica over the Pd metal surface. It is not possible to estimate the surface coverage of silica since TEM provides a 2-D image of a 3-D sample. Only the silica overlayer at the edge is visible. Since these are randomly oriented particles, one would expect the presence of silica on the top and bottom of the metal particle, which is not visible because the lattice image dominates the contrast. Based on the thickness of the layer, we can state that the coverage is less than one monolayer.

Pd foil

Before reaction, the palladium foil was cleaned as described above and then examined by XPS. Only features corresponding to palladium metal were observed with Pd 3d5/2 Binding Energy (BE) 334.50 eV. The minimal atomic concentration of Si that could be detected by XPS was 1%. The number of active sites during methane oxidation was calculated based on a Pd atom density of 1.27×10^{19} m^{-2} [48].

4.3.2 Surface Coverage by Silicon Compounds During Reaction

Supported Model Catalysts

All Pd/ZrO_2 catalysts showed activation and deactivation stages during reaction, independently of pre-reduction or pre-oxidation treatment (Figure 4-5). Activation and

deactivation stages were also observed for reduced Pd/SiO_2; however, only deactivation was observed for oxidized Pd/SiO_2 (Figure 4-6). After 24 hours on stream, the reduced catalysts generally had lower turnover rates than the oxidized ones. In particular, the turnover rate for the reduced Pd/SiO_2 was 1/15 of the one for oxidized Pd/SiO_2. Oxidized Pd/SiO_2 was examined by TEM after reaction and its image showed that the palladium particles were covered with an amorphous layer (Figure 4-7). This amorphous layer was less distinct than the one observed after reduction at 923 K (Figure 4-4).

Foil Catalyst

A batch reactor was used for measuring rates. Before the results are presented, we will explain how to interpret the data on this type of reactor when inhibition by one of the products is present. For lean fuel methane combustion at 598 K, the methane reaction rate can be expressed as

$$r=-k[CH_4]^1[O_2]^0[H_2O]^{-1}[CO_2]^0. \quad (2)$$

At low conversion, the methane concentration is almost constant and the rate expression can be simplified to $r=A/[H_2O]$, where A is a constant. Since the reaction rate was measured in a batch reactor, the water concentration can be related to the change of methane concentration

$$[H_2O]=2[CH_4]_0 \cdot \chi, \quad (3)$$

where $[CH_4]_0$ is the initial methane concentration and χ is methane conversion. The final expression can be written as

$$r = B/\chi, \tag{4}$$

where B is a constant. The reaction rate can also be expressed by methane consumption rate as

$$r = -V[CH_4]_0 \cdot \frac{d\chi}{dt} \tag{5}$$

where V is the reactor volume and t is reaction time. By combining the two rate expressions (4) and (5),

$$\frac{d\chi}{dt} = \frac{C}{\chi} \tag{6}$$

where C is a constant. After integration, a linear relation can be obtained between the square of conversion and time

$$\chi^2 = 2Ct. \tag{7}$$

Since a relation between methane conversion and number of methane turnovers can be expressed as

$$(\text{Number of Turnovers}) = D\chi, \tag{8}$$

where D is a constant, a linear relation can be obtained between square of Number of Turnovers and reaction time as

$$(\text{Number of Turnovers})^2 = Et, \tag{9a}$$

where

$$E = 2D^2C. \tag{9a}$$

Monteiro *et al.* [10] reported a linear relationship between $(\text{Number of Turnovers})^2$ and reaction time for palladium foil. In this study, the plot of $(\text{Number of Turnovers})^2$ to reaction time was used to monitor catalyst performance.

Figure 4-8 shows the plot of $(\text{Number of Turnovers})^2$ versus reaction time for a typical deactivation process. Since a stable foil produces a straight line, a change in slope indicates deactivation. On the deactivated foil, palladium, oxygen, silicon (Figure 4-9) and carbon were observed on the surface. Carbon on the was mainly deposited during transfer from the reactor to the UHV chamber [10]. For this reason, carbon was not considered during surface composition analysis. The binding energy of the $Pd3d_{5/2}$ at 336.3 eV was shifted by 1.8 eV from the position of metallic Pd (334.5 eV), indicating the surface was PdO. The Si 2s peak is quite broad and centered at 152.5 eV. According to the literature data, the Si 2s peak position for silicon is 150.5-150.7 eV [86-88] .

Therefore the 2 eV shift towards higher BE points to an oxidation state of silicon after the reaction. On the other hand, silica (SiO_2) is characterized by the Si 2s peak set at approximately 154.2-154.8 eV[89-92]. The factors, which cause the smaller BE shift, will be discussed below.

To understand how Si appeared on the surface, a series of experiments were carried out on the clean foil to investigate the effect of H_2O and O_2. The joint effect from H_2O and O_2 was tested by treating the clean foil at 598 K for 30 minutes with a gas mixture of 2 Torr H_2O, 638 Torr N_2 and 160 Torr O_2. XPS analysis on this foil showed features corresponding to Pd, O, Si and C. The rate of methane oxidation on the treated foil was tested at 598 K; no CO_2 was detected in 40 minutes, indicating that the foil was deactivated. After the methane oxidation experiment, the foil was transferred to the UHV chamber and annealed at 873 K for 1 minute. XPS analysis of the sample revealed O and Si (Figure 4-10), also metallic Pd on the surface. The nominal atomic concentration assuming a uniformly distributed concentration over the probing volume was 5.2% Si, 16.3% O and 78.5% Pd.

The O_2 effect on Si was tested by treating the clean foil with 160 Torr O_2 at 598 K for 1 hour. No Si was detected by XPS on the oxidized foil. XPS after TPD showed metallic Pd peaks, but did not show O Auger peaks and Si 2s peak (Figure 4-10).

The water effect on Si was tested by treating the clean foil with a gas mixture of 3 Torr H_2O and N_2 balanced to 800 Torr for 1 hour at either room temperature or 598 K. Silicon

was detected by XPS on the foil treated at 598 K, but was not detected on the one treated at room temperature.

The information depth of XPS is in the range of 50-100 Å, therefore additional experiments were performed to determine the depth profile of the Si distribution (Figure 4-11). The deactivated catalyst was sputtered by 0.5 kV Ar^+ beam with beam current passing through the sample of 0.24 μA. It can be seen that the signal intensity ratio of silicon to palladium (I_{Si}/I_{Pd}) decreased with sputtering time. A distribution of silicon on the sample based on this profile will be derived in the next section.

4.4 DISCUSSION

Deactivation by coverage with silicon oxides

Silicon and oxygen were observed on the surface of the deactivated foil after annealing at 873 K (Figure 4-10). The oxygen is associated with Si because PdO decomposes to Pd at the prevalent vacuum pressure. No oxygen signal is observed by XPS following annealing of a foil that did not show deactivation during reaction (Figure 4-10). Bader *et al.* [93] observed that thermal decomposition of PdO to 1173 K could not decompose the co-existing Si-stabilized oxide, so annealing at 873 K could leave Si-stabilized oxide on the foil surface. Two kinds of oxidized silicon, including silica (SiO_2) and silicon monoxide (SiO), could be the specie on the surface [94]. Solid SiO is a metastable state, thermodynamically stable only as a gas at high temperatures; it dissociates to Si and SiO_2 at 400-700^oC [94].

The BE of the Si 2s peak was 152.5 eV. This number is by approximately 2 eV higher than those for silicon[86-88] . On the other hand, this BE is lower by approximately 2 eV than the BE of the Si 2s peak (154.2-154.8 eV) characterized SiO_2 [89-92]. The relatively small chemical shift might be due to the "surface" nature of the silica. The silica layer covering the surface might consist of the silicon atoms bound to various number of oxygen atoms. Bekkay *et al* [95] reported non-stoichiometric oxide formation and the silicon atoms coordinated to one and to four oxygen atoms were characterized by the Si 2s peaks at 150.2 and 153.9 eV correspondently. In our case the Si 2s peak is broad and the state of Si could not be unambiguously identified because the signal to noise level on the Si 2s peak was low. The other factor, which might cause the relatively low BE of the Si 2s peak observed in our experiments, is the relaxation energy.

The variation of the relaxation energy is the final-state effect corresponding to a reorganization of the electrons of the neighboring atoms that provide the screening of the photoelectron hole remaining after electron emission. The effects of relaxation could cause a low BE shift whereas the effect of the initial states for a positive ionic state should result in a high BE shift. For instance, a large extra-atomic relaxation energy contribution for CdO reduces the binding energy [96]. Silver is another example of the exceptions, which show a low BE shift in the oxide states [96-99] . Therefore, the relatively low BE shift of the Si 2s peak, observed in our experiments, might be governed by the difference in the relaxation energy for a thin layer and a bulk material. Thus, we believe the silicon compound on the surface was silica.

Silicon and carbon were two impurities found on the surface of the deactivated foil. Previous work showed that the carbon deposition does not result in the catalyst deactivation [10], thus silica must be the compound deactivating the foil. One possible source of silica was the bulk of the foil. If the conditions are favorable, silicon compounds can migrate to the surface and then agglomerate to form large particles. Our hypothesis is that these large particles, with low concentration and small surface area to volume, generate a low intensity XPS signal that could not be detected on the clean foil. These particles are probably concentrated at grain boundaries. At reaction temperature (598 K) and with help from water formed during reaction, silicon from the large particles could oxidize, spread and cover the foil. The silica coverage in this case is high and XPS could detect it. The cleaning process could only remove thin layers of silica spreading on the surface, but could not eliminate the large particles that are the source of silica.

XPS depth profiling indicates that silica was on the top layer of the foil surface. By using Ar^+ with 500 eV ion energy, the sputtering yields for single-element solids are 0.5 Si atom per Ar^+ and 2 Pd atoms per Ar^+ [100]. If Pd was surface segregated compared to Si or the distribution of Pd and Si was homogeneous, then I_{Si}/I_{Pd} should have increased with time-on-sputtering because Pd has a higher sputtering yield. This hypothesis does not agree with the experimental results. The only reasonable element distribution to explain the data is that Si was surface segregated so that I_{Si}/I_{Pd} could drop from the beginning of sputtering even though Si has a lower sputtering yield than Pd.

Assuming silica spreading on top of PdO, the Si2s and Pd3d signal intensity could be expressed as a function of silica coverage using a mathematical model for photoelectron

attenuation during XPS analysis [101]. The coverage on the deactivated foil was obtained by fitting the signal intensities from the experiment to the mathematical model. The inelastic-mean-free-path was supplied by the National Institute of Standards and Technology [102]. The thickness of one monolayer of silica was estimated at 0.34 nm. It was calculated based on the parameters for quartz using the equation $1000\rho a^3 N=A$ where ρ is the quartz density (kg m^{-3}), "a" is the monolayer thickness we are estimating, N is the Avogadro number and A is the atomic weight. The XPS data was recorded with fixed emission angle of the photoelectron, which was between 0^o and 45^o with respect to the sample normal. In such cases, the coverage was found to be in the range of 0.8 to 1.0 monolayer.

Our experimental results showed that water and reaction temperature were the two key factors promoting silica migration, which was in agreement with previous work. Lund *et al.* [77] observed silica migration on Pt/SiO_2 at 660 K and on Fe_3O_4/SiO_2 at 670 K when water vapor was present. Huber *et al.* [80] attributed the loss of H_2 chemisorption capacity and BET surface area of Co/SiO_2 catalyst during Fischer-Tropsch at 220^oC (493 K) to silica migration and formation of cobalt-silicates.

Lund *et al.* [79] explained the migration of silica on Fe_3O_4 by Si^{4+} substitution into the tetrahedral sites of Fe_3O_4 and displacement of Fe^{3+} to adjacent octahedral sites, which occurred over the entire surface of Fe_3O_4, rather than being confined to the interface. The substituted Fe_3O_4 retained 80% capacity to adsorb NO but showed one order of magnitude lower turnover rate for water-gas shift reaction because there were still octahedrally coordinated iron cations on the surface that could adsorb NO but this

compound was not active for catalytic reaction. A similar explanation may be applicable to the Pd system. Another possibility for silica migration is that silica interacted with water to form a mobile compound that migrated to the palladium particle surface.

Silica migration was also observed by TEM on the supported Pd/SiO_2 samples after reduction and after reaction. Similar migration of titania on rhodium during reduction has been seen after high temperature reduction [103], and is believed to be the explanation for the phenomenon of strong metal support interaction. If the surface overlayers were caused by Pd oxide, they would not be amorphous since PdO is generally crystalline (Figure 4-2, Figure 4-3, and Figure 4-7). Hydrogen reduction of silica-supported palladium catalysts can also lead to strong chemical interaction between metal and support and the growth of palladium silicides [73-75]. If we use the rate per gram of Pd as an indication of the surface area of Pd available during reaction (Table 4-1), it can be concluded that silica coverage must be higher on the sample reduced in H_2 than on the sample oxidized in O_2 since the rate is 45 times lower on the former sample. The TEM results confirm the higher concentration of silica on the reduced sample; the amorphous layer is clearly visible on the reduced sample but is diffuse on the oxidized sample after reaction. Juszczyk and Karpinski [74] proposed that overlayers of oxidized silicon species on palladium were formed only when the catalyst was first reduced at high-temperature and then oxidized. During reduction, palladium silicides (Pd_xSi_y) were formed by palladium atoms taking oxygen vacancies in the silica support. When exposed to O_2 at room temperature, silicon in Pd_xSi_y was oxidized and then moved to the top of the surface; at the same time palladium atoms agglomerated and formed palladium particles, which were covered by silica.

Pd surface area and rates of reaction

The effects of oxidation and reduction on the surface area and reactivity of palladium catalysts has been studied [104]. In this study (Table 4-1), the higher surface area for the oxidized catalysts was caused probably by palladium surface roughening during O_2 oxidation although the TEM pictures presented here do not suggest a substantial difference in surface roughening between reduced and oxidized samples. Ruckenstein and Chen [105] suggested that a particle breakup, not observed by TEM in our experiments either, could be the explanation for higher surface area. Datye [82] suggested based on TEM results that the surface of Rh catalysts was roughened when the sample was oxidized in O_2 and then reduced in H_2 at a mild temperature. The roughening is caused by an expansion of the metal structure upon oxidation, a situation similar to the one we have here. Results from our group on a Pd foil [10] show that the surface of PdO surface increases by a factor of two after the combustion reaction. The increase in surface area by a factor of 1.5 for Pd/ZrO_2 after oxidation observed in our work is thus reasonable. Note also that for the samples supported on zirconia, the surface increase corresponded to a proportional increase in the rate per gram so that the turnover rate was constant. For the samples supported on silica, the decline in the chemisorption uptake by a factor of three after reduction seems to be affected by the coverage of Pd by silica. The decrease in chemisorptive properties (factor of 3) is much smaller than the decrease observed in the rate per gram (factor of 45) (Table 4-1). One explanation for this difference is that the overlayers of oxidized silicon formed during H_2 reduction might have moved during the surface area measurement by the H_2-O_2 titration procedure, causing a higher coverage. This is a feasible mechanism as the titration involves

oxidation and reduction steps at 373 K. In this case, more active sites could be counted by H_2-O_2 titration than could be available during reaction of methane oxidation. This over-counting translates into a lower turnover rate than the correct one and would explain why the turnover rate of reduced Pd/SiO_2 was 1/15 of that for oxidized Pd/SiO_2 after 24 hours on stream.

The rates of reaction for the foil and supported sample were in good agreement with the rates reported in the literature (Table 4-1). The general behavior of activation and deactivation are also the same as reported in the literature. For example, the zero rate of reaction at time zero for the pre-reduced samples observed in Figure 4-5 and Figure 4-6 have been observed before [9, 106]. In this study, activation followed by deactivation was observed on Pd/ZrO_2 samples. Literature results suggest, for example, that during the activation stage new surface morphologies that are more active in oxidizing methane are formed and that palladium oxide particles sinter during the deactivation stage [23-26, 42, 43, 107]. There was only deactivation observed on oxidized Pd/SiO_2, which was different from the other three catalysts tested and can probably be explained by silica migration. For oxidized Pd/SiO_2, silica started to spread once water was formed at the start of reaction. The initial activation caused possibly by a surface morphology change of PdO particle overlapped with deactivation by silica migration. The magnitude of deactivation was larger than the magnitude of activation, so deactivation, not activation, was observed at the first stage. Experimental results from Muto *et al*. [25, 26] showed that in Pd/SiO_2 and Pd/SiO_2-Al_2O_3 samples with enough silica loading to cover the surface, only the deactivation stage was observed, which is in agreement with our results.

4.5 CONCLUSION

Silica from the support could migrate on to the palladium particles during H_2 reduction or spread from silicon impurities present on the foil during methane oxidation. Migration during reaction was caused by water formed in the reaction and migration during H_2 reduction of silica-supported catalyst was possibly caused by the formation of palladium silicides, subsequently oxidized by O_2. The migration of silica deactivated the catalyst by covering active sites. We conclude that silica is not a good support for Pd catalysts when they are used in reactions where water is present and also that they should not be reduced in H_2 at temperatures close to 900 K. These results explain the deactivation observed in this work on foil during methane oxidation. It points to possible problems when Pd massive catalysts (foil and wires) are used in reaction media containing water and H_2. When bulk Pd is used, surface science techniques need to be available to measure the state of the surface. When Pd is supported on zirconia, no deleterious effects caused by H_2 or H_2O are observed.

Table 4-1 - Surface area and corrected turnover rates for Pd catalysts

Catalyst	Pds[a] $\mu mol\ g^{-1}$	Diameter[b] nm	Rate[c] $\mu mol\ g^{-1}\ s^{-1}$	TOR[d] $10^{-2}\ s^{-1}$	Reference
5% Pd/SiO_2-Reduced	11	45	1.6	0.7	This work
5% Pd/SiO_2-Oxidized	33	15	72	11	This work
10% Pd/ZrO_2-Reduced	43	20	37	9	This work
10% Pd/ZrO_2-Oxidized	65	15	71	11	This work
10% Pd/ZrO_2	32	30	0.7	3	[8]
1.0% Pd/ZrO_2	2.4-21	4.6-39	0.05-2.1	0.5-11	[43]
Pd foil	-	-	-	70	[10]
Pd black	990[e]	-	-	6	[10]

a - Pd surface area measured by H_2-O_2 titration at 373 K

b- calculated using d(nm)=100/(Percentage of metal exposed)

c - Reaction rate based on mass of Pd

c, d - Rate and Turnover rate (TOR) calculated at 553 K, 16 Torr CH_4 and 1 Torr H_2O by assuming reaction order of 1 for CH_4, –1 for H_2O, and 0 for O_2 and CO_2.

e - Calculated based on BET surface area 47 m^2g^{-1}

Figure captions:

Figure 4-1 TEM of Pd/ZrO2 after reduction in H2 at 923 K for 2 h.

Figure 4-2 TEM of Pd/ZrO2 after oxidation in O2 at 923 K for 2 h.

Figure 4-3 TEM of Pd/SiO2 after oxidation in O2 at 923 K for 2 h.

Figure 4-4 TEM of Pd/SiO2 (reduced in H2 at 923 K for 2 h) after chemisorption. Note amorphous silica overlayers.

Figure 4-5 Turnover rates as function of time for 10% Pd/ZrO2 (calculated at 553 K, 16 Torr CH4, 160 Torr O2 and 1 Torr H2O using reaction orders 1 for CH4, -1 for H2O and 0 for O2)

Figure 4-6 Turnover rates as function of time for 5% Pd/SiO2 (calculated at 553 K, 16 Torr CH4, 160 Torr O2 and 1 Torr H2O using reaction orders 1 for CH4, -1 for H2O and 0 for O2)

Figure 4-7 TEM of oxidized Pd/SiO2 after methane oxidation reaction at 553 K for 22 h with 2% CH4, 20% O2 and N2 balanced to 800 Torr.

Figure 4-8 (Number of Turnovers)2 as function of reaction time for a deactivated foil. Reaction at 598 K with 2% CH4, 20% O2 and N2 balanced to 800 Torr.

Figure 4-9 Si 2s core level XPS spectra of deactivated foil

Figure 4-10 XPS survey spectra of (a) deactivated foil after TPD (b) oxidized clean palladium foil after TPD

Figure 4-11 ISi/IPd change as function of time-on-sputtering (ISi: XPS signal intensity of Si 2s; IPd: XPS signal intensity of Pd 3d)

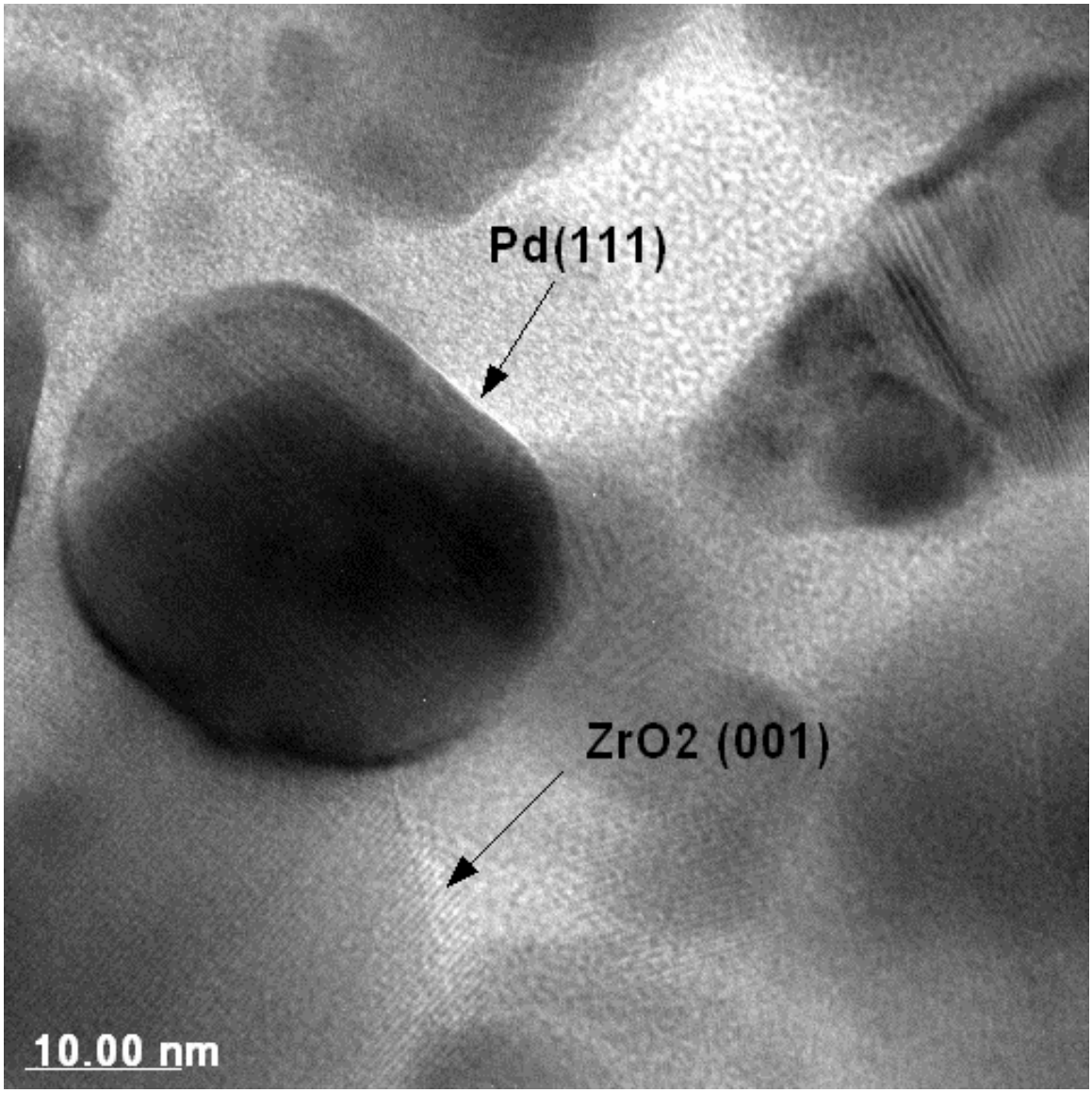

Figure 4-1 TEM of Pd/ZrO_2 after reduction in H_2 at 923 K for 2 h.

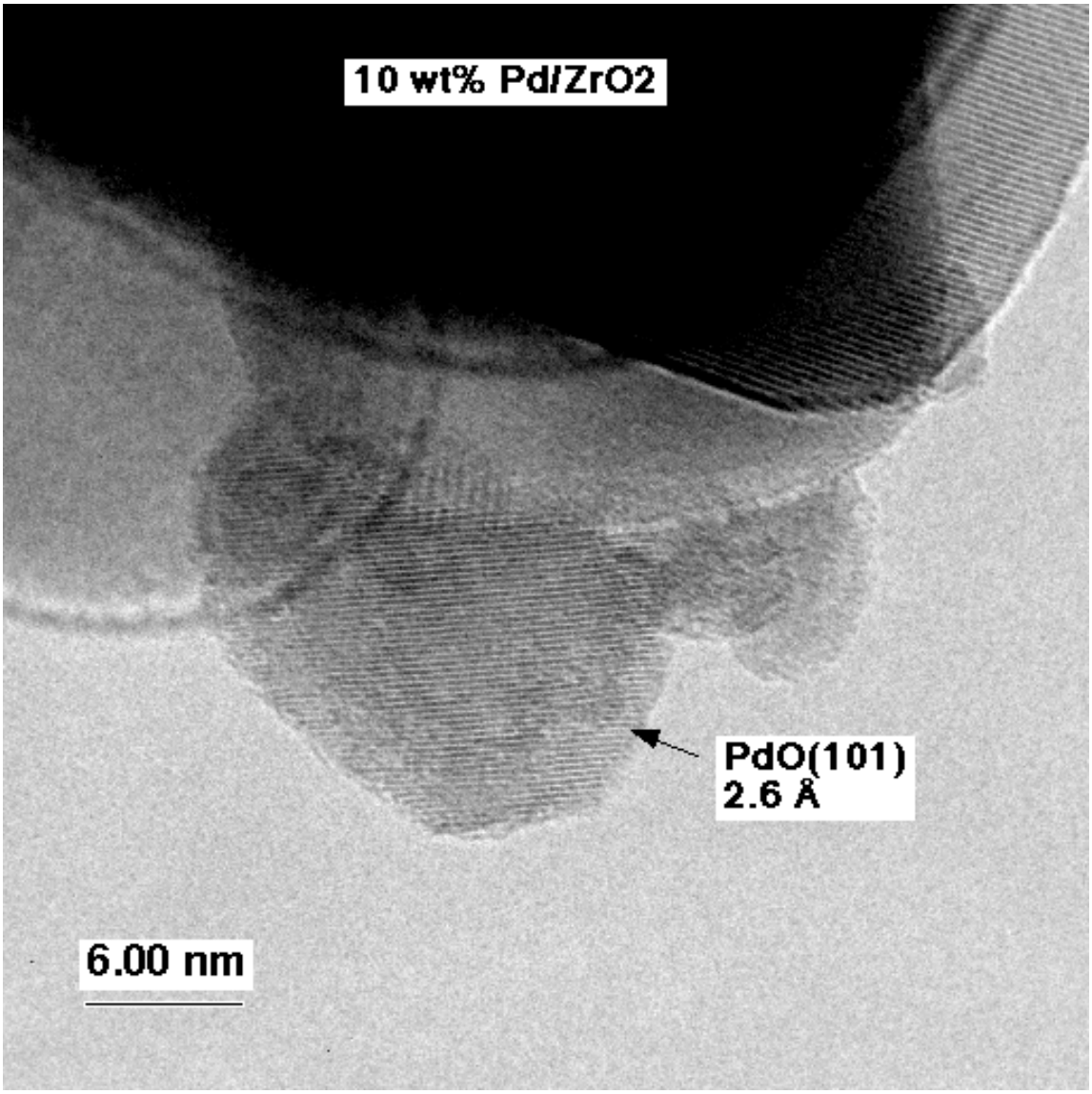

Figure 4-2 TEM of Pd/ZrO_2 after oxidation in O_2 at 923 K for 2 h.

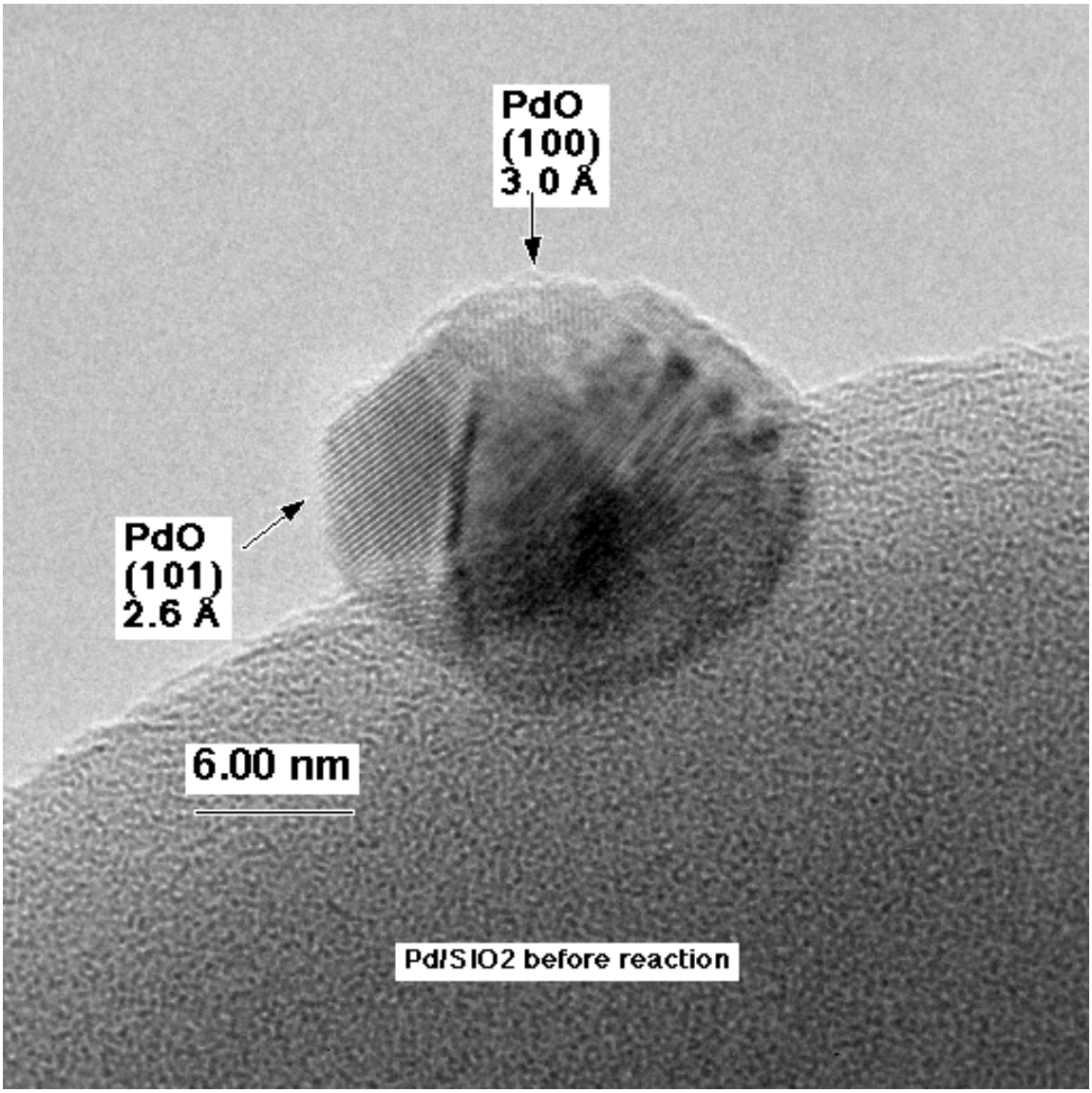

Figure 4-3 TEM of Pd/SiO_2 after oxidation in O_2 at 923 K for 2 h.

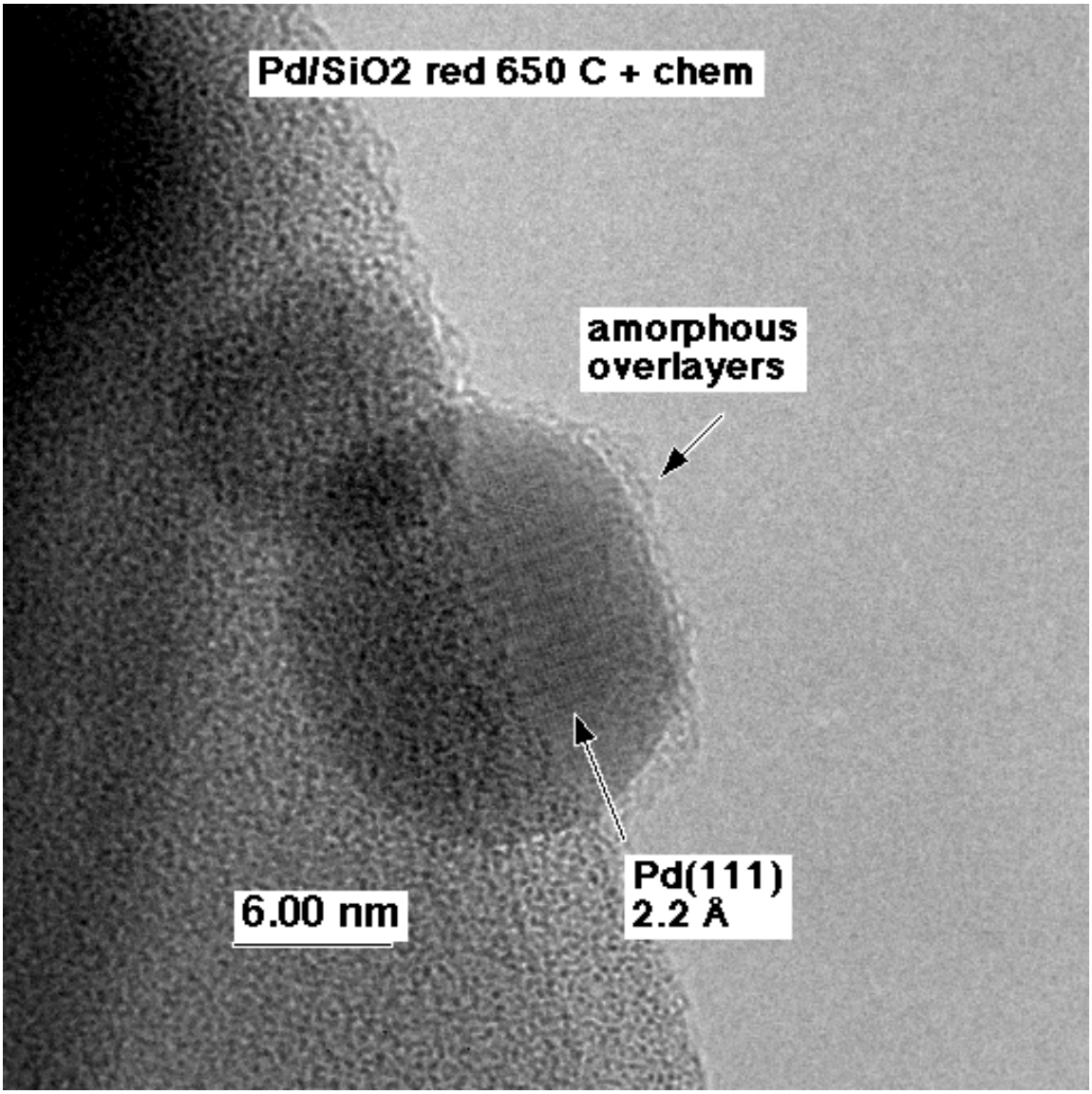

Figure 4-4 TEM of Pd/SiO_2 (reduced in H_2 at 923 K for 2 h) after chemisorption. Note amorphous silica overlayers.

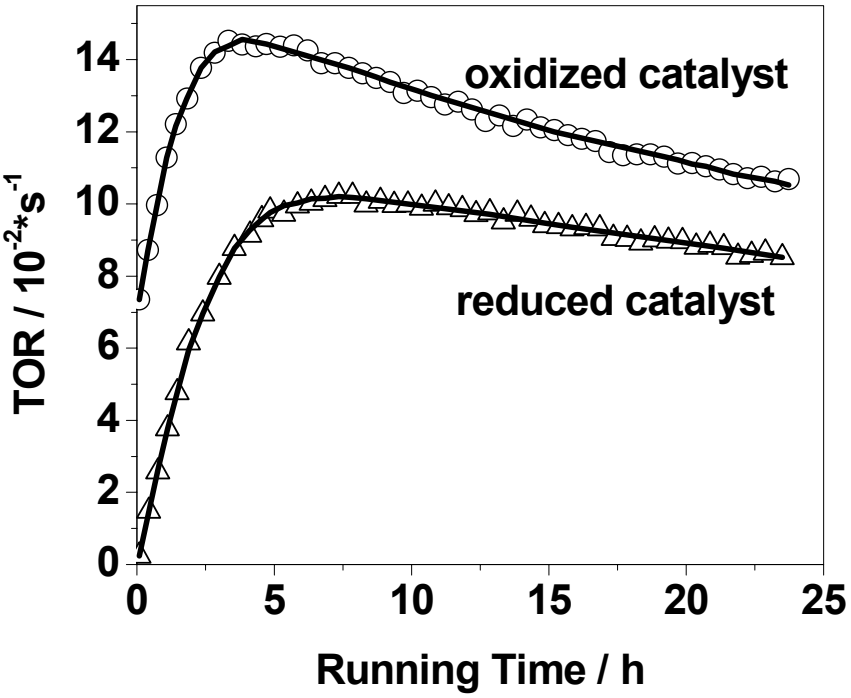

Figure 4-5 Turnover rates as function of time for 10% Pd/ZrO_2 (calculated at 553 K, 16 Torr CH_4, 160 Torr O_2 and 1 Torr H_2O using reaction orders 1 for CH_4, -1 for H_2O and 0 for O_2)

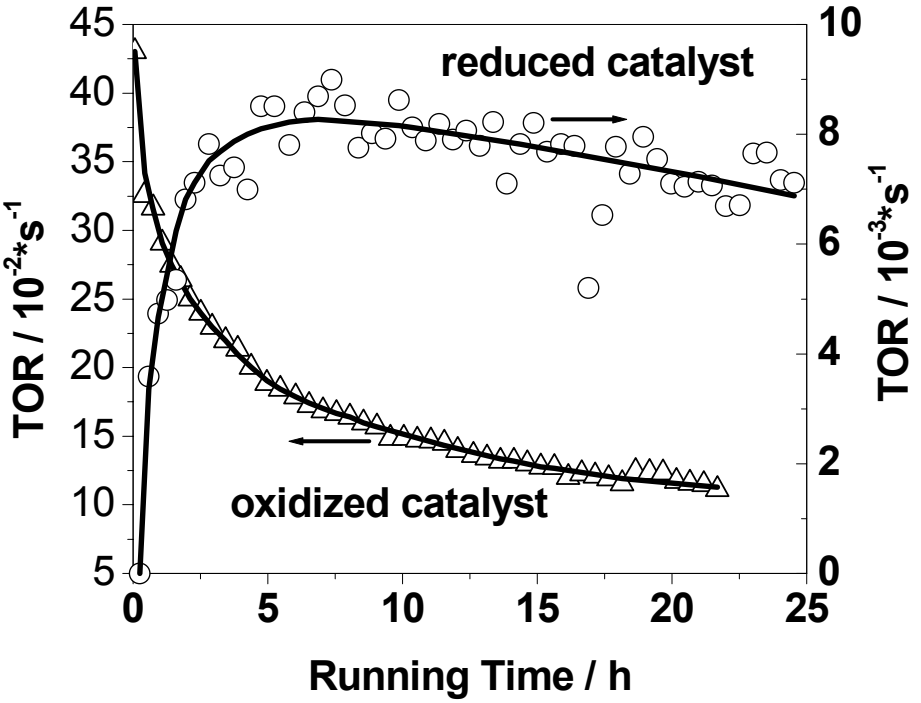

Figure 4-6 Turnover rates as function of time for 5% Pd/SiO_2 (calculated at 553 K, 16 Torr CH_4, 160 Torr O_2 and 1 Torr H_2O using reaction orders 1 for CH_4, -1 for H_2O and 0 for O_2)

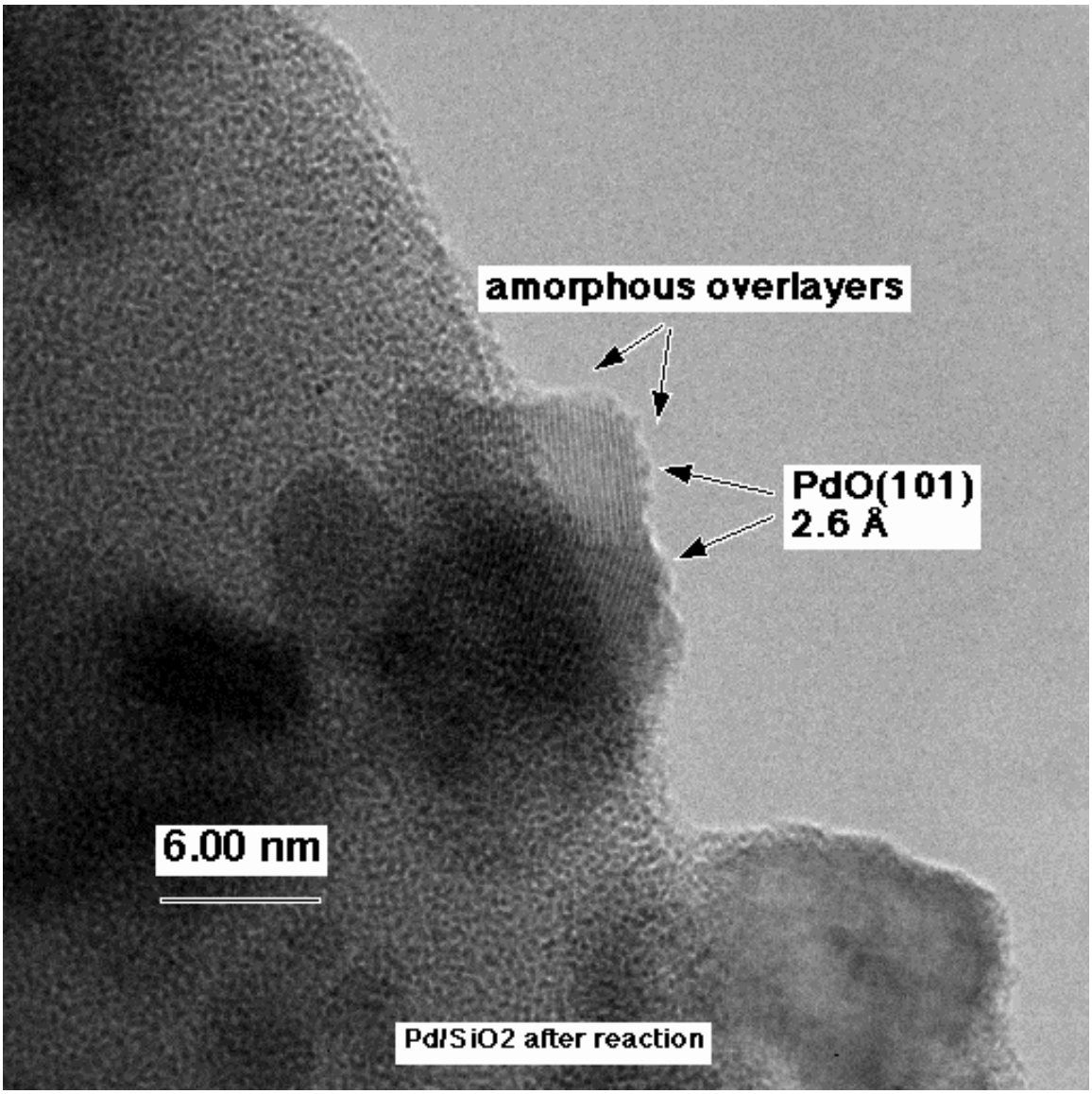

Figure 4-7 TEM of oxidized Pd/SiO_2 after methane oxidation reaction at 553 K for 22 h with 2% CH_4, 20% O_2 and N_2 balanced to 800 Torr.

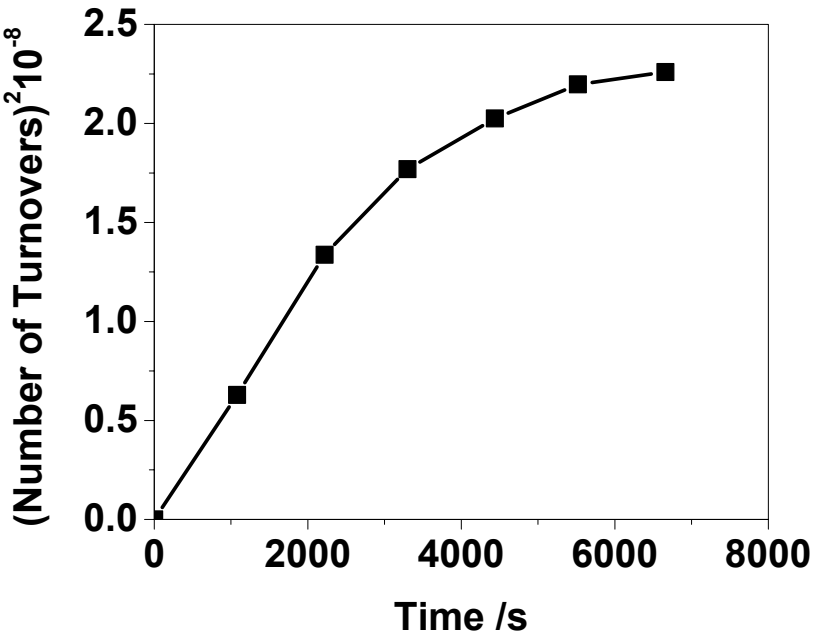

Figure 4-8 (Number of Turnovers)^2 as function of reaction time for a deactivated foil. Reaction at 598 K with 2% CH_4, 20% O_2 and N_2 balanced to 800 Torr.

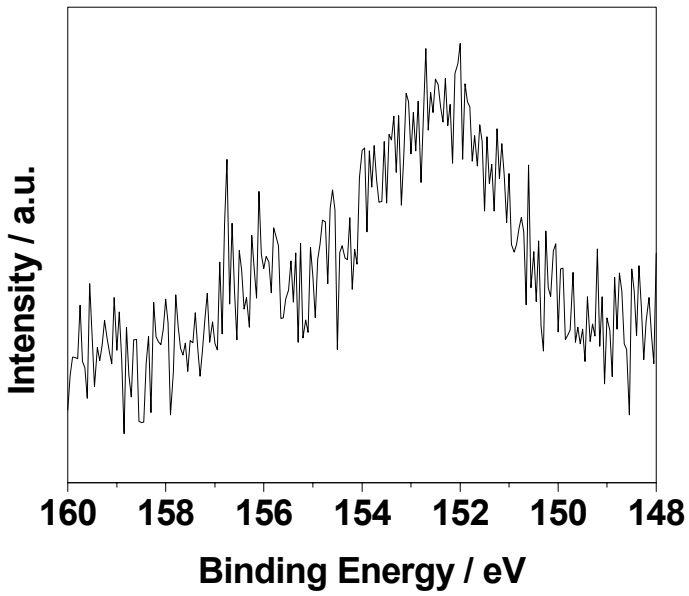

Figure 4-9 Si 2s core level XPS spectra of deactivated foil

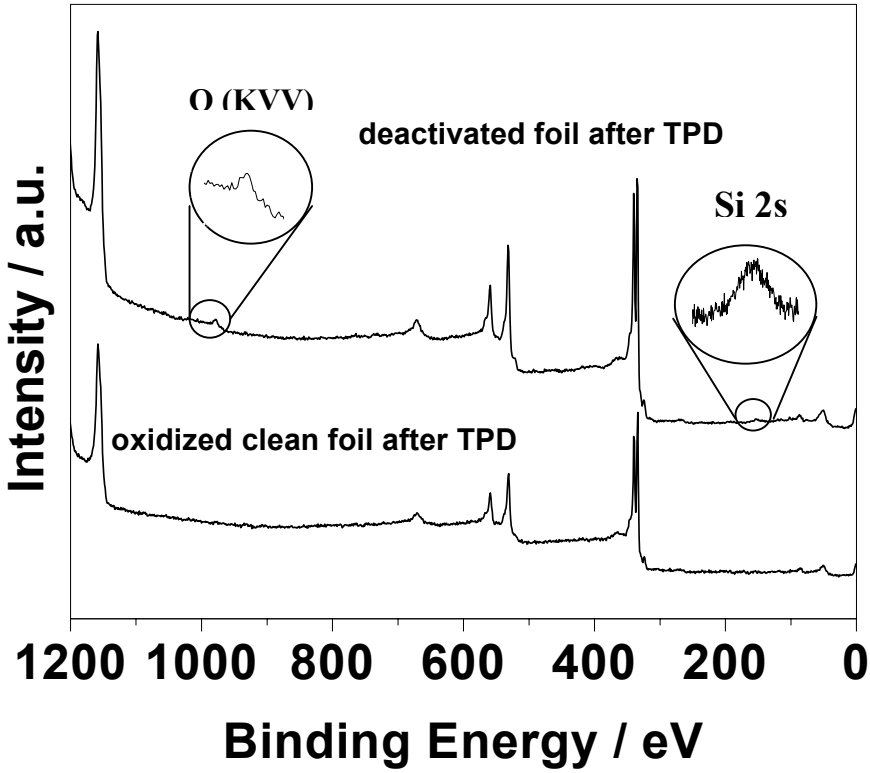

Figure 4-10 XPS survey spectra of (a) deactivated foil after TPD (b) oxidized clean palladium foil after TPD

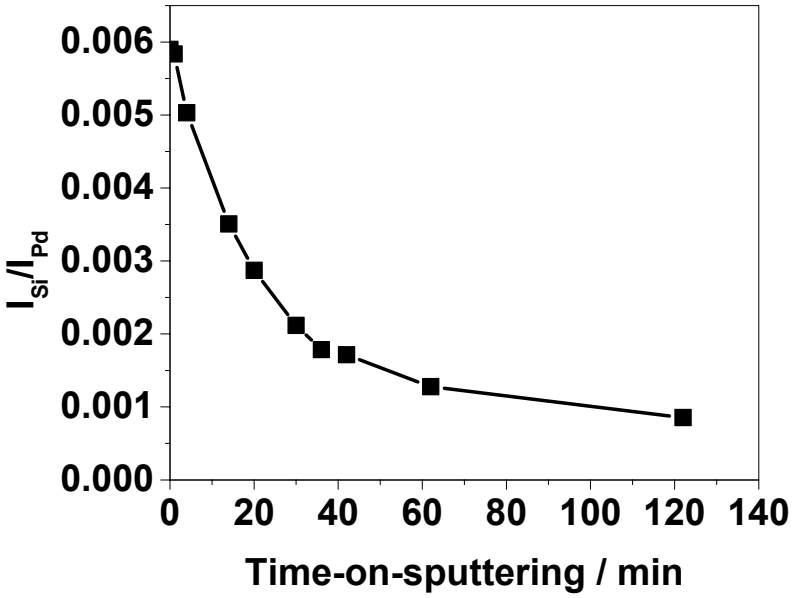

Figure 4-11 I_{Si}/I_{Pd} change as function of time-on-sputtering (I_{Si}: XPS signal intensity of Si 2s; I_{Pd}: XPS signal intensity of Pd 3d)

5 Study of Catalyst Reactivity Hysteresis during Phase Transition

Abstract:

The palladium catalyst exhibited activity hysteresis for methane oxidation at the temperatures between PdO decomposition and reformation. The hysteresis was studied using temperature-programmed methane oxidation with 0.76 Torr O_2 and 0.15 Torr CH_4, which included heating and cooling cycles. In the heating cycle, the methane conversion initially increased as expected up to 873 K when PdO started to decompose to Pd. The conversion decreased by 90% after PdO fully decomposed to Pd. Methane conversion started to increase again as the temperature increased after PdO had fully decomposed. When temperature reached 1003 K, the cooling cycle started. The conversion decreased initially in the cooling cycle as expected; but as the transition temperature was reached, the conversion remained at a level more than 90% lower than in the heating cycle. As the temperature reached 828 K, methane conversion increased to the same level observed in the heating cycle. We have thus observed a 45 K difference in the Pd-PdO transition temperature. Additional experiments showed that in the hysteresis temperature range (828-873 K), palladium oxidation could occur only if PdO could be first formed in the catalyst. This observation indicates that the PdO reformation at lower temperature was not limited by the rate of oxidation but possibly by the formation of nucleation sites.

Keywords: methane oxidation on palladium, catalyst activity hysteresis, palladium oxidation, model catalyst

5.1 Introduction

As the most active catalysts for methane combustion, supported Pd catalysts have been extensively studied and currently are being used in the commercial catalytic combustion systems [3]. Due to the wide operating temperature range of the catalytic combustor, the palladium catalyst presents unusual situation that the thermodynamic stable phase could be PdO or Pd, depending on the oxygen pressure and the reaction temperature. Palladium catalyst exhibited hysteresis in the reaction rate for methane oxidation due to the PdO decomposition and reformation. Temperature-programmed methane oxidation, including heating and cooling cycles, was usually carried out to study this issue. In the heating cycle, the methane conversion initially increased as expected up when PdO started to decompose to Pd. Methane conversion started to increase again as the temperature increased after PdO had fully decomposed. The process was then reversed by decreasing the temperature from some point where PdO has fully decomposed to the initial point. The conversion decreased as expected; but as the transition temperature was reached, the conversion remained at a level lower than in the heating cycle. The methane conversion increased to the same level observed in the heating cycle only at a temperature below the PdO decomposition temperature [17, 35-38]. The temperature range for hysteresis and the difference of catalytic activity in the hysteresis window were also found strongly dependent on support materials [47, 108, 109].

Some hypotheses have been raised to explain the unusual behavior of PdO reformation. McCarty [35] and Datye *et al.* [37] attributed this behavior to formation of passive layers of chemisorbed oxygen on palladium metal, which prevented the oxidation of palladium. Salomonsson *et al.* [110] proposed a non-ideal three-phase system in the hysteresis region composed of palladium metal, palladium metal with oxygen and palladium oxide. In this phase diagram, the palladium oxidation and reformation took different paths which caused the hysteresis of oxide formation. A more complex four-phase diagram was proposed by Wolf *et al.* [111] to simulate the hysteresis of palladium oxidation. These four phases included Pd, PdO, surface PdO and chemisorbed oxygen.

It is noteworthy that the hysteresis has been, so far, mainly studied on supported Pd catalysts, which could be strongly affected by the support-metal interactions. Also there were no detailed kinetic data in this region to help understand this issue. In this study, the hysteresis issue was addressed using a Pd polycrystalline foil which is free of support effect. Possible mechanism based on the study results was proposed.

5.2 Experimental Methods

The experiment system includes a high-pressure reactor cell and an ultrahigh vacuum (UHV) surface analysis chamber. The reactor cell can be operated as continuous-stirred tank reactor (CSTR) and batch reactor. At temperature above 700 K, experiments were performed in CSTR mode to avoid total conversion of methane because of the high reaction rate; at temperature below 700 K, experiments were performed in batch mode so that CO_2 could accumulate inside the reactor to the level which the GC detector could precisely monitor. Gas circulation pumps (Metal Bellows, MB-21) were employed to

speed up reactants flow rate to avoid mass transfer limitation. The maximum flow rate was 4600 cc min^{-1}. The UHV chamber was equipped with AES, XPS, mass spectrometer and sputtering gun for surface analysis and cleaning. The sample could be transferred between the reactor cell and the UHV chamber without exposing to air. Details about this system were described in previous paper[10].

The palladium catalysts were 0.1 mm thickness polycrystalline foil with surface area about 0.5 cm^2 (Alfa Aesar, 99.9%). It was spot-welded on the power pins so that current can go through to achieve resistive heating. Thermocouple wires were spot-welded on the back of the foil for temperature reading. Sample temperature was automatically controlled by interfacing a temperature controller (Euortherm Model 2408) with a TCR power supply (Electronic Measurements Inc). An infrared lamp was mounted outside the reactor facing the viewport on the reactor. Infrared light generated by the lamp could go through the viewport and be focused on the palladium foil. The sample was heated by both methods at the same time during the experiment. To clean the impurities, the foil was treated by methane oxidation at 773 K and 873 K for 100 minutes respectively with reactants mixture of 4.5 Torr CH_4, 18 Torr O_2 and inert gases (He and N_2) balanced to atmospheric pressure. After the treatment, the foil was annealed at 873 K for 1 minute in vacuum, and then sputtered with 2.0 keV Ar^+ to remove the surface impurities. Surface was regarded clean when no sulfur-, phosphorus- and silicon- species were detected by XPS. Before each independent experiment, the sample was sputtered by 2.0 keV Ar^+ and then annealed at 873 K for 1 minute.

To study hysteresis, the operating temperature should vary between room temperature to some level above the PdO decomposition temperature. Considering the possible mass transfer limitation and the limit of the equipment tolerance to high temperature oxidation, the PdO decomposition temperature should be set as low as possible, which means the O_2 pressure should be as low as possible. At the same time, the concentration has to be high enough to be detectable by GC detector. By comprising these two contradictive factors, most experiment in this study was performed with oxygen pressure of 0.76 Torr, which corresponds to PdO decomposition temperature of 888 K.

Except notation, turnover rate was calculated using the geometric Pd metal surface area assuming an average Pd surface atom density for a polycrystalline foil of $1.27*10^{15}$ atoms cm^{-2}[48].

The real PdO surface area was measured by a surface exchange experiment with labeled oxygen (^{18}O isotope), which was done by exposing the oxidized foil to 5 Torr $^{18}O_2$ at 598 K for 12 seconds. These conditions were designed based on the results from Au-Yeung *et al.* [49] and ensured the exchange between ^{16}O in PdO and $^{18}O_2$ isotope mostly occur at the surface, without appreciable diffusion into the bulk. The reference point for oxygen coverage was made by assuming that a foil exposed to O_2 at room temperature will form an oxygen layer with 0.25 ML coverage at saturation. Since this coverage was well established for a Pd(111) single crystal [50, 51] and a foil is composed of mostly (111) planes, the reference point is reasonable. The exchange was proved to be an effective method to measure PdO surface area [10, 52]. The surface area of the metal phase under reaction conditions was assumed to be the same as the surface area for clean Pd foil.

5.3 Results

5.3.1 System Test

A stainless steel foil with same size as palladium foil was used to test the background activity of the catalytic reactor. The turnover rate was less than 0.15 s^{-1} compared with the turnover rate of 9.3 s^{-1} on Pd foil under conditions of 6 Torr O_2, 1.5 Torr CH_4, and at 1023 K. Therefore, the contribution from the background of the catalytic reactor was less than 2%.

To obtain kinetic data, the experiment must be free of mass and heat transfer limitation. The palladium foil was non-porous solid metal, so there was no internal mass and heating transfer limitation. The temperature of the foil was automatically controller by a thermal controller, which enabled the reaction free of external heat transfer limitation inherently. The only possible transport limitation for this system was external mass transfer. Figure 5-1 shows the methane conversion as a function of gas circulation rate. The results indicate that under the test conditions, there was no external mass transfer limitation when circulation rate was higher than 3800 cc min^{-1} since methane conversion did not increase any more when the circulation rate was increased above this level. The circulation rate was higher than 3800 cc min^{-1} during experiment, so no mass transfer limitation was involved in the experiment results.

5.3.2 Hysteresis of Methane Oxidation

Temperature-programmed methane oxidation was performed with 0.76 Torr O_2, 0.15 Torr CH_4 and inert gases balanced to atmospheric pressure. The temperature program included heating and cooling cycles. The heating cycle included two ramps: from room temperature to 863 K, the heating rate was 0.5 K s^{-1}; from 863-1003 K, the heating rate was 1 K s^{-1}. During cooling cycle, the catalyst was cooled down from 1003 K to 600 K at 1 K s^{-1} and then the sample was quenched inside the gas mixture. Since the volume of the reactor cell was 840 ml and the feed rate was only 50 ml min^{-1}, the response of reactants concentration to reaction rate or feed concentration change was very slow. At each temperature where data were collected, the temperature program was held for at least one hour so that steady-state data could be obtained.

Figure 5-2 shows the methane conversion during the heating and cooling cycles. Since it took at least one hour to get stabilized data for each point on the figure and the circulation pump could not tolerate extensive operation time, the data on the figure were collected from three heating-cooling cycles. There was at least one point shared by each two cycles to check that these cycles were repeatable.

The first point was collected at 733 K with methane conversion of 13%. Methane conversion increased at elevated temperature until 873 K where it reached 40%. Conversion decreased to 20% when the temperature was increased further to 893 K and decreased to 5% when temperature reached 903 K. Methane conversion started to pick up again from 903 K. In the experiment, the temperature on the foil was not very uniform

and 15 K variation was possible. Thus, it was normal to have both PdO and Pd on the foil at temperature around PdO decomposition point and the decrease of methane conversion did not show a straight vertical line. The cooling cycle started from 1003 K. The methane conversion decreased initially until 823 K. At 823 K, the methane conversion increased to the level observed in the heating cycle. As temperature was further decreased, the methane conversion started to decrease again. There was a hysteresis of 50 K between the starting point of conversion increase during cooling and the starting point of conversion decrease during heating.

Was the hysteresis caused by cooling from temperatures above PdO decomposition point? A special experiment was designed to answer this question. The clean Pd metal foil was heated in N_2 to 863 K (below PdO decomposition temperature). Because the gas phase was pure N_2, no PdO was formed during catalyst heating up. Then, the feed was changed from N_2 to reactant mixture with 0.76 Torr O_2 and 0.15 Torr CH_4. No CO_2 was detected for 80 minutes after changing the feed composition. Then the temperature was decreased to 828 K (out of hysteresis range), and was held at 828 K for 80 minute before returning to 863 K. Methane conversion of 25% was obtained when temperature returned to 863 K.

5.3.3 Palladium Oxide Decomposition and Reformation

The hysteresis of catalyst activity during cooling is related with the PdO reformation at lower temperature than the PdO decomposition. To understand the hysteresis of methane oxidation, it is imperative to study the PdO decomposition and reformation.

Clean metal palladium foil was heated under vacuum in the reactor to 863 K at 0.8 K s^{-1}, then 0.76 Torr O_2 was introduced inside. The foil was held at 863 K for 30 minutes in 0.76 Torr O_2 before being quenched with oxygen inside. During the quenching stage, the temperature dropped to 543 K after 30 seconds and to 473 K after another 30 seconds. XPS analysis after quenching indicated the surface was palladium metal (Figure 5-3). Oxygen desorption was observed during TPD after XPS analysis, but desorption peak was not observed even when temperature reached 950 K (Figure 5-4). Since XPS showed the foil was in metal state, the oxygen could possibly come from the surrounding power pins on the mounting cart. In another experiment, the foil was heated up with 0.76 Torr O_2 inside the reactor using the same temperature program. After quenching, PdO was the only surface species observed on the surface. Following TPD revealed that 440 monolayers of PdO were formed. Note that the oxygen released from power pins, obtained from the previous experiment, was subtracted during the calculation of PdO formation. By comparison, only 270 ML of PdO was formed if the foil was quenched immediately after temperature reached 863 K inside 0.76 Torr O_2. Therefore, there were 170 monolayers of PdO formed during the 30 minutes holding at 863 K inside oxygen, but it only occurred after 270 ML of PdO formed during the heating up.

5.3.4 Effect of Rich Treatment on Hysteresis

The clean metal foil was heated in N_2 to 863 K, and then the feed was changed from N_2 to fuel lean mixture (0.76 Torr O_2, 0.15 Torr O_2, inert gases balanced to atmospheric pressure). After 3 hours, methane conversion was stabilized at ~5%. Then, the feed was changed to fuel rich mixture (0.76 Torr O_2, 1.5 Torr CH_4 and inert gases balanced to

atmospheric pressure). The methane conversion during the rich treatment was 10%. After 2 hours of rich treatment, the feed was change back to fuel lean mixture. A stabilized methane conversion of about 55% was obtained under the fuel lean reaction. Then the catalyst was quenched. The XPS analysis after quenching indicated that the foil surface was palladium metal (Figure 5-3).

Another experiment of the lean-rich-lean treatment was performed at 853 K. Since the temperature was still at the hysteresis window, the results were similar as the results at 863 K, with the lean reaction after rich treatment had much higher methane conversion than the one before rich treatment. By assuming the catalyst surface area was the same before arich treatment and after rich treatment, the turnover rate increased 6 times. After the lean-rich-lean experiment, the reactor was loaded with 160 Torr O_2, 16 Torr CH_4 and N_2 balanced to 800 Torr, and reaction was performed in batch reactor mode at 598 K. The nominal turnover rate was 5 s^{-1} after correcting to 550 K, 16 Torr CH_4 and 1 Torr H_2O without considering surface area change. Note that if starting the reaction at 598 K with a clean metal palladium foil, the nominal turnover rate was 0.4 s^{-1}.

5.3.5 Effect of O_2 Pressure on Hysteresis

Previous experiment showed that when hysteresis occurred, the catalyst could keep in metal state though the thermodynamically stable phase was PdO. This experiment tested whether increasing the oxygen pressure could eliminate hysteresis.

A new palladium foil was used to perform this experiment. For this foil, PdO started to decompose at 863 K, which was lower than the one obtained on the previous foil. The reasons could be the non-uniform temperature distribution on the foil and the different position of the thermocouple. The foil was heated up to 903 K in the fuel lean mixture (0.76 Torr O_2 and 0.15 Torr CH_4) at 0.5 K s^{-1}. The temperature was kept at 903 K for 5 minutes, and then decreased to 853 K. The final methane conversion at 853 K was 10%. Then oxygen pressure in the feed was increased to 1.5 Torr, which was double of the initial pressure. Under this oxygen pressure, the methane conversion increased to 30%. XPS analysis after reaction indicated that the surface was palladium oxide.

5.4 Discussion

An experiment in batch mode was carried out at 598 K with 160 torr O_2, 16 Torr CH_4 and N_2 balanced to 800 Torr. The turnover rate was 3.8 s^{-1} calculated at 598K, 160 Torr O_2, 16 Torr CH_4, 1 Torr H_2O. A comparison of turnover rates from literature reports was summarized in Figure 5-1. The value of turnover rate in study is close to the turnover rate obtained in our laboratory on Pd foil (5.3 s^{-1}), and is among the highest for all the palladium catalysts reported.

McCarty [35] and Datye *et al.* [37] attributed the hysteresis to the formation of a passive chemisorbed oxygen layer on the metal surface. Since heat of formation of chemisorbed oxygen (220 kJ mol^{-1} [50, 51, 66, 112]) is greater than heat of bulk PdO formation (120 kJ mol^{-1} [7]), the chemisorbed oxygen should bind Pd stronger than the oxygen in bulk PdO. Thus, it could form a passive layer on the metal surface to prevent oxygen adsorption, in turn to prevent PdO formation and methane reaction. The challenge for

this theory is why the chemisorbed oxygen could not prevent PdO formation at lower temperatures such as 783 K.

Dissolved oxygen/subsurface oxygen was able to form at subsurface region of Pd metal at temperature above the PdO decomposition point in oxygen environment, and this oxygen was regarded as the precursor for bulk PdO formation [60, 113-120]. The interaction between oxygen and Pd was simplified as the following stages: (i) formation of surface chemisorbed oxygen O(c) from gas phase oxygen O_2(g): (ii) chemisorbed oxygen O(c) migration into the bulk to form dissolved/subsurface oxygen O(d): (iii) oxide O(b) formation from dissolved/subsurface oxygen O(d) [118]. A similar mechanism is proposed here to explain the unusual behavior for PdO decomposition and reformation. In our mechanism, an equilibrium could be reached between O_2(g) and O(d) (step 1); but formation of O(b) from O(d) is irreversible and only starts when the O(d) concentration is saturated.

$$O_2(g) \Leftrightarrow O(d) \qquad (1)$$
$$O(d) \rightarrow O(b) \qquad (2)$$

The O(d) should be more strongly bonded than O(b) considering the lower O/Pd ratio for O(d). Since the formation of O(b) from the oxygen in gas phase is an exothermic reaction with heat of formation 120 kJ mol^{-1}[121], the formation of O(d) from oxygen in the gas phase should be exothermic. Therefore, the equilibrium of step 1 will shift to O(d) as temperature decreases. We proposed that at temperatures slightly lower than PdO decomposition temperature, the equilibrium concentration of O(d) could not saturate to

form PdO. Further decreasing the temperature would allow O(d) to build up in the near surface region until it is saturated to form O(b).

Thurmer *et al*. [122] reported that for oxidation of lead single crystal, the oxide initially was formed around impurity sites, and then the oxide acted as a catalyst for the further oxidation. Zheng *et al.* [50] observed the formation of PdO islands on Pd(111) surface at the beginning of oxidation. These results indicate that oxidation of palladium is very possible an auto-catalytic reaction like the oxidation of lead, and it starts with PdO seeds. The formation of the PdO seeds may occur at the defects where the O(d) could saturate at higher temperature. Once the seeds were created, further growth of oxide is only a kinetic issue. The mechanism we proposed is for the initial PdO seeds formation. Further oxidation after the formation of PdO seeds may not be restricted by the concentration of O(d) as it became auto-catalytic process. This would explain why at 863 K with 0.76 Torr O_2, palladium oxide grew further if oxide has already formed, but did not grow if there was no oxide. Increasing O_2 pressure will increase the O(d) concentration., thus will allow O(d) to saturate at temperature inside the hysteresis temperature window to form oxide, which explains why an increase of O_2 pressure could eliminate hysteresis.

The PdO decomposition is proposed not to go through the dissolved oxygen, and only depends on the thermodynamic equilibrium between PdO and gas phase oxygen.

$$2O(b) \rightarrow O_2(g)$$

In this mechanism, both O(b) and O(d) could be the stable phase on the surface region at temperatures between PdO decomposition and reformation, and the choice just depends on the starting point.

Rich treatment was proved to be able to increase the catalyst surface area of palladium oxide, thus to increase the methane conversion [52]. Could rich treatment increase the surface area of palladium metal? The nominal turnover rate was 5 s^{-1} at 550 K with 160 Torr O_2, 16 Torr CH_4 and 1 Torr H_2O on the foil after the lean-rich-lean experiment, which was 12 times the nominal turnover rate (0.4 s^{-1}) based on a clean palladium metal foil without rich treatment history. It is possible that the surface area increased after rich treatment even though the surface was still palladium metal.

5.5 Conclusion

During temperature-programmed methane oxidation, methane conversion decreased as PdO decomposed to Pd metal; however the methane conversion could not be fully recovered to the level in heating cycle until temperature decreased to the point lower than where PdO should be reformed. This hysteresis in the rate of reaction was caused by PdO reformation at a lower temperature than PdO decomposition. The hysteresis could be eliminated by either increasing the O_2 pressure, or treating with rich fuel mixture.

A mechanism was presented to explain the hysteresis by assuming different reaction pathways for PdO decomposition and reformation. Dissolved/subsurface oxygen is regarded as the precursor for initial PdO formation, and palladium oxide is formed until the concentration of dissolved/subsurface oxygen reaches certain level. On the contrary,

PdO decomposition will not go through subsurface oxygen. In such cases, the PdO decomposition and reformation may occur at different temperatures.

Table 5-1: Comparison of Turnover Rates on Palladium Catalysts

Catalyst	Activation Energy[a]		TOR[b] (s^{-1})	Reference
	Value ($kJ\ mol^{-1}$)	Measure Range (K)		
Pd foil	-	-	3.8	This work
Pd foil	125	570-630	5.3	[10]
Pd/Si-Al_2O_3	170-184	500-640	0.1[e]	[8]
Pd/Al_2O_3	150	500-640	0.07-0.16[e]	[8]
Pd/ZrO_2	170	500-640	0.1-0.7[e]	[8]
Pd/ZrO_2	185	-	0.5-3.0[e]	[43]
Pd/ZrO2	N/A	-	0.3[e]	[45, 71]

[a] Assuming reaction order for water is –1, the activation energy was corrected for the water inhibition effect.

[b]TOR calculated at 598 K, 16 Torr CH_4, 1 Torr H_2O, and N_2 balanced to 800 Torr. Reaction orders were assumed to be 1 for CH_4, 0 for O_2 and –1 for H_2O

[c]Surface area measured from $^{18}O_2$ exchange

[d]Number of sites measured from BET surface area (47 m^2g^{-1})

[e] For plug flow reactor, partial pressures for reactants and products are the average of values of inlet and exit concentration

Table of Figure

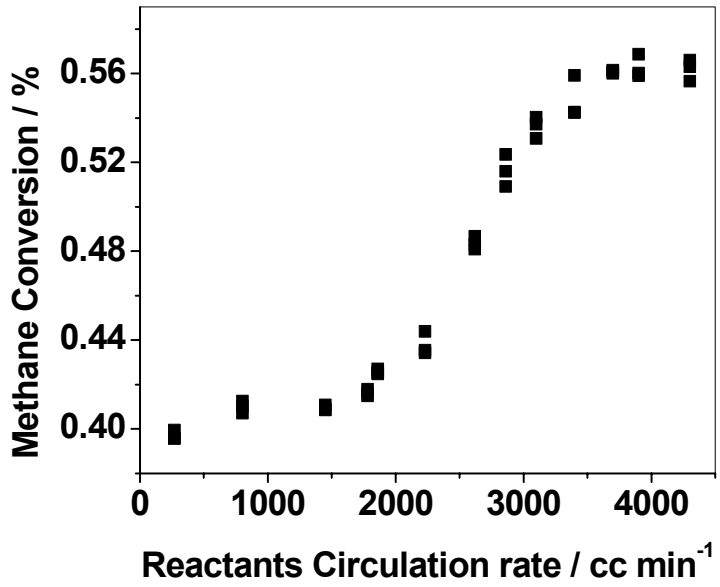

Figure 5-1 Methane conversion as a function of reactants circulation rate at 863 K with 1.5 Torr O_2, 0.38 Torr CH_4 and inert gases balanced to atmospheric pressure

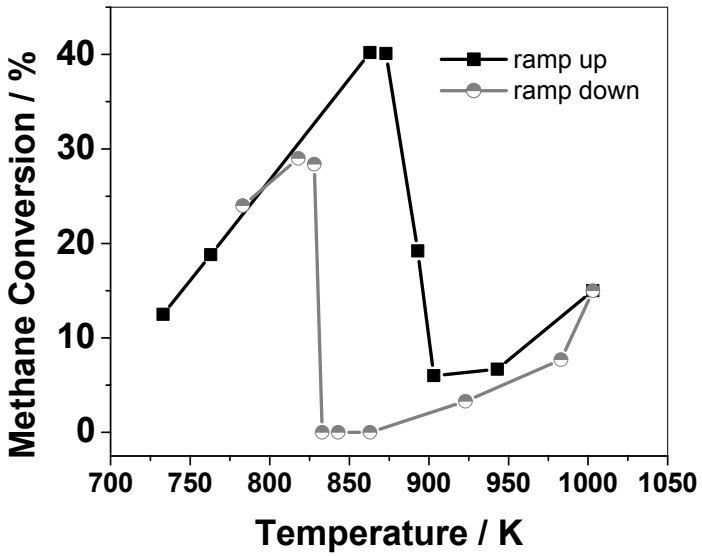

Figure 5-2 Catalytic methane oxidation on palladium foil as function of temperature and treat methods. The rate of ramp up was 0.5 $K \cdot s^{-1}$ from room temperature to 863 K and 1 $K \cdot s^{-1}$ from 863 K to 1003 K; rate of ramp down was 1 $K \cdot s^{-1}$ from 1003 K to 783 K and then the sample was quenched. Reactant mixture was composed of 0.75 Torr O_2, 0.15 Torr O_2 and inert gases balanced to atmospheric pressure

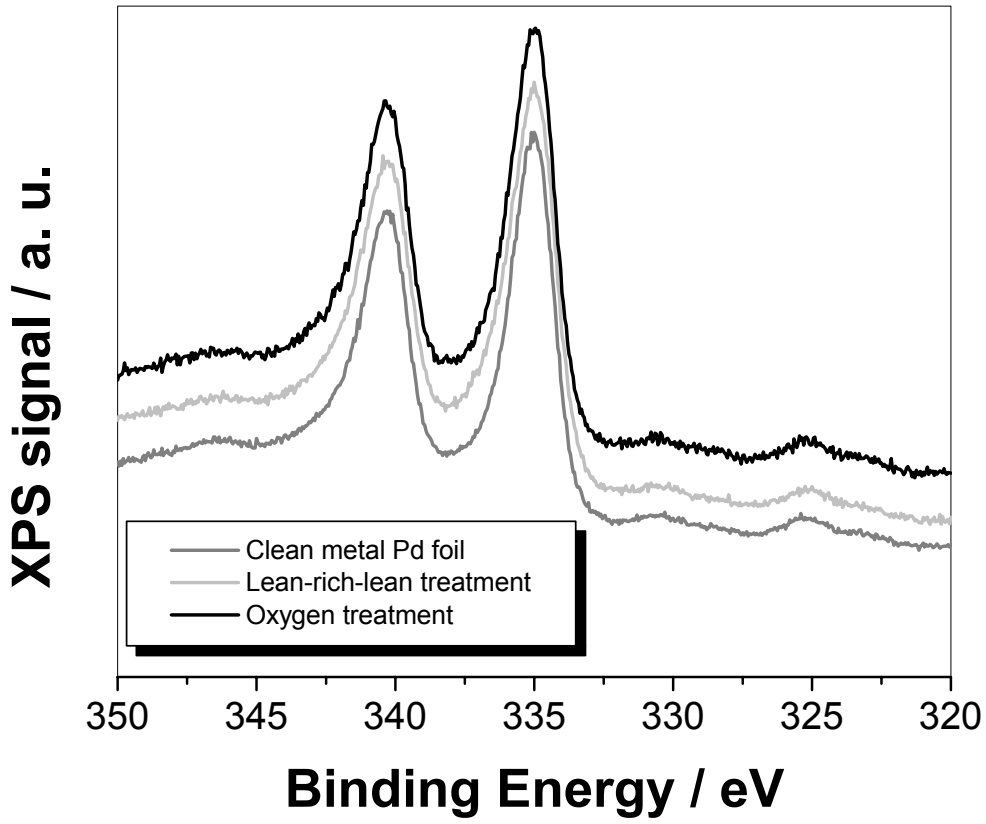

Figure 5-3 Comparison of XPS Pd 3d5/2 core level peak on clean metal foil and foils after two kinds of treatment. O_2 treatment was done by heating up clean metal palladium foil under vacuum to 863 K at 0.8 $K \cdot s^{-1}$ and then introducing 0.76 Torr O_2 inside. Lean-rich-lean experiment was performed by heating up clean metal palladium foil to 863 K in N_2, then switch to fuel lean, rich and lean mixture.

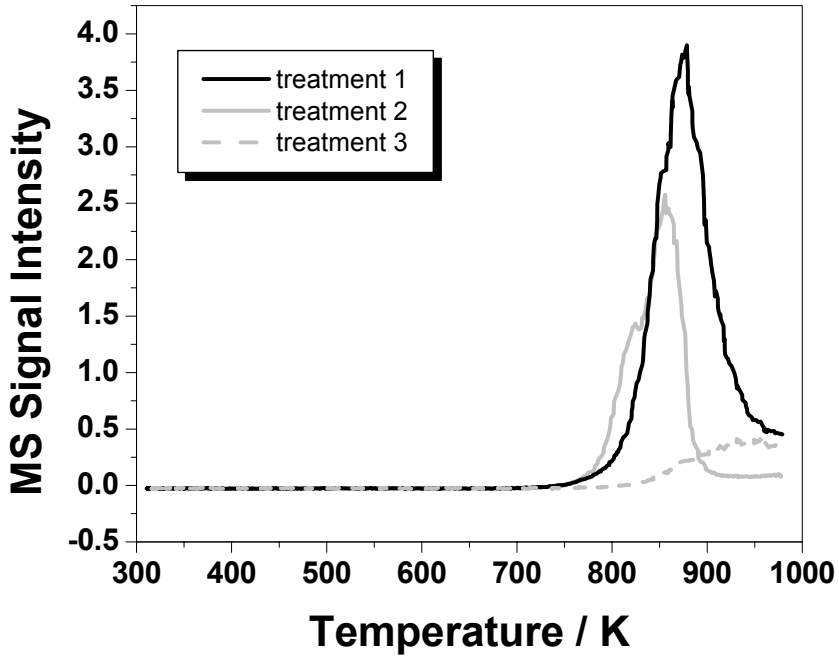

Figure 5-4 Temperature-programmed desorption of palladium foil after three kinds of oxygen treatment (*Treatment 1*: heat up foil in 0.76 Torr O_2 to 863 K and hold for 30 min before quenching; *Treatment 2*: heat up foil in 0.76 Torr O_2 to 863 K and quench; *Treatment 3*: introduce 0.76 Torr O_2 into reactor after heating up the foil to 863 K, hold 30 min before quenching.)

6 Reaction Sensitivity of Methane Oxidation on Palladium Catalysts*

*contribution from Jinyi Han is acknowledged.

Abstract

Catalytic methane combustion was studied on palladium polycrystalline foil and palladium single crystals including Pd(111), Pd(100) and Pd(110). Reaction kinetics was investigated under fuel lean conditions both at low temperatures where PdO was the thermodynamic stable phase and at high temperatures where Pd metal was thermodynamic stable phase. The reaction on both PdO and Pd metal was structure insensitive to the original metal surface orientations. The turnover rate on the oxide phase was 2.8 s^{-1} for Pd(111), 4.7 s^{-1} for Pd(100) and 1.3 s^{-1} for Pd(110) after correcting to 160 Torr O_2, 16 Torr CH_4 and 1 Torr H_2O at 598 K. And the turnover rate on the metal phase was 2.8 s^{-1} for Pd(111), 2.0 s^{-1} for Pd(100) and 2.2 s^{-1} for Pd(110) after correcting to 2.3 Torr O_2, 0.46 Torr CH_4 and 0.05 Torr H_2O at 973 K.

Keywords: methane oxidation on palladium, structure sensitivity, model catalysts

6.1 Introduction

Natural gas-fueled gas turbines are a preferred technology for power generation. One reason is that many of the large reserves of natural gas, which are composed mainly of methane, have very small amounts of sulfur and nitrogen compounds; as a consequence, when the natural gas is burned, the emission gases will contain correspondingly a low concentration of SOx and NOx formed from S and N compounds. Another reason is that methane has the highest hydrogen-to-carbon ratio of all the hydrocarbons, thus, combustion of methane can produce less carbon dioxide, a greenhouse gas, per unit of power produced. Catalytic combustion, which enables the combustion reaction to take place on the catalyst surface without flame, could be operated at a lower temperature. Thus, it has the potential to reduce NOx emission at much lower cost while avoiding the problems of conventional flame combustors. Palladium based catalysts have been regarded as the choice for catalytic methane combustion because of their high catalytic activity [5]. Catalytic methane combustion technology based on palladium catalyst has recently been used on commercial combustors [3, 6].

One of the questions regarding methane combustion on palladium catalyst is structure sensitivity. For a real catalyst, when metal particles are in the critical size of nanometer diameter, the relative concentrations of surface sites with given coordination neighbors changes rapidly when the particle size changes. This means the catalyst surface structure changes. If the turnover rates changes as the catalyst surface structure changes, then the reaction is structure sensitive. Turnover rate is commonly used as the quantitative

measure for comparison of catalyst performance. Thus, it is necessary to specify whether the reaction is structure sensitive before comparing the turnover rate.

Baldwin and Burch [24] found a change in turnover rate (TOR) of two orders of magnitude on a series of catalysts with no correlation between particle size and TOR. The catalysts used in their study were prepared from two different kinds of palladium sources: palladium chloride and palladium nitrate. Comparing TOR on those catalysts is not sound as chlorine, which was deposited during catalyst preparation, could inhibit the rate of methane oxidation[41]. Hicks *et al.* [20, 41] reported higher TORs on catalysts with larger Pd particles. They found that during experiments small Pd crystallites were completely oxidized, while large crystallites were partially oxidized. The completely oxidized palladium dispersed over the alumina as PdO, while the partially oxidized palladium was broken into smaller crystallites which were covered with a layer of oxygen. Based on these results, the authors suggested that the palladium oxide dispersed over the alumina was much less active than the oxide covering the FCC palladium crystallites. Garbowski *et al.* [42] proposed that crystal planes with low atom density, like Pd(110) and Pd(100), were able to form PdO in a near epitaxial structure with the sublayer metal. If the metal itself is also in epitaxy with the support, there is no need for reorganization of the sublayer metal structure. On the other hand, for planes with high atom density, such as Pd(111) plane, are not related to a square structure, thus catalytic activity, (i.e., oxidation and reduction of the surface) cannot occur without profound metal reorganization. Ribeiro *et al.* [8] found that for catalysts with different supports and prepared with different metal precursors, the rates were the same with particles ranging from 2 nm to 110 nm. Fujumoto *et al.* [15] found a "weak" structure sensitivity

on Pd/ZrO2 as particle size varied from 3 to 10 nm. Muller *et al.* [45, 71] found that TOR on Pd/ZrO_2 with palladium particle size of 12 nm was about 5 times the TOR on Pd/ZrO_2 with palladium particle size of 6 nm.

In general, most of the experiments to address this issue have been carried out on supported catalysts. However, supported catalysts are not ideal systems in this case because multiple factors, such as particle size, interaction with support, deactivation by impurities, spreading of oxide and measurement of support area, can affect the rate substantially and are difficult to identify individually. Another key issue did not get touched on in previous studies is the reaction sensitivity on palladium metal. Studying methane oxidation on palladium metal requires high temperatures so that metal state could be maintained under reaction conditions.

This study addressed the sensitivity issue using palladium single crystals and polycrystalline palladium foil under both oxide and metal states. The results on single crystals were straightforward because the structure of the metal could be modified by changing the low Miller index plane exposed on the catalyst and there was no support effect. Polycrystalline palladium foil was used as comparison standard because its surface was composed of various planes. This method has been effectively used to identify the structure sensitive reaction of ammonia synthesis on iron catalysts and rhenium catalysts [123, 124]. The surface during methane oxidation could be PdO or Pd metal, depending on the oxygen pressure and the reaction temperature; therefore, both phases need to be studied.

6.2 Experimental Methods

The experiment system includes a methane combustion reactor and an ultrahigh vacuum (UHV) surface analysis chamber. The reactor could be operated under either a batch mode or a continuous-stirred tank (CSTR) mode. At low temperatures, a batch mode was employed so that CO_2 could accumulate inside the reactor to reach a high enough concentration to be monitored using GC detector. At high temperatures, experiments were performed under CSTR mode to avoid total consumption of methane due to the high reaction rate. For batch reactor mode, the reaction gases were introduced into the reactor cell from a gas manifold in the order of (H_2O), N_2, O_2 and CH_4. The reaction mixture was well mixed after 25 min circulation before the reaction started. For CSTR mode, the reaction gases were mixed before entering the reactor cell. Desired gas concentrations in reactor were obtained by adjusting flow rate of different gases using mass flow controllers. In order to eliminate external mass transfer limitation, the reaction mixture was circulated in the reactor using gas circulation pumps (Metal Bellows, MB-21), and the circulation rate was adjusted using an adjustable valve. The maximum flow rate could reach 4600 ml min^{-1}.

The palladium catalysts used for catalytic CH_4 combustion in this research were polycrystalline foil (Alfa Aesar, 99.9%) and single crystals Pd(111), Pd(110) (both Princeton Scientific Corp., 1 mm thickness x 8.5 mm diameter, mis-alignment < 0.5^o), and Pd(100) (Accumet Materials Co. 1 mm thickness x 8.5 mm diameter, mis-alignment < 0.5^o). These catalysts were held on the cart by two power pins. Electric current was applied through the power pins to resistively heat the sample. Sample temperature was

measured by an alumel-chromel thermocouple spot-welded on the back of the foil or on the side of the single crystals. Automatic control of the sample temperature was achieved by interfacing temperature controller (Eurotherm Model 2408) with TCR DC power supply (Electronic Measurements Inc). An infrared lamp was mounted outside the reactor, facing the viewport on the reactor. Infrared light generated could go through the glass viewport and be focused on the catalyst. Catalysts were heated up using both IR heating and resistive heating. The gas phase composition was analyzed using a HP 6890 series gas chromatograph equipped with a 15-ft Carbonxen 1000, 60/80 mesh column, and a thermal conductivity detector.

The UHV analysis chamber was equipped with a double-pass cylindrical mirror analyzer (PHI Model 15-255G) used for X-ray Photoelectron Spectroscopy (XPS), a 15 kV double-anode X-ray gun (PHI 4-548), a UTI-100C quadrupole mass spectrometer, a OCI Low Energy Electron Diffraction analyzer (LEED) and a sputtering gun. The X-ray gun was performed using Alk_α (1486.6 eV) radiation at a power of 300 W. Survey spectra on XPS were recorded using analyzer pass energy of 100 eV; whereas, on the core level measurement the analyzer pass energy was 50 eV. The temperature programmed desorption (TPD) analysis was performed at a constant heating rate of 5 K s^{-1}. A Labview program was designed to monitor the desorption species. Catalysts could be transferred between the CH_4 combustion reactor and the UHV analysis chamber without being exposed to air by means of a transfer arm sealed inside a metal bellow. Thus, the surface details could be studied before and after reactions without contamination from air.

Cleaning of the fresh Pd catalysts consisted of two steps, namely methane combustion under high temperature and Ar^+ ion sputtering. The fresh palladium foil was treated by methane combustion at 773 K for 100 minutes with 4.5 Torr CH_4, 18 Torr O_2 and inert gases (He and N_2) balanced to atmospheric pressure. The oxidized foil was then sputtered by 2 keV Ar^+ followed by annealing at 873 K for 1 minute in vacuum. The single crystals were first treated by methane combustion at 673-723 K for more than one hour with reactant mixture of 1.7 Torr CH_4, 7 Torr O_2 and inert gases balanced to atmospheric pressure. The oxidized crystals were then sputtered by 2.0 keV Ar^+ followed by annealing at 873 K for 1 min. These cleaning procedures have proven to be effective to remove the impurities from the near surface region of the catalysts. Before each independent experiment, the sample was sputtered by 2.0 keV Ar^+ ions and then annealed at 873 K for 1 minute under UHV conditions to resume the surface structure.

Except notation, the turnover rate was calculated using the geometric Pd metal surface area assuming an average Pd surface atom density of $1.27*10^{15}$ atom cm^{-2} on polycrystalline foil [48], $1.53*10^{15}$ atom cm^{-2} on Pd(111), $0.94*10^{15}$ atom cm^{-2} on Pd(110) and $1.34*10^{15}$ atom cm^{-2} on Pd(100) . The surface area should not change or change slightly with the variation of temperature for activation energy measurement or the variation of reactant concentration for reaction order measurement. Thus, using geometric Pd metal surface area was feasible to measure reaction orders and activation energies.

The surface morphologies of Pd oxide were studied by scanning-tunneling microscopy (STM). The experiments were carried out in a specially designed system consisting of

three stainless steel chambers: an Ultra-High Vacuum (UHV) analysis chamber, a UHV STM chamber and a high-pressure reaction cell. The catalytic CH_4 combustion reaction was carried out in the reaction cell in batch reactor mode. The single crystals were mounted on a standard RHK sample holder (RHK, Inc.). The temperature was measured by a chromel-alumel thermocouple spot-welded onto the side of the sample. An infrared lamp was mounted outside the reaction cell to heat up the single crystal catalyst sample by focusing the infrared light onto the surface of the single crystals. A Eurotherm 2408 temperature controller controlled the power output to the lamp based on the temperature reading from the catalyst. STM images were obtained in UHV at ambient temperature using home-made Pt/Ir tips. The catalyst sample was scanned at a bias voltage of 0.1-1 V and tunneling current of 0.1-1 nA.

6.3 Experimental Results

6.3.1 System Test

A stainless steel foil with similar geometric surface area as Pd foil or single crystals was used to test background effect. The turnover rate was less than 0.15 s^{-1} compared with the turnover rate of 9.3 s^{-1} on Pd foil under conditions of 6 Torr O_2, 1.5 Torr CH_4, and at 1023 K. Therefore, the contribution from background was less than 2%.

To obtain kinetics data, the experiment must be free of mass and heat transfer limitation. The catalysts were non-porous solid metal, so there was no internal mass and heating transfer limitation. The temperature of catalyst was automatically controlled by external

heating system, so the system was free of external heat transfer limitation. The only concern in this system was external mass transfer limitation. Figure 6-1 shows the methane conversion as function of gas circulation rate. The results indicated that under the test conditions, there was no external mass transfer limitation when the circulation rate was higher than 3800 cc min^{-1} since methane conversion did not increase any more when the circulation rate was above this level. The circulation rate was higher than 3800 cc min^{-1} during experiment, so no mass transfer limitation was involved in the experiment results

6.3.2 Constancy of Single Crystal Surface Structure

Figure 6-2 demonstrates the arrangement of surface atoms on the palladium single crystals with the simplest orientations, and Figure 6-3 shows corresponding LEED patterns obtained on the three single crystals used in this study. The LEED patterns were consistent throughout the study once the samples were cleaned.

6.3.3 Surface Area Measurement

The oxygen coverage on Pd single crystals was calibrated by assuming that exposure of Pd(111) to O_2 at room temperature would form an oxygen overlayer with 0.25 ML saturated coverage [11, 12]. The TPD spectrum after 0.25 ML adsorption on Pd(111) did not show oxygen desorption in our system. The amount of oxygen corresponding to 0.25 ML was calculated from the desorption of $H_2{}^{18}O$, $C^{18}O$, $C^{16}O^{18}O$ and $C^{18}O_2$ after adsorption of $^{18}O_2$ at room temperature. The carbon or hydrogen might come from

hydrocarbon species deposited on the surface from the environment and carbon dissolved into the crystals during methane oxidation.

The calibration of oxygen coverage on Pd(100) and Pd(110) was derived from the results on Pd(111). The following equation demonstrates the way to get the calibration of oxygen coverage on Pd(100) surface.

$$M_{100} = \frac{\mathrm{D}_{100}}{\mathrm{D}_{111}} * \frac{A_{100}}{A_{111}} M_{111}$$

Where M_{abc} is the integral area of O_2 desorption peak corresponding to 1 ML coverage on the surface of Pd(abc) crystal

D_{abc} is the atom density on the surface of Pd(abc) crystal

A_{abc} is the geometric surface area of Pd(abc) single crystal

The calibration on Pd(110) was obtained following the same derivation.

After methane oxidation, the PdO surface area was measured by a surface exchange experiment with labeled oxygen (^{18}O isotope), which was performed by exposing the oxidized catalyst to 5 Torr $^{18}O_2$ at 598 K for 12 seconds. These conditions are chosen based on results from Au-Yeung *et al.* [49] to ensure the exchange between ^{16}O in PdO and $^{18}O_2$ isotope mostly occur at the surface, without appreciable diffusion into the bulk.

The oxygen uptake was calculated from the desorption of $^{18}O_2$, $^{16}O^{18}O$, $H_2{}^{18}O$, $C^{18}O$, $C^{16}O^{18}O$ and $C^{18}O_2$.

The surface area was also measured using STM images. The method using STM images relies on the generation of the surface topographic image by STM. Therefore, it can be used for samples that are conductive and can be outlined by the microscope tip. The surface area was then calculated by taking discrete image pixels and joining them using a series of triangles. Integration of the area of individual triangles gives the total area.

The results of the surface area measurement on palladium after oxidation in O_2 and catalytic combustion of a lean CH_4 mixture (O_2:CH_4=10:1) at 600 K are summarized in Table 6-2. The two proposed methods, integration of STM data and ^{18}O exchange, agreed within ±20%.

6.3.4 Structure Sensitivity of Reaction on Oxide Phase

Single crystals of PdO with different orientations are not commercially available. Considering PdO in real catalysts is created by oxidizing the Pd particles which are composed mainly by facets of (111), (100) and (110), the oxide in this study was obtained by oxidizing the surface of the three crystals which should give the same PdO surface structure as on the corresponding facet in real catalysts. The kinetic data obtained on PdO, including turnover rates, reaction orders and activation energies, were measured in a batch mode. By assuming reaction order of 1 for CH_4, -1 for H_2O, 0 for O_2 and CO_2,

the methane conversion (X) has linear relationship with the square of time (t) in batch reactor [10].

$$X = C * t^2$$

The rate constant could be derived from the slope C, and then the turnover rate under certain reaction conditions was calculated.

Figure 6-4 presents the comparison in XPS Pd 3d region taken from a clean Pd(111), a Pd(111) after 130 minutes methane oxidation at 598 K and a Pd(110) after 130 minutes methane oxidation at 598 K. The clean Pd(111) is characterized by the Pd $3d_{5/2}$ peak at 335.0 eV, which is in good agreement with the one in the literature [53]. For Pd(111) after 130 minutes methane oxidation, the Pd $3d_{5/2}$ peak shifted to a higher binding energy by *ca*. 1.8 eV with new position at 336.8 eV, characteristic of PdO [53]. The Pd $3d_{5/2}$ peak obtained on Pd(111) after methane oxidation did not show broadening compared with the Pd $3d_{5/2}$ peak obtained on clean Pd(111), indicating that the major compound in the surface region was PdO. For Pd(110) after methane oxidation, broadening of Pd $3d_{5/2}$ peak was observed at lower binding energy region. The broadening was contributed by a palladium metal peak, indicating that Pd metal was in the detectable range and the oxide formation on Pd(110) was slower than on Pd(111). To know how faster the oxidation process was on the Pd(111), XPS analysis was performed on Pd(111) after methane oxidation for 10 minutes. Comparing with the Pd $3d_{5/2}$ peak for Pd(110) after 130 minutes methane oxidation, the broadening was much smaller for the Pd $3d_{5/2}$ peak obtained on Pd(111) only after 10 minutes methane oxidation (Figure 6-5). It was

unknown whether the metal in the near surface region would affect the methane oxidation rate. To compare the kinetics on PdO phas, Pd(110) was first oxidized at 700 K in 160 Torr O_2 for 30 minutes before the methane oxidation experiment started. No peak broadening was observed from the XPS after pre-oxidation, indicating that the only compound in the near surface region was PdO. No pre-oxidation was performed on Pd(100) before methane oxidation as the rate of PdO formation on Pd(100) was close to the rate on Pd(111).

The reaction orders for CH_4, O_2 and H_2O were measured on three single crystals at 598 K and the activation energy was measured at temperature between 558 K and 623 K. Figure 6-6 and Figure 6-7 gives an example of reaction orders and activation energy on Pd(110). Each turnover rate on the figure corresponds to one individual experiment in the batch reactor. Before each individual experiment, the sample was sputtered and then annealed at 973 K for 1 min. The reaction orders and activation energies were summarized in Table 6-1. The PdO surface area and the turnover rates were summarized in Table 6-2.

6.3.5 Surface Morphology on Oxide phase

The surface morphology of oxidized single crystals was studied by STM after methane oxidation at 598 K for 60 minutes. The oxide phase on three single crystals presented qualitatively similar surface structure with the formation of amorphous or polycrystalline PdO (Figure 6-8). This conclusion was also supported by LEED, which did not show spots except for bright background. The oxide clusters were in “semi-spherical

cauliflower" shape and 10-30 nm in diameter. It is difficult to tell whether the oxide clusters grew along any preferential direction due to the aggressive roughening of the surface.

6.3.6 Structure Sensitivity of Reaction on Metal Phase

The turnover rates, reaction orders and activation energies were measure on Pd metal under CSTR mode on Pd foil, Pd(111), Pd(100) and Pd(110). The metallic state was confirmed by XPS after quenching the sample inside the reaction mixture (Figure 6-9). During the quenching, temperature decreased from 907 K to 600 K in 30 seconds, and to 520 K in 60 seconds, and then slowly cooled down to room temperature.

The kinetic results on Pd metal were summarized in Table 6-1. Generally, the reaction orders and the activation energy are almost the same on the three single crystals and the palladium foil. Reaction order is 0.7 for CH_4, 0 for O_2 and –1 for H_2O, and activation energy is in the range of 125 $kJ \cdot mol^{-1}$ to 140 $kJ \cdot mol^{-1}$. After correcting to 2.3 Torr O_2, 0.46 Torr CH_4 and 0.05 Torr H_2O, the turnover rate was 1.3 s^{-1} on Pd foil [10], 2.8 s^{-1} on Pd(111), 2.0 s^{-1} on Pd(110) and 2.2 s^{-1} on Pd(110) as shown in Table 6-2. The surface area under reaction conditions was assumed to be identical to the geometric surface area of the clean metal phase.

6.4 Discussion

The constancy of LEED patterns throughout the study indicates that the original surface structure of the three single crystals could be restored even after surface reconstruction during methane oxidation.

The turnover rates obtained in this study on model catalysts are generally higher than the turnover rates reported in the literature on supported catalysts and palladium black (Table 6-3). For the model catalysts without initial cleaning procedure to remove the surface impurities, the turnover rate usually decreased to zero in 1 hour under standard conditions (598 K, 160 Torr O_2 and 16 Torr CH_4). Therefore, surface impurities and support effect might be the reasons for the lower turnover rates reported in the literature.

6.4.1 Reaction Structure Sensitivity on Oxide Phase

The turnover rates on PdO were similar on all model catalysts studied after correcting to the same reaction conditions (Table 6-2). The similar turnover rates indicate that methane oxidation is not sensitive to the PdO which grew from metal surface with different orientations.

Only amorphous PdO was observed by STM in this study after methane oxidation (Figure 6-8). However, high resolution TEM (HRTEM) studies by Datye *et al.* [37] and Lyubovsky *et al.* [125] and In-situ Raman studies by Su *et al*. [126] suggested the simultaneous growth of crystalline PdO during catalytic CH_4 combustion. However, thin

layers of amorphous PdO was observed by HRTEM covering on the surface of PdO crystals [37, 125]. Su *et al.* [126] found that amorphous PdO formed at first, and then it transformed to crystalline PdO. The rate of transformation accelerated at higher temperatures. These results indicate that amorphous PdO was more readily formed than crystalline PdO, and the transformation from amorphous PdO to crystalline PdO had to overcome an activation barrier. This is reasonable by thinking the Pd atom density in the oxide is only 60% of the density in the metal structure and a major lattice expansion should occur during PdO formation. In summary, it could be possible that crystalline PdO was formed during methane oxidation, but was covered by a thin layer of amorphous PdO. In this case, STM could only reflect the amorphous layer, but HRTEM and Raman could detect the crystalline PdO in the sublayer. Since the structure of the surface PdO, not the bulk PdO, affects the methane oxidation, it becomes trivial to know whether there was crystalline PdO formed in the bulk. As long as the surface oxide is amorphous, the rate of methane oxidation would not be different on different metal substrate. Even if there were small domains of crystalline PdO on the surface that STM did not identify, theses PdO would not make major contribution to methane oxidation because the amount of defects was overwhelming comparing with the amount of crystalline PdO on the surface.

Garbowski *et al.* [42] proposed that crystal planes with low atom density, like Pd(110) and Pd(100), were able to form PdO in a near epitaxial structure with the sublayer metal. If the metal itself is also in epitaxy with the support, there is no need for reorganization of the sublayer metal structure. On the other hand, for planes with high atom density, such as Pd(111) plane, are not related to a square structure, thus catalytic activity, (i.e.,

oxidation and reduction of the surface) cannot occur without profound metal reorganization. This issue did not occur when the oxide was thermodynamic stable phase such as the case in this study. A thick layer of oxide was either formed in the first few minutes of reaction (Pd(111) and Pd(100)), or created before reaction (Pd(110)). The methane oxidation afterwards was performed on thick amorphous oxide instead of monolayer PdO on top of Pd crystal. When such thickness of PdO on top of metal phase, the lattice structure advantages of Pd(110) and Pd(100) do not exist any more.

6.4.2 Reaction Structure Sensitivity on Metal Phase

The turnover rates on Pd metal phase are close to each other after corrected to same conditions (Table 6-2), indicating that methane oxidation is not sensitive to the original metal surface orientations.

Here we use Pd(110) as an example to calculate what species could be on the surface during reactions. For the heat of O_2 adsorption on Pd(110), Ertl *et al.* [58] reported 80 kcal mol^{-1} when the coverage reached some point where LEED image gave a (1x3) pattern; 77 kcal mol^{-1} for a (1x2) pattern; 62 kcal mol^{-1} for a c(2x4) pattern and 48 kcal mol^{-1} for a c(2x6) pattern. The heat of adsorption was obtained using Clausius-Clapeyron equation assuming a LEED pattern corresponds to same saturated oxygen coverage at different temperatures. A saturated coverage of 0.23 ML was reported for the (1x3) LEED pattern [59] and 0.48-0.5 ML for c(2x4) LEED pattern [59, 60]. Jo *et al.* [61] believed that the (1x3) and (1x2) LEED patterns observed by Ertl *et al.* [58] corresponds to the streaky pattern they observed with coverage between (2x3)-1D and c(2x4). A

coverage of 0.2 ML for the (2x3)-1D pattern and a coverage of 0.3 ML were reported for the streaky pattern [62]. For Ni(110), which has the same crystal structure and has the same surface atom orientation as Pd(110), a coverage of 0.33-0.35 ML was reported for the (2x1) pattern [63, 64]. Considering the same LEED patterns correspond to same saturated coverage of oxygen as long as the single crystals have the crystal same structure and surface orientation, the streaky LEED pattern reported on Pd(110) might be the (1x2) pattern observed by Ertl *et al.* [58]. Thus, the coverage of 0.3 ML for the streaky pattern could be used for the corresponding oxygen coverage for (1x2) LEED pattern. The c(2x6) LEED pattern was observed in our lab with the coverage in the range of 0.6-0.7 ML. On Rh(110), the oxygen coverage for the structure of c(2x2n) (n=3, 4 and 5) was proposed to be (n-1)/n [65], which agrees well with experimental results. Considering Rh(110) and Pd(110) have same crystal structure and surface orientation, the c(2x6) on Pd(110) should correspond to the same oxygen coverage of 0.67 ML. In summary, the heat of adsorption at corresponding coverage is 80 kcal mol^{-1} at 0.23 ML, 77 kcal mol^{-1} at 0.30 ML, 62 kcal mol^{-1} at 0.50 ML and 48 kcal mol^{-1} at 0.67 ML. With those four sets of data, the equilibrium pressure at our experiment temperature (973 K) with certain oxygen coverage could be obtained using Clausius-Clapeyron equation. Using empirical equation of Freundlich, the equilibrium oxygen pressure was found to be 0.8 Torr for 1 ML coverage at 973 K by extrapolating from the available equilibrium pressure at other coverage. Thus, from the thermodynamic point of view, the surface of Pd(110) should be mostly covered by adsorbed oxygen at 973 K when exposing to 2.3 Torr O_2.

One concern is whether the oxygen adsorption rate could surpass the methane adsorption rate under reaction conditions so that thermodynamically favored situation mentioned above could be reached. At temperature between 273 K and 673 K, the sticking probability of oxygen on Pd(110) was about 1 at zero coverage, and dropped to 0.1 at coverage about 0.5 ML [66]. The sticking probability at 973 K with coverage less than 0.5 ML was found greater than 0.1 by extrapolating the sticking probability at lower temperature. The initial sticking probability of methane on Pd(110) was found to increase exponentially with the average translational energy of methane which was calculated as:

$$E = \frac{m_h}{\overline{M}} \overline{C}_p T_g$$

Where m_h is the molecular mass of heavy species, $\overline{C}_p$ is the average heat capacity of the gas mixture, and $\overline{M}$ is the average molecular mass of the gas mixture[67, 68]. Meanwhile, The initial sticking probability was also found to increase strongly with methane molecule vibrational energy, but increase weakly with solid phase temperature [67-69]. The gas phase temperature during experiment could not be precisely determined but was estimated in the range between 600 K and 973 K. The average translational energy was then between 22 kJ mol^{-1} and 31 kJ mol^{-1} based on the fact that N_2 was the majority composition of gas mixture (>90 vol%) and also the heavy species. The initial sticking probability was, therefore, in the range of $3*10^{-4}$ to $3*10^{-3}$ assuming it did not change with solid phase temperature. The sticking probability of methane on Pd(110) decreased linearly with oxygen coverage [68],

$$S_{tot}(\theta_0) = S_{0,tot}(1 - \alpha\theta_0)$$

Where α has value about 2.3

S_{tot} is the sticking probability of methane at oxygen coverage of θ_0

$S_{0,tot}$ is the sticking probability of methane at oxygen coverage of 0

Based on these facts, the sticking probability of oxygen should be at least two orders of magnitude higher than the sticking probability of methane even with 0.5 ML oxygen coverage. Though the sticking probability of oxygen continues to drop as coverage increases, the large difference between the sticking probability of oxygen and methane indicate that oxygen adsorption rate should still surpass methane adsorption rate at a oxygen coverage higher than 0.5 ML. Thus, from the kinetic point of view, the Pd(110) surface should be mostly covered by adsorbed oxygen under reaction conditions. The similar turnover rates on the three single crystals and the Pd foil indicate that the same situation occurred on the surface of the other single crystals and the Pd foil.

Methane dissociation is regarded as the rate-determining step for methane oxidation on metal phase. Since methane oxidation is structure insensitive to the original surface orientation, methane dissociation should be structure insensitivity to the original surface orientation. Methane dissociation on clean metal Pd was reported as structure sensitive reaction [67, 68, 127-129]. Calculation showed that the dissociation barrier for $CH_4 \rightarrow CH_3+H$ is 0.66eV for flat Pd(111), 0.38eV for step on Pd(111) and 0.41 for kink on Pd(111)[129]. Since the metal surface was covered by adsorbed oxygen under reaction conditions, methane dissociation should occur predominantly on Pd sites bonded with oxygen instead of bare metal sites, which agrees with the reaction order of near zero for oxygen. Oxygen adsorption on palladium single crystals could modify the surface structure at low temperature [50, 112]. The similar turnover rates on Pd(111), Pd(100)

and Pd(110) indicate that modified surfaces have the same chemical properties toward methane dissociation.

6.5 Conclusion

Catalytic methane oxidation on palladium was insensitive to the original surface orientation, when both PdO and Pd metal were the thermodynamic stable phases. Study of the oxide surface morphology by STM revealed qualitatively similar surface structure with the formation of amorphous PdO even though the initial metal structure of Pd(111), Pd(100) and Pd(110) was quite different, which explains the similar turnover rates on the oxide which grew from different crystal phases. Estimated calculation suggests that under reaction conditions, the metal phase should be fully covered by chemisorbed oxygen. The oxygen-covered surface should have the same chemical properties for methane oxidation, even though the underneath crystal structure is different.

Table 6-1

(a) Activation Energy for Catalytic Methane Combustion

Catalyst	On PdO		On Pd	
	Temp Range (K)	Ea (kJ mol^{-1})	Temp Range (K)	Ea (kJ mol^{-1})
Pd foil	558-623	125	933-1003	125
Pd(111)	558-623	136	928-978	127
Pd(100)	558-623	121	928-978	127
Pd(110)	558-623	154	928-978	140

(b) Reaction Orders for Catalytic Methane Combustion

Catalyst	On PdO				On Pd			
	Temp	Reaction Orders			Temp	Reaction Orders		
	(K)	CH_4	O_2	H_2O	(K)	CH_4	O_2	H_2O
Pd foil	598	0.7	0.2	-0.9	973	0.7	0.0	0.0
Pd(111)	598	0.7	0.0	-1.1	953-973	0.7	-0.15	0.0
Pd(100)	598	0.8	0.1	-0.1	953	0.9	0.0	0.0
Pd(110)	598	0.7	0.26	-1.0	953-973	0.9	-0.1	0.0

Table 6-2: **Turnover Rates on Model Catalysts**

Catalyst	On PdO			On Pd
	Surface Area by $^{18}O_2$ exchange (cm^2/cm^2)	Surface Area by STM (cm^2/cm^2)	TOR[a] (s^{-1})	TOR[b] (s^{-1})
Pd foil	2.2	N/A	2.5	1.3
Pd(111)	2.6	3.2	2.8	2.8
Pd(100)	2.0	2.2	4.7	2.0
Pd(110)	1.9	1.6	1.3	2.2

[a]corrected to 598 K, 160 Torr O_2, 16 Torr CH_4 and 1 Torr H_2O

[b]corrected to 973 K, 2.3 Torr O_2, 0.46 Torr CH_4 and 0.05 Torr H_2O

Table 6-3 Summary of Turnover Rates from Literature

Catalyst	Particle Size (nm)	Activation Energy[a] (kJ mol^{-1})	Reaction Order			TOR[b] (s^{-1})	Reference
			CH_4	O_2	H_2O		
Pd black	10	135	0.7	0.1	-0.8	0.5[d]	[10]
Pd/Si-Al_2O_3	2.6-6.2	170-184	-	-	-1.0	0.1[e]	[8]
Pd/Al_2O_3	49-134	150	-	-	-	0.07-0.16[e]	[8]
Pd/ZrO_2	4.3-81	170	-	-	-	0.1-0.7[e]	[8]
Pd/ZrO_2	3-9	185	1.1	0.1	-1.0	0.5-3.0[e]	[43]
Pd/ZrO2	5.5-12.5	N/A	-	-	-	0.3[e]	[45, 71]

[a] Assuming reaction order for water is –1, the activation energy was corrected for the water inhibition effect.

[b]TOR calculated at 598 K, 16 Torr CH_4, 1 Torr H_2O, and N_2 balanced to 800 Torr. Reaction orders were assumed to be 1 for CH_4, 0 for O_2 and –1 for H_2O

[c]Surface area measured from $^{18}O_2$ exchange

[d]Number of sites measured from BET surface area (47 m^2g^{-1})

[e] For plug flow reactor, partial pressures for reactants and products are the average of values of inlet and exit concentration

Figure Captions:

Figure 6-1 Methane conversion as a function of reactants circulation rate at 863 K with 1.5 Torr O2, 0.38 Torr CH4 and inert gases balanced to atmospheric pressure

Figure 6-2 Schematic Drawing of Atom Orientation on (a)Pd(111) (b)Pd(100) (c)Pd(110)

Figure 6-3 LEED patterns for (a) bare Pd(111) surface (b) bare Pd(100) surface (c) bare Pd(110) surface

Figure 6-4 XPS core level scan on clean Pd(111), Pd(111) and Pd(110) after methane oxidation at 598 K for 130 minutes

Figure 6-5 XPS core level scan of Pd3d5 after methane oxidation at 598 K

Figure 6-6 Reaction Order dependence for Pd(111) on methane (10-32 Torr CH4, 160 Torr O2, N2 balanced to 800 Torr), oxygen (80-320 Torr O2, 16 Torr CH4, N2 balanced to 800 Torr), and water (4-8 Torr H2O, 160 Torr O2, 16 Torr CH4, N2 balanced to 800 Torr)

Figure 6-7 Arrhenius plot for the combustion of CH4 over Pd(110) at 16 Torr CH4, 160 Torr O2 and N2 balanced to 800 Torr. The apparent activation energy was 150 kJ mol-1

Figure 6-8 STM images of (a) Pd(111) after CH4 oxidation in 16 Torr CH4, 160 Torr O2 and 624 Torr N2, at 600 K for 60 min. (b) Pd(110) after CH4 oxidation in 16 Torr CH4, 160 Torr O2 and 624 Torr N2, at 600 K for 60 min. (c) Pd(100)

after CH4 oxidation in 16 Torr CH4, 160 Torr O2 and 624 Torr N2, at 600 K for 60 min. The sample bias is 0.1-1 V, the tunneling current is 0.5 nA

Figure 6-9 Comparison of XPS Pd3d core level scan of clean metal foil, foil after lean reaction at 903 K with 0.76 Torr O2, 0.15 Torr CH4 and inert gases (N2 and He) balanced to atmospheric pressure.

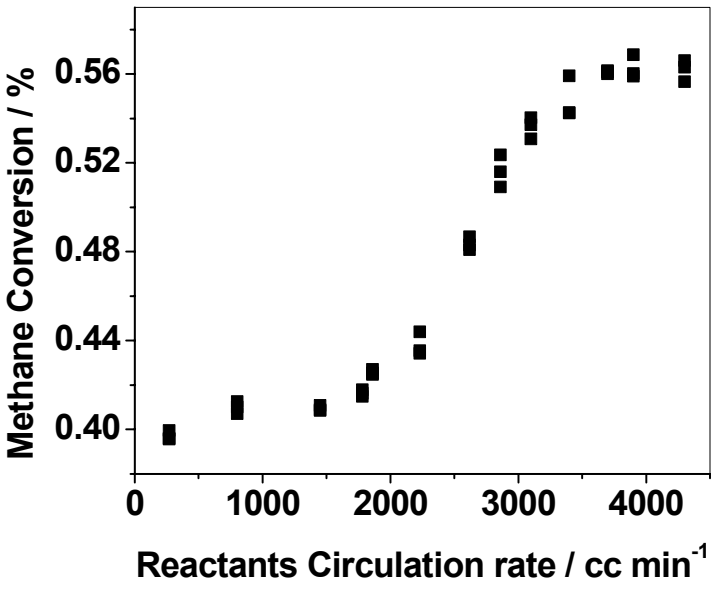

Figure 6-1 Methane conversion as a function of reactants circulation rate at 863 K with 1.5 Torr O_2, 0.38 Torr CH_4 and inert gases balanced to atmospheric pressure

(a) **(b)** **(c)**

Figure 6-2 Schematic Drawing of Atom Orientation on (a)Pd(111) (b)Pd(100) (c)Pd(110)

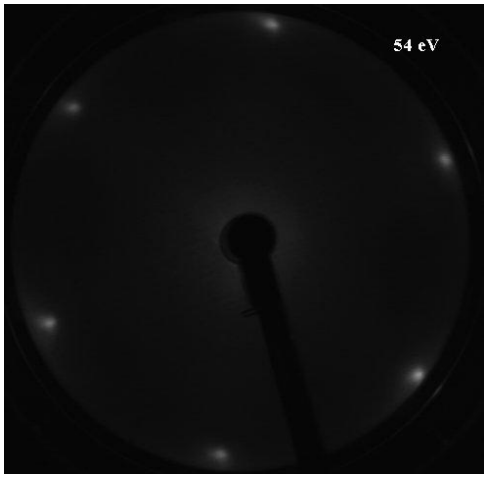

(a)

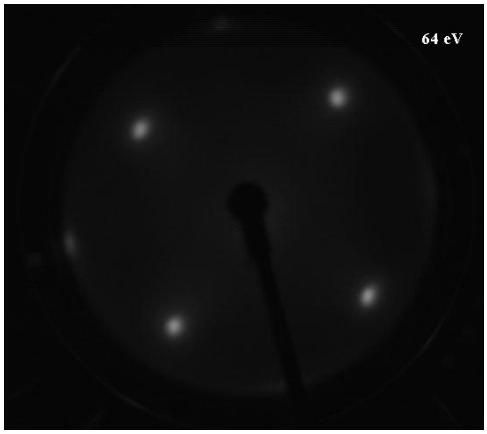

(b)

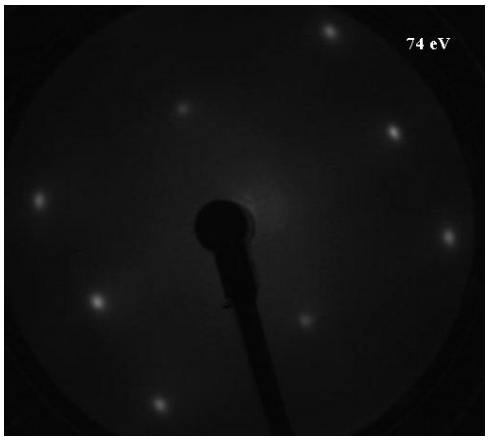

(c)

Figure 6-3 LEED patterns for (a) bare Pd(111) surface (b) bare Pd(100) surface (c) bare Pd(110) surface

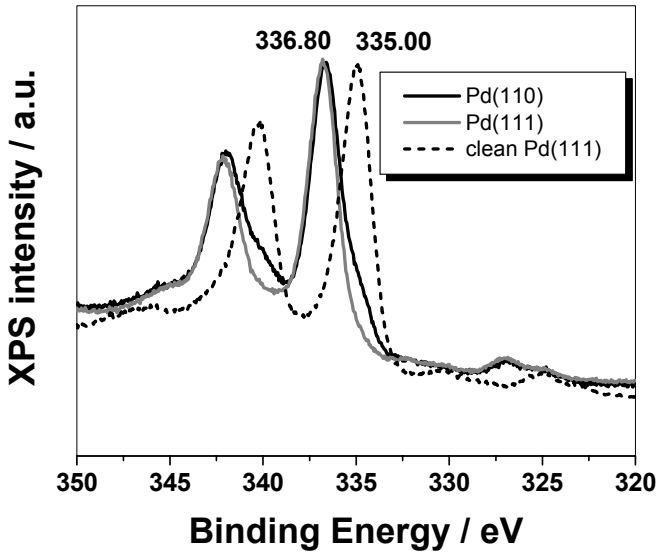

Figure 6-4 XPS core level scan on clean Pd(111), Pd(111) and Pd(110) after methane oxidation at 598 K for 130 minutes

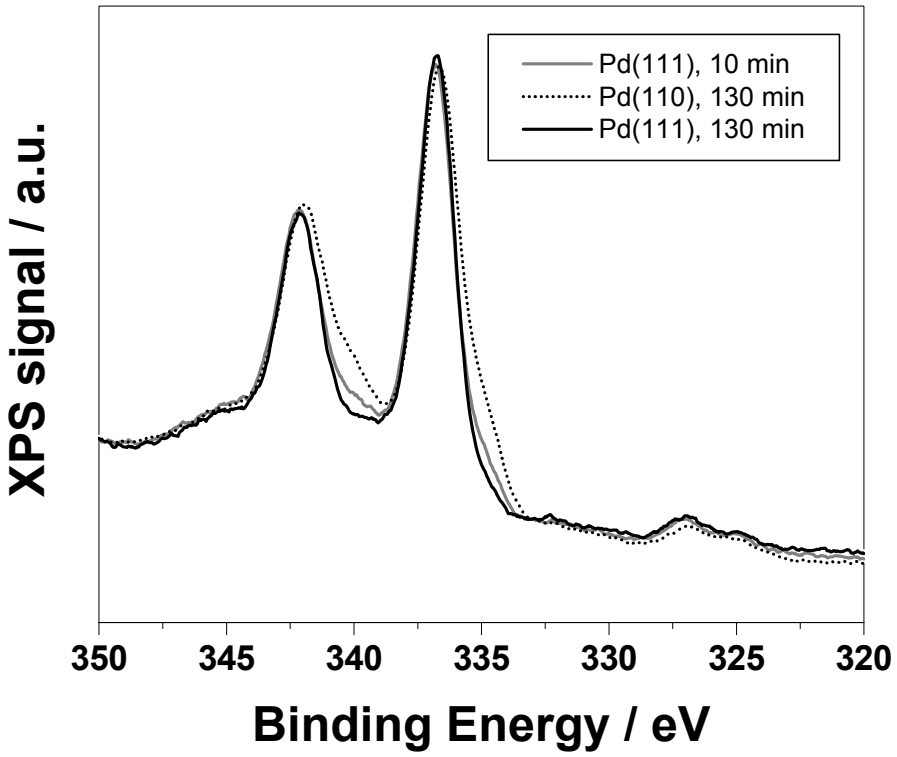

Figure 6-5 XPS core level scan of Pd3d5 after methane oxidation at 598 K

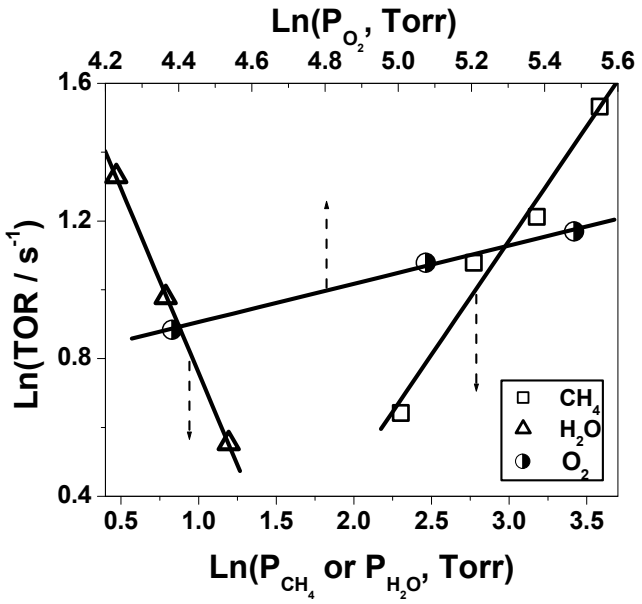

Figure 6-6 Reaction Order dependence for Pd(111) on methane (10-32 Torr CH_4, 160 Torr O_2, N_2 balanced to 800 Torr), oxygen (80-320 Torr O_2, 16 Torr CH_4, N_2 balanced to 800 Torr), and water (4-8 Torr H_2O, 160 Torr O_2, 16 Torr CH_4, N_2 balanced to 800 Torr)

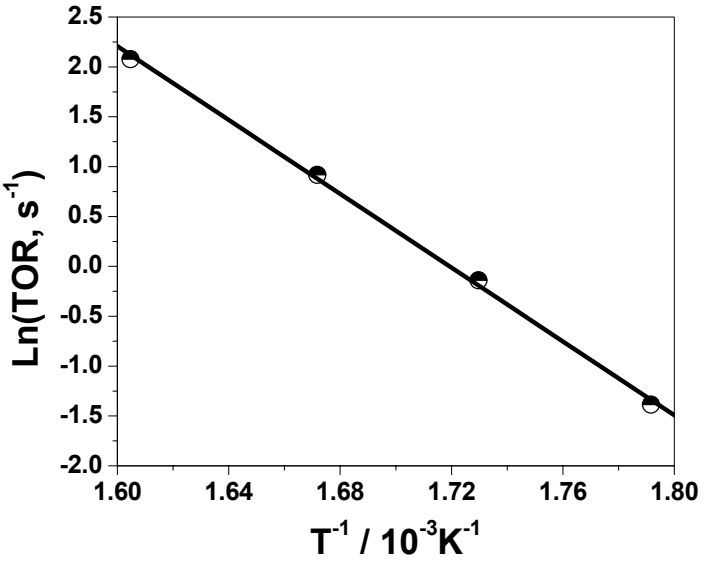

Figure 6-7 Arrhenius plot for the combustion of CH_4 over Pd(110) at 16 Torr CH_4, 160 Torr O_2 and N_2 balanced to 800 Torr. The apparent activation energy was 150 kJ mol^{-1}

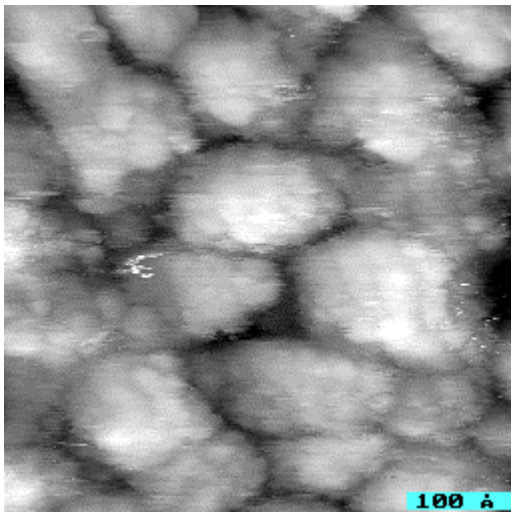

(a)

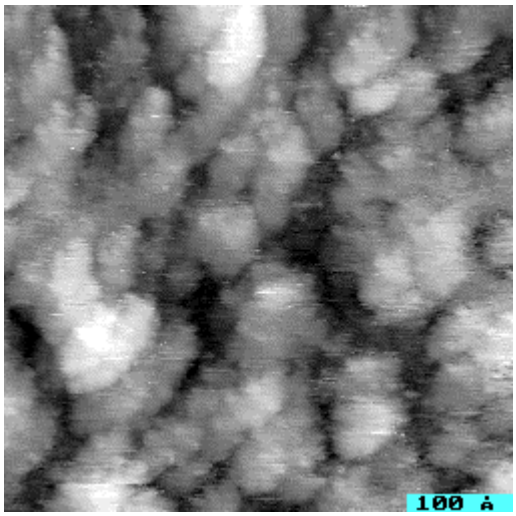

(b)

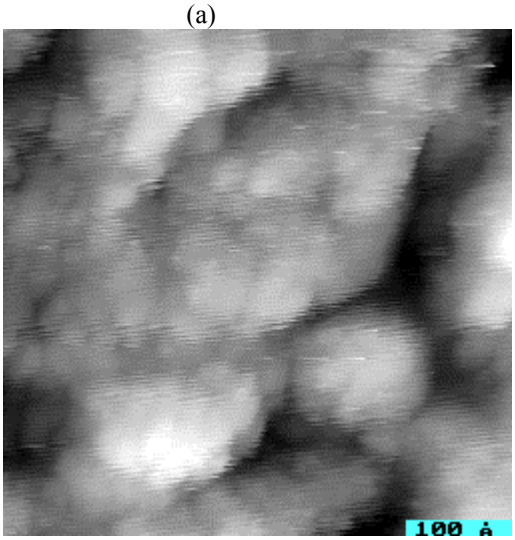

(c)

Figure 6-8 STM images of (a) **Pd(111) after CH_4 oxidation in 16 Torr CH_4, 160 Torr O_2 and 624 Torr N_2, at 600 K for 60 min.** (b) **Pd(110) after CH_4 oxidation in 16 Torr CH_4, 160 Torr O_2 and 624 Torr N_2, at 600 K for 60 min.** (c) **Pd(100) after CH_4 oxidation in 16 Torr CH_4, 160 Torr O_2 and 624 Torr N_2, at 600 K for 60 min. The sample bias is 0.1-1 V, the tunneling current is 0.5 nA**

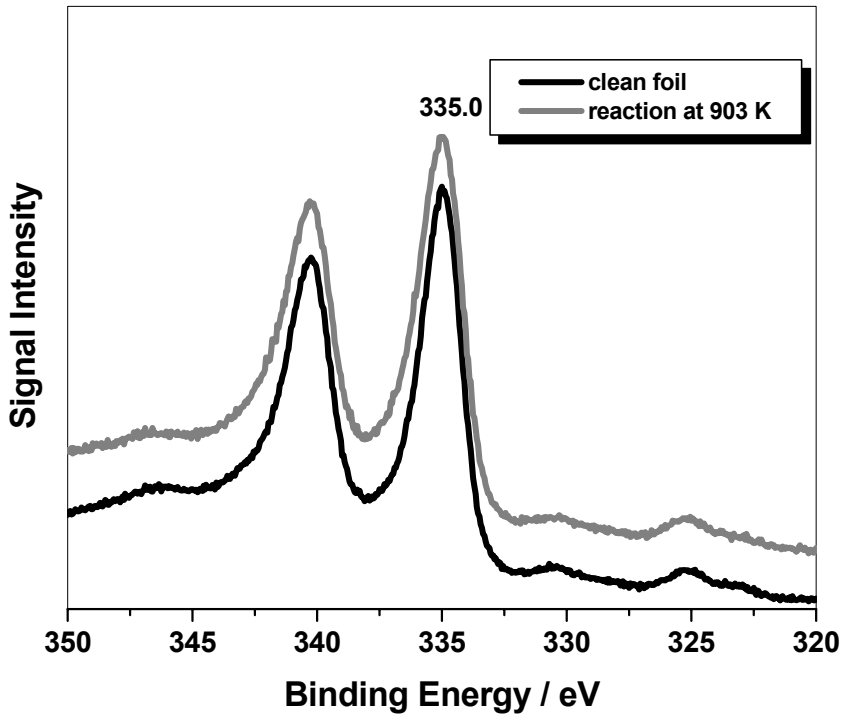

Figure 6-9 Comparison of XPS Pd3d core level scan of clean metal foil, foil after lean reaction at 903 K with 0.76 Torr O_2, 0.15 Torr CH_4 and inert gases (N2 and He) balanced to atmospheric pressure.

7 Reference

1. Ertl, G., Knozinger, H., and Weitkamp, J., *in "Environmental Catalysis."* Wiley-VCH, Weinheim, 1999, 236.
2. Dalla Betta, R. A., Schlatter, J. C., Yee, D. K., Loffler, D. G., and Shoji, T., *Catal. Today* **26**, 329 (1995).
3. Dalla Betta, R. A., and Rostrup-Nielsen, T., *Catal. Today* **47**, 369 (1999).
4. Forzatti, P., and Groppi, G., *Catal. Today* **54**, 165 (1999).
5. Anderson, R. B., Stein, K. C., Feenan, J. J., and Hofer, L. J. E., *Ind. Eng. Chem.* **53**, 809 (1961).
6. Kajita, S., and Dalla Betta, R., *Catalysis Today* **83**, 279 (2003).
7. Warner, J. S., *J. Electrochem. Soc.* **114**, 68 (1967).
8. Ribeiro, F. H., Chow, M., and Betta, R. A. D., *J. Catal.* **146**, 537 (1994).
9. Burch, R., Urbano, F. J., and Loader, P. K., *Appl. Catal., A* **123**, 173 (1995).
10. Monteiro, R. S., Zemlyanov, D., Storey, J. M., and Ribeiro, F. H., *J. Catal.* **199**, 291 (2001).
11. Hayes, R. E., Kolaczkowski, S. T., Li, P. K. C., and Awdry, S., *Chem. Eng. Sci.* **56**, 4815 (2001).
12. Cullis, C. F., Nevell, T. G., and Trimm, D. L., *J. Chem. Soc. Faraday Trans. I* **1**, 1406 (1972).
13. Cullis, C. F., and Willatt, B. M., *J. Catal.* **86**, 187 (1984).
14. Ahlstroem-Silversand, A. F., and Ulf Ingemar Odenbrand, C., *Appl. Catal., A* **153**, 157 (1997).
15. Fujimoto, K., Ribeiro, F. H., Iglesia, E., and Avalos-Borja, M., *Prepr. - Am. Chem. Soc., Div. Pet. Chem.* **42**, 190 (1997).

16. van Giezen, J. C., van den Berg, F. R., Kleinen, J. L., van Dillen, A. J., and Geus, J. W., *Catal. Today* **47**, 287 (1999).

17. Ciuparu, D., Katsikis, N., and Pfefferle, L., *Applied Catalysis A: General* **216**, 209 (2000).

18. Lyubovsky, M., and Pfefferle, L., *Appl. Catal., A* **173**, 107 (1998).

19. Lyubovsky, M., and Pfefferle, L., *Catal. Today* **47**, 29 (1999).

20. Hicks, R. F., Young, M. L., Lee, R. G., and Qi, H., *J. Catal.* **122**, 280 (1990).

21. Cullis, C. F., and Willatt, B. M., *J. Catal.* **83**, 267 (1983).

22. Baldwin, T. R., and Burch, R., *Appl. Catal.* **66**, 337 (1990).

23. Baldwin, T. R., and Burch, R., *Appl. Catal.* **66**, 359 (1990).

24. Baldwin, T. R., and Burch, R., *Catal. Lett.* **6**, 131 (1990).

25. Muto, K.-i., Katada, N., and Niwa, M., *Appl. Catal., A* **134**, 203 (1996).

26. Muto, K.-i., Katada, N., and Niwa, M., *Catal. Today* **35**, 145 (1997).

27. Mowery, D. L., Graboski, M. S., Ohno, T. R., and McCormick, R. L., *Appl. Catal., B* **21**, 157 (1999).

28. Euzen, P., Le Gal, J.-H., Rebours, B., and Martin, G., *Catal. Today* **47**, 19 (1999).

29. Augustine, S. M., Alameddin, G. N., and Sachtler, W. M. H., *J. Catal.* **115**, 217 (1989).

30. Briot, P., and Primet, M., *Appl. Catal.* **68**, 301 (1991).

31. Feuerriegel, U., Klose, W., Sloboshanin, S., Goebel, H., and Schaefer, J. A., *Langmuir* **10**, 3567 (1994).

32. Yu, T.-C., and Shaw, H., *Appl. Catal., B* **18**, 105 (1998).

33. Roth, D., Gelin, P., Primet, M., and Tena, E., *Appl. Catal., A* **203**, 37 (2000).

34. Hoyos, L. J., Praliaud, H., and Primet, M., *Appl. Catal., A* **98**, 125 (1993).

35. McCarty, J. G., *Catal. Today* **26**, 283 (1995).

36. Farrauto, R. J., Hobson, M. C., Kennelly, T., and Waterman, E. M., *Appl. Catal., A* **81**, 227 (1992).

37. Datye, A. K., Bravo, J., Nelson, T. R., Atanasova, P., Lyubovsky, M., and Pfefferle, L., *Appl. Catal., A* **198**, 179 (2000).

38. Groppi, G., Artioli, G., Cristiani, C., Lietti, L., and Forzatti, P., *Studies in Surface Science and Catalysis* **136**, 345 (2001).

39. Furuya, T., Sasaki, K., Hanakata, Y., Ohhashi, T., Yamada, M., Tsuchiya, T., and Furuse, Y., *Catal. Today* **26**, 345 (1995).

40. Lyubovsky, M., Smith, L. L., Castaldi, M., Karim, H., Nentwick, B., Etemad, S., LaPierre, R., and Pfefferle, W. C., *Catalysis Today* **83**, 71 (2003).

41. Hicks, R. F., Young, M. L., Lee, R. G., and Qi, H., *J. Catal.* **122**, 295 (1990).

42. Garbowski, E., Feumi-Jantou, C., Mouaddib, N., and Primet, M., *Appl. Catal., A* **109**, 277 (1994).

43. Fujimoto, K.-i., Ribeiro, F. H., Avalos-Borja, M., and Iglesia, E., *J. Catal.* **179**, 431 (1998).

44. Muller, C. A., Maciejewski, M., Koeppel, R. A., and Baiker, A., *J. Catal.* **166**, 36 (1997).

45. Muller, C. A., Maciejewski, M., Koeppel, R. A., and Baiker, A., *Catal. Today* **47**, 245 (1999).

46. Burch, R., and Urbano, F. J., *Appl. Catal., A* **124**, 121 (1995).

47. Farrauto, R. J., Lampert, J. K., Hobson, M. C., and Waterman, E. M., *Appl. Catal., B* **6**, 263 (1995).

48. Anderson, J. R., *in "Structure of Metallic Catalysts."*1975, 478 pp.

49. Au-Yeung, J., Bell, A. T., and Iglesia, E., *J. Catal.* **185**, 213 (1999).

50. Zheng, G., and Altman, E. I., *Surf. Sci.* **462**, 151 (2000).

51. Conrad, H., Ertl, G., Kueppers, J., and Latta, E. E., *Surf. Sci.* **65**, 245 (1977).

52. Monteiro, R. S., Zemlyanov, D., Storey, J. M., and Ribeiro, F. H., *J. Catal.* **201**, 37 (2001).

53. Wagner, C. D., Naumkin, A. V., Kraut-Vass, A., Allison, J. W., Powell, C. J., and Rumber, J. R. J. (NIST,

54. Au-Yeung, J., Chen, K., Bell, A. T., and Iglesia, E., *J. Catal.* **188**, 132 (1999).

55. Ciuparu, D., Altman, E., and Pfefferle, L., *J. Catal.* **203**, 64 (2001).

56. Mueller, C. A., Maciejewski, M., Koeppel, R. A., Tschan, R., and Baiker, A., *J. Phys. Chem.* **100**, 20006 (1996).

57. Ciuparu, D., and Pfefferle, L., *Catalysis Today* **77**, 167 (2002).

58. Ertl, G., and Rau, P., *Surface Science* **15**, 443 (1969).

59. Goschnick, J., Wolf, M., Grunze, M., Unertl, W. N., Block, J. H., and Loboda-Cackovic, J., *Surface Science* **178**, 831 (1986).

60. He, J. W., Memmert, U., Griffiths, K., and Norton, P. R., *Journal of Chemical Physics* **90**, 5082 (1989).

61. Jo, M., Kuwahara, Y., Onchi, M., and Nishijima, M., *Chemical Physics Letters* **131**, 106 (1986).

62. Tanaka, H., Yoshinobu, J., and Kawai, M., *Surf. Sci.* **327**, L505 (1995).

63. Smeenk, R. G., Tromp, R. M., and Saris, F. W., *Surface Science* **107**, 429 (1981).

64. Baro, A. M., Binnig, G., Rohrer, H., Gerber, C., Stoll, E., Baratoff, A., and Salvan, F., *Physical Review Letters* **52**, 1304 (1984).

65. Murray, P. W., Leibsle, F. M., Guo, Q., Bowker, M., and Thornto, G., *Physical Review B* **47**, 12976 (1993).

66. Yagi, K., Sekiba, D., and Fukutani, H., *Surface Science* **442**, 307 (1999).

67. Valden, M., Pere, J., Xiang, N., and Pessa, M., *Chem. Phys. Lett.* **257**, 289 (1996).

68. Valden, M., Pere, J., Hirsimaki, M., Suhonen, S., and Pessa, M., *Surf. Sci.* **377-379**, 605 (1997).

69. Hirsimaki, M., Paavilainen, S., JNieminen, J. A., and Valden, M., *Surf. Sci.*, 717 (2001).

70. Zhu, G., Han, J., Zemlyanov, D., and Ribeiro, F. H., *to be published*,

71. Mueller, C. A., Maciejewski, M., Koeppel, R. A., and Baiker, A., *J. Catal.* **166**, 36 (1997).

72. McCarty, J. G., Gusman, M., Lowe, D. M., Hildenbrand, D. L., and Lau, K. N., *Catal. Today* **47**, 5 (1999).

73. Lamber, R., Laeger, N., and Schulz-Ekloff, G., *J. Catal.* **123**, 285 (1990).

74. Juszczyk, W., and Karpinski, Z., *J. Catal.* **117**, 519 (1989).

75. Juszczyk, W., Lomot, D., Pielaszek, J., and Karpinski, Z., *Catal. Lett.* **78**, 95 (2002).

76. Crozier, P. A., Sharma, R., and Datye, A. K., *Microsc. Microanal.* **4**, 278 (1998).

77. Lund, C. R. F., and Dumesic, J. A., *J. Catal.* **72**, 21 (1981).

78. Lund, C. R. F., and Dumesic, J. A., *J. Catal.* **76**, 93 (1982).

79. Lund, C. R. F., and Dumesic, J. A., *J. Phys. Chem.* **86**, 130 (1982).

80. Huber, G. W., Guymon, C. G., Conrad, T. L., Stephenson, B. C., and Bartholomew, C. H., *Stud. Surf. Sci. Catal.* **139**, 423 (2001).

81. Moss, R. L., Pope, D., Davis, B. J., and Edwards, D. H., *J. Catal.* **58**, 206 (1979).

82. Datye, A. K., *Top. Catal.* **13**, 131 (2000).

83. Stoeber, W., Fink, A., and Bohn, E., *J. Colloid Interface Sci.* **26**, 62 (1968).

84. Benson, J. E., Hwang, H. S., and Boudart, M., *J. Catal.* **30**, 146 (1973).

85. Wagner, C. D., Davis, L. E., Zeller, M. V., Taylor, J. A., Raymond, R. H., and Gale, L. H., *SIA, Surf. Interface Anal.* **3**, 211 (1981).

86. Baptist, R., Pellissier, A., and Chauvet, G., *Solid State Commun.* **68**, 555 (1988).

87. Ogama, T., *J. Appl. Phys.* **64**, 753 (1988).

88. Puppin, E., Lindau, I., and I., A., *Solid State Commun.* **77**, 983 (1991).

89. Gorlich, E., Haber, J., Stoch, A., and Stoch, J., *J. Solid State Chem.* **33**, 121 (1980).

90. Seyama, H., and Soma, M., *J. Chem. Soc. Faraday Trans.* **I 81**, 485 (1985).

91. Anpo, M., Nakaya, H., Kodama, S., Kubokawa, Y., Domen, K., and Onishi, T., *Journal of Physical Chemistry* **90**, 1633 (1986).

92. Paparazzo, E., *J. Phys.* **D. 20**, 1091 (1987).

93. Bader, S. D., Richter, L., and Orent, T. W., *Surf. Sci.* **115**, 501 (1982).

94. Samsonov, G. V., and Editor, *in "The Oxide Handbook."*1973, 524 pp.

95. Bekkay, T., Sacher, E., and Yelon, A., *Surface Science* **217**, L377 (1989).

96. Gaarenstroom, S. W., and Winograd, N., *Journal of Chemical Physics* **67**, 3500 (1977).

97. Bowker, M., *Surface Science* **155**, L276 (1985).

98. Tjeng, L. H., Meinders, M. B. J., van Elp, J., Ghijsen, J., Sawatzky, G. A., and Johnson, R. L., *Phys. Rev.* **41**, 3190 (1990).

99. Zemlyanov, D. Y., Nagy, A., and Schlogl, R., *Applied Surface Science* **133**, 171 (1998).

100. Behrisch, R., *in "Sputtering by Particle Bombardment I: Physical Sputtering of Single-Element Solids."*Topics in Applied Physics, Springer-Verlag, Berlin, Heidelberg, New York, 1981, vol. 47.

101. Seah, M. P., *SIA, Surf. Interface Anal.* **2**, 222 (1980).

102. Powell, C. J., and Jablonski, A., *in "NIST Electron Inelastic-Mean-Free-Path Database."* 1.1 ed., National Institute of Standards and Technology, Gaithersburg, 2000.

103. Logan, A. D., Braunschweig, E. J., Datye, A. K., and Smith, D. J., *Langmuir* **4**, 827 (1988).

104. Ciuparu, D., Lyubovsky, M. R., Altman, E., Pfefferle, L. D., and Datye, A., *Catal. Rev. - Sci. Eng.* **44**, 593 (2002).

105. Ruckenstein, E., and Chen, J. J., *J. Colloid Interface Sci.* **86**, 1 (1982).

106. Burch, R., Loader, P. K., and Urbano, F. J., *Catal. Today* **27**, 243 (1996).

107. Garbowski, E., Feumi-Jantou, C., Mouaddib, N., and Primet, M., *Appl. Catal., A* **125**, 185 (1995).

108. Deng, Y., and Nevell, T. G., *Catal. Today* **47**, 279 (1999).

109. Sekizawa, K., Machida, M., Eguchi, K., and Arai, H., *J. Catal.* **142**, 655 (1993).

110. Salomonsson, P., Johansson, S., and Kasemo, B., *Catal. Lett.* **33**, 1 (1995).

111. Wolf, M. M., Zhu, H., Green, W. H., and Jackson, G. S., *Applied Catalysis, A: General* **244**, 323 (2003).

112. Zheng, G., and Altman, E. I., *Surface Science* **504**, 253 (2002).

113. Campbell, C. T., Foyt, D. C., and White, J. M., *J. Phys. Chem.* **81**, 491 (1977).

114. Leisenberger, F. P., Koller, G., Sock, M., Surnev, S., Ramsey, M. G., Netzer, F. P., Klotzer, B., and Hayek, K., *Surf. Sci.* **445**, 380 (2000).

115. Bondzie, V. A., Kleban, P., and Dwyer, D. J., *Surface Science* **347**, 319 (1996).

116. Bondzie, V. A., Kleban, P. H., and Dwyer, D. J., *Surface Science* **465**, 266 (2000).

117. Weissman, D. L., Shek, M. L., and Spicer, W. E., *Surf. Sci.* **92**, L59 (1980).

118. Weissman-Wenocur, D. L., Shek, M. L., Stefan, P. M., Lindau, I., and Spicer, W. E., *Surface Science* **127**, 513 (1983).

119. Peuckert, M., *J. Phys. Chem.* **89**, 2481 (1985).

120. Guiot, J. M., *Journal of Applied Physics* **39**, 3509 (1968).

121. Bayer, G., and Wiedemann, H. G., *Thermochim. Acta* **11**, 79 (1975).

122. Thurmer, K., Williams, E., and Reutt-Robey, J., *SCIENCE FIELD Publication Date:2002 Sep 20* **297**, 2033 (2002).

123. Asscher, M., and Somorjai, G. A., *Surface Science* **143**, L389 (1984).

124. Spencer, N. D., Schoonmaker, R. C., and Somorjai, G. A., *Journal of Catalysis* **74**, 129 (1982).

125. Lyubovsky, M., Pfefferle, L., Datye, A., Bravo, J., and Nelson, T., *J. Catal.* **187**, 275 (1999).

126. Su, S. C., Carstens, J. N., and Bell, A. T., *J. Catal.* **176**, 125 (1998).

127. Wang, Y.-N., Herman, R. G., and Klier, K., *Surface Science* **279**, 33 (1992).

128. Klier, K., Hess, J. S., and Herman, R. G., *Journal of Chemical Physics* **107**, 4033 (1997).

129. Liu, Z.-P., and Hu, P., *Journal of the American Chemical Society* **125**, 1958 (2003).

8 Acknowledgements

I would like to express my sincere gratitude to the people and organizations that have supported my Ph.D. study at Worcester Polytechnic Institute.

First, I would like to thank Professor Fabio H. Ribeiro for giving me the opportunity to be his Ph.D. student. Catalysis and surface science is a fascinating research field, and I gained great insights and understanding of this subject under his kind guidance. His broad knowledge and scholarly attitude set an example for me, not limited to the past five years but for the rest of my life. He offered generous help not only to my research but also to my daily life.

I also want to thank my Ph.D. committee members, Professor William M. Clark from the chemical engineering department and Professor Richard D. Sission from the mechanical engineering department, for their time in reviewing my dissertation and participating my defense.

Secondly, I would like to thank my former and current lab colleagues, Dr. Robson S. Monteiro, Dr. Dmitri Y. Zemlyanov, Dr. Yury Zvinevich, Dr. Natalia A. Koryabkina, Dr. Nan Chen, Jinyi Han, Abhijit Phatak, Nada M. Al-Ananzeh and Vinay Medhekar, for all the happy time together. I especially thank Jinyi Han and Dr. Dmitri Y. Zemlyanov for discussing experimental results and sharing ideas. They made great contribution to my dissertation.

Additionally, I want to thank all the faculty and staff memebers of the chemical engineering department at WPI. Special thank to Giacomo Ferraro and Douglas White for their sincere help to maitain and modify my experiment system throughout the last five years.

Finally, I would like to dedicate my dissertation to my wife and my parents for their constant love, support, and patience during my years of study.

Also, I thank US Department of Energy for financial support.